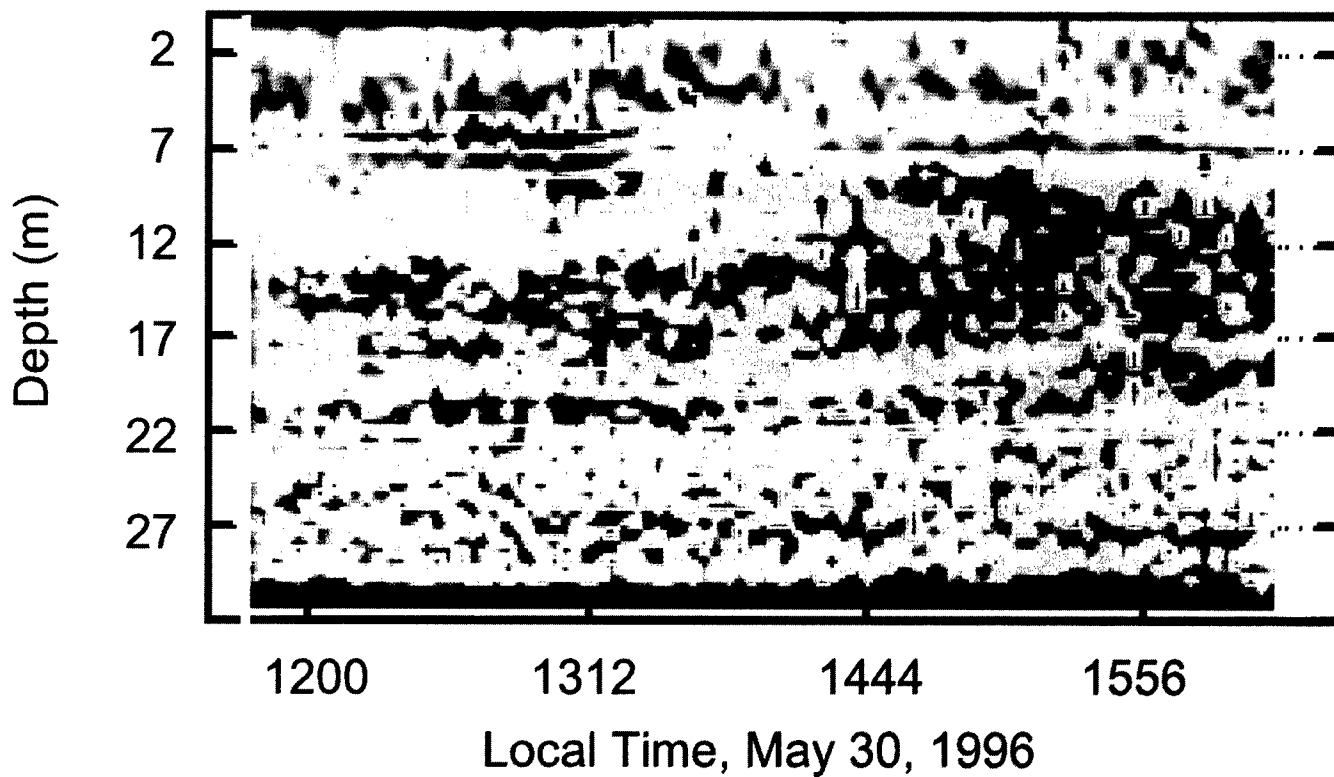


OCEANOGRAPHY

PUBLISHED BY THE OCEANOGRAPHY SOCIETY

Zooplankton Aggregation on Phytoplankton Layer near 7m depth



19990323 130

Special Issue: Focus on Thin Layers

DEIC QUALITY INSPECTED 1

MicroCAT sets the **NEW** standard in *accurate* moored C-T instruments

- Higher Accuracy
- Increased Resolution
- Better Stability
- Direct Digital Output
- Proven Fouling Resistance

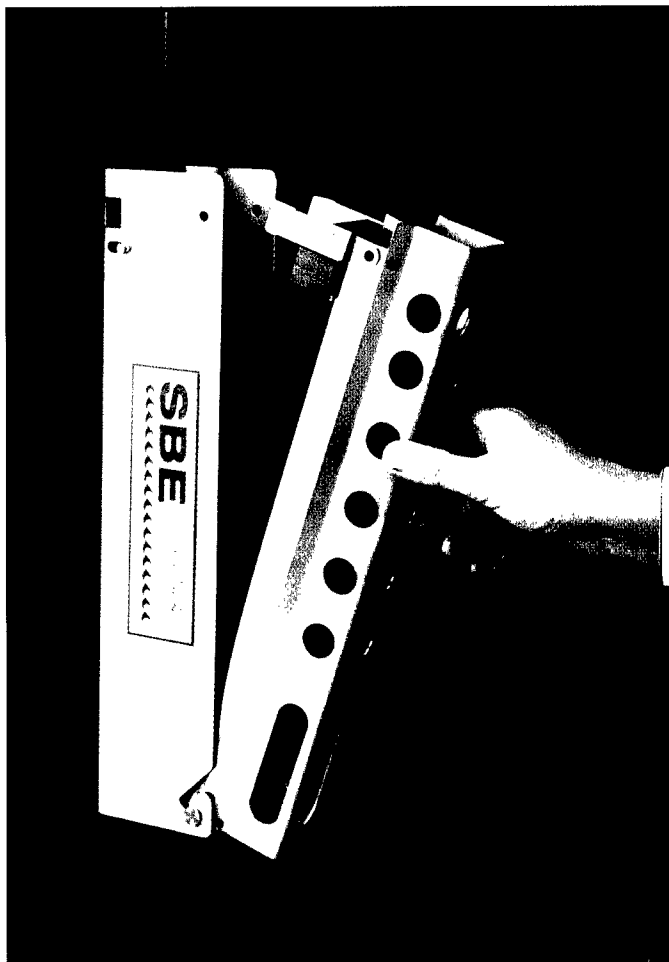
An evolution of the legendary SEACAT, proven by a decade of ocean research; MicroCAT combines our unique internal-field conductivity cell and ultra-stable thermistor with new microelectronics and calibration technology.

Three New Models with Surprisingly Low Prices!

SBE 37-SI with serial interface (no memory or battery) for real-time monitoring or integration with current meters, ROVs, etc.

SBE 37-SM with serial interface and large flash memory for conventional moorings or synchronization with ADCP sampling.

SBE 37-IM with DPSK inductive modem telemetry (shown at right), outperforms FSK inductive telemetry types. The SBE 37-IM clamp attaches to a jacketed cable, the MicroCAT snaps in place and is then secured in the clamp with two bolts. Up to 100 addressable MicroCATs communicate (half duplex) with an Inductive Modem Controller (sold separately) over cables up to 7000 meters long.



Other MicroCAT Features

All titanium construction for 7,000 meters depth, RS-232C or RS-485 interface choices, real-time clock, optional strain gauge pressure sensor, non-restricted lithium battery gives endurance for over 100,000 samples, internal references for automatic error correction, calibration coefficients stored in EEPROM allow data output in degrees C, Siemens/meter, decibars and time (month, day, year, hours, minutes, seconds). Data format compatible with SEASOFT® or virtually any spread sheet or data base.



SEA-BIRD ELECTRONICS, INC.
1808 - 136th Place Northeast
Bellevue, Washington, 98005 USA

web site: www.seabird.com

Fax (425) 643-9954

Telephone (425) 643-9866

VOL. 11, NO. 1

OCEANOGRAPHY

PUBLISHED BY THE OCEANOGRAPHY SOCIETY

DISTRIBUTION STATEMENT A
Approved for Public Release
Distribution Unlimited

Style Guide and Information for Contributors

Philosophy. *Oceanography* exists to promote and chronicle all aspects of ocean science and its applications. It publishes brief articles, critical essays and concise reviews that deal with topics of broad interest to the ocean-science community. In addition, *Oceanography* solicits and publishes news and information, meeting reports, book reviews, and other items of current interest.

Manuscript Requirements: All manuscripts must be typewritten and double spaced. Manuscripts must include the title, name and affiliation (including city, state and zip code) of each author. Acknowledgements, references and figures should follow the stylistic conventions outlined below. Please submit four hard copies of the manuscript and a copy on disk to: Larry P. Atkinson, Center for Coastal Physical Oceanography, Old Dominion University, Crittenton Hall, Norfolk, VA 23529. Submitted material will be reviewed for style, relevance and quality by the editors and by anonymous external reviewers.

Language Style: The desired style of writing is less technical and more compact than that typically used in scientific papers. The readership includes oceanographers from all traditional disciplines, as well as scientifically literate persons with a broad range of interests and responsibilities. Authors should strive for clarity and simplicity and avoid technical and mathematical jargon. Perhaps the best description of the expected style is the following.

Vigorous writing is concise. A sentence should contain no unnecessary words, a paragraph no unnecessary sentences, for the same reason that a drawing should have no unnecessary lines and a machine no unnecessary parts. This requires not that the writer make all his sentences short, or that he avoid all detail and treat his subjects only in outline, but that every word tell.

—William Strunk, Jr. and E. B. White
The Elements of Style, third ed.,
© 1979 Macmillan Pub. Co., Inc.
Reprinted with permission.

Length Limitations (Maximum length of articles must be strictly followed):

*** Feature Articles:**

10–12 double-spaced, typed pages; 4–5 figures.

*** Review and Comment Pieces:**

5–8 pages, 2–3 figures.

*** Other** (e.g., News and Information, Meeting and Workshop Reports, or Book Reviews) should be as concise as possible. Meeting reports should describe goals, activities and accomplishments; not agendas, programs and attendance.

References: *Oceanography* does not use numbered footnotes. Instead, textual references should be given parenthetically as: (author, year). Complete and correct references are the author's responsibility. A complete list of references should be ordered alphabetically by the first author's last name, and placed at the end of the manuscript in following format.

Article in Journal:

Author(s), year: Title of article. *Title of Journal (abbreviated)*, volume number, inclusive pages.

*** Example:**

Levin, M.E., 1979: Ahab as Socratic philosopher: The Myth of the Cave inverted. *Am. Transcendental Quar.*, 41, 61–73.

*** Article in Book:**

Author(s), year: Title of article. In: *Title of Book*. Editor's name, ed., Publisher, inclusive pages.

*** Example:**

Skirrow, G., 1975: The dissolved gases-carbon dioxide. In: *Chemical Oceanography*, vol. 2, 2nd edition. J.P. Riley and G. Skirrow, eds., Academic Press, New York, 1–192.

Book:

Author(s), year: *Title of Book*. Publisher, city, total pages.

*** Example:**

Baker, B.B. and E.T. Copson, 1939: *The Mathematical Theory of Huygens' Principle*. Clarendon, Oxford, 155 pp.

*** Thesis:**

Author, year: Name of thesis. Masters/Ph.D. thesis, name of university, total pages.

*** Example:**

Rintoul, S., 1988: Mass, heat and nutrient fluxes in the Atlantic Ocean determined by inverse methods. Ph.D. thesis, Massachusetts Institute of Technology/Woods Hole Oceanographic Institution Joint Program, 287 pp.

*** Proceedings:**

Author(s), year: Name of report. In: *Name of Proceedings*. Name of conference, publisher, city, inclusive pages.

*** Example:**

Knauss, J.A. and M.H. Katsouras, 1986: Recent experiences of the United States in conducting marine scientific research in coastal state Exclusive Economic Zones. In: *The Law of the Sea: What Lies Ahead?*. Proceedings of the Twentieth Annual Conference on the Law of the Sea Institute, 1986, Univ. of Hawaii Press, Honolulu, 297–309.

Abbreviations should conform to the current Chemical Abstracts Service Source Index published by The American Chemical Society, or see the American Meteorological Society's Author's Guide. Works "in progress" or "submitted" may be cited only as "personal communication." Articles that have been accepted for publication may be cited, if the journal name and volume number are provided in the list of references. "In press" citations are acceptable. The correct citation for this publication is *Oceanography*.

Figures/Tables: Each figure or table should be accompanied by a complete caption and be cited and explained in the text. All figures and drawings should be of exceptional quality to allow for clear reproduction and reduction. Articles generally are limited to four or five figures. Review and Comment pieces generally are limited to three figures. Line drawings and black-and-white or color photos are acceptable; authors must pay the additional costs of color processing.

REPORT DOCUMENTATION PAGE

Form Approved

OMB No. 0704-0188

Public reporting burden for this collection of information is estimated to average 1 hour per response, including the time for reviewing instructions, searching existing data sources, gathering and maintaining the data needed, and completing and reviewing the collection of information. Send comments regarding this burden estimate or any other aspect of this collection of information, including suggestions for reducing this burden to Washington Headquarters Services, Directorate for Information Operations and Reports, 1215 Jefferson Davis Highway, Suite 1204, Arlington, VA 22202-4302, and to the Office of Management and Budget, Paperwork Reduction Project (0704-0188), Washington, DC 20503.

1. AGENCY USE ONLY (Leave blank)		2. REPORT DATE 11 MAR 1999	3. REPORT TYPE AND DATES COVERED FINAL 15 JUN 97 - 31 DEC 98
4. TITLE AND SUBTITLE Publication and distribution of two special issues of "Oceanography" - High Frequency Radar and Ocean Thin Layers			5. FUNDING NUMBERS N00014-97-1-0851
6. AUTHOR(S) Larry P. Atkinson, editor, plus various authors (see Table of Contents attached)			
7. PERFORMING ORGANIZATION NAME(S) AND ADDRESS(ES) The Oceanography Society (TOS) 4052 Timber Ridge Drive Virginia Beach, VA 23455			8. PERFORMING ORGANIZATION REPORT NUMBER 2 - Final
9. SPONSORING / MONITORING AGENCY NAME(S) AND ADDRESS(ES) Office of Naval Research 800 North Quincy Street Arlington, VA 22217-5660			10. SPONSORING / MONITORING AGENCY REPORT NUMBER
11. SUPPLEMENTARY NOTES			
12. DISTRIBUTION / AVAILABILITY STATEMENT V10:N2 High Frequency Radar - 500 delivered to ONR V11:N2 Thin Layers in the Ocean - 500 delivered to ONR Both issues were also sent to all members of TOS and additional copies are available through the TOS office.			13. DISTRIBUTION CODE
14. ABSTRACT (Maximum 200 words) The Table of Contents of both V10:N2 and V11:N1 are attached here. Also attached are the introductory articles to each each which together summarize the importance and significant information contained in the two special issues.			
15. SUBJECT TERMS high-frequency radar, remote sensing, small-scale patterns, upper ocean processes			16. NUMBER OF PAGES 1
			17. PRICE CODE
18. SECURITY CLASSIFICATION OF REPORT Unclassified	19. SECURITY CLASSIFICATION OF THIS PAGE Unclassified	20. SECURITY CLASSIFICATION OF ABSTRACT Unclassified	21. LIMITATION OF ABSTRACT UL

OCEANOGRAPHY

SERVING OCEAN SCIENCE AND ITS APPLICATIONS

TABLE OF CONTENTS

QUARTERDECK / 2

FEATURES

SMALL-SCALE PLANKTONIC STRUCTURE: PERSISTENCE AND TROPHIC CONSEQUENCES
By Timothy J. Cowles, Russell A. Desiderio, and Mary-Elena Carr / 4

**MICRO- TO FINE-SCALE CHEMICAL GRADIENTS AND LAYERS
IN STRATIFIED COASTAL WATERS**
By Alfred K. Hanson, Jr. and Percy L. Donaghay / 10

**ACOUSTICAL SENSING OF SMALL-SCALE VERTICAL STRUCTURES
IN ZOOPLANKTON ASSEMBLAGES**
By D.V. Holliday, R.E. Pieper, C.F. Greenlaw and J.K. Dawson / 18

SIMULTANEOUS IMAGING OF PHYTOPLANKTON AND ZOOPLANKTON DISTRIBUTIONS
By Jules F. Jaffe, Peter J.S. Franks and Andrew W. Leising / 24

**ECOLOGY OF A *CHAETOCEROS SOCIALIS* LAUDER PATCH ON GEORGES BANK:
DISTRIBUTION, MICROBIAL ASSOCIATIONS, AND GRAZING LOSSES**
By Michael E. Sieracki, Dian J. Gifford, Scott M. Gallager
and Cabell S. Davis / 30

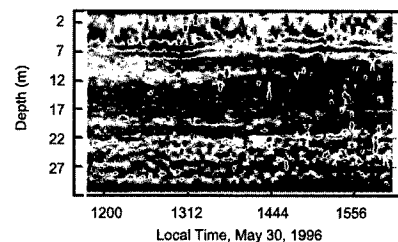
FINESTRUCTURE, MICROSTRUCTURE, AND THIN LAYERS
By Thomas Osborn / 36

**A MODEL FOR THE REFLECTANCE OF THIN LAYERS, FRONTS, AND INTERNAL
WAVES AND ITS INVERSION**
By J. Ronald V. Zaneveld and W. Scott Pegau / 44

EFFECTS OF A THIN LAYER ON REFLECTANCE AND REMOTE-SENSING REFLECTANCE
By A.A. Petrenko, J.R.V. Zaneveld, W.S. Pegau, A.H. Barnard
and C.D. Mobley / 48

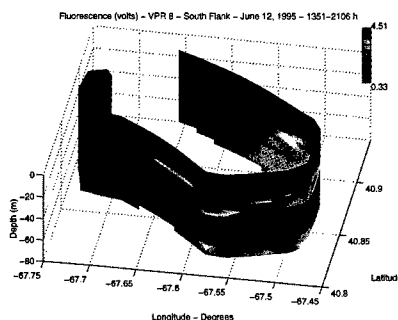
A QUANTITATIVE LITTORAL CLASSIFICATION SYSTEM
By A. Brandt, J. Calman and J.R. Rottier / 51

Zooplankton Aggregation on Phytoplankton Layer near 7m depth



FRONT COVER

Zooplankton aggregation on a phytoplankton layer near 7m depth in West Sound in the San Juan Islands, Washington.



BACK COVER

Vertical section of *in situ* fluorescence. See Sieracki *et al.*, this issue.

Oceanography (ISSN 1042-8275) is published by The Oceanography Society, 4052 Timber Ridge Drive, Virginia Beach, VA 23455 USA. © 1997, The Oceanography Society, Inc. All rights reserved. Permission is granted to copy an article in this publication for use in teaching or research. For more extensive copying, a fee of \$1.00 per article can be paid through the Copyright Clearance Center, 21 Congress Street, Salem, MA 01970. Republication, systemic reproduction, or collective redistribution of any material in this publication is permitted only with the approval of The Oceanography Society. Send change-of-address information to the Society address. Postmaster: Bulk mail postage paid Lancaster, PA 17603; Permit 161.

THIN LAYERS: OBSERVATIONS OF SMALL-SCALE PATTERNS AND PROCESSES IN THE UPPER OCEAN

FOR DECADES, marine scientists have been asking questions about the response of planktonic distributions and processes to physical forcing across a range of temporal and spatial scales. The mismatch in measurement capabilities in physical, chemical, and biological oceanography, however, often frustrated attempts to link planktonic responses to physical forcing over equivalent time and space scales. The compelling nature of these questions about linkages and scale, coupled with technological advances in optical and acoustical methods, has resulted in the development of new instrumentation packages and sampling approaches that permit us to quantify and evaluate small-scale planktonic processes and physical processes on coincident temporal and spatial scales. The technical advances in optics and acoustics have included improved sensitivity and accuracy as well as greatly improved spatial and spectral resolution. The sensors resulting from these technical advances now have been deployed on a wide variety of platforms, including moorings, bottom-mounted inverted echo sounders, remotely operated vehicles (ROVs), autonomous underwater vehicles (AUVs), towed vehicles, and free-falling or buoyancy-controlled packages that decouple the instruments from the "smearing" effects of ship motion.

We now have the ability to resolve the vertical structure of biological, chemical, and physical properties on spatial scales of a few centimeters. As illustrated by the papers in this issue of *Oceanography*, many of the observations with these new optical and acoustical systems have revealed previously unresolved "thin layers" of phytoplankton and zooplankton <1 m in vertical extent. These submeter vertical structures often have local concentrations many times larger than found just above or below the layer. Some of these small-scale structures have been observed to persist for days over horizontal scales of kilometers.

These observations of small structure raise questions about the impact of such structure on planktonic processes, including those of nutrient flux, phytoplankton growth, feeding by zooplankton, reproductive behavior, and predation by animals at higher trophic levels. What physical mechanisms are involved in the formation, maintenance, and dissipation of small-scale planktonic structure? To what extent do small-scale planktonic structures in the upper ocean influence, or bias, observations obtained from satellite-based, ocean color sensors? The papers in this volume address some of these questions, while providing examples of the rich structure that, just a few years ago, was invisible to us.

This issue of *Oceanography* attempts to focus attention on "critical scale" phenomena that involve physics, chemistry, and biology. It is our contention that the sampling approaches described in these papers provide the means for new insights into upper ocean processes. It is likely that further observations of these "critical scale" phenomena may force us to reassess some of our existing ideas about planktonic processes, trophic dynamics, and physical-chemical-biological coupling. We hope that this collection of papers illustrates the need for that reassessment and stimulates readers to explore the role of small-scale distributions and the processes that occur within them. A sound understanding of these structures and processes is essential as we address questions ranging from how an individual organism finds sufficient food for growth and reproduction, to how ocean physics is linked to the amount of life the sea can sustain.

—Tim Cowles and Percy Donaghay



THE OCEANOGRAPHY SOCIETY

4052 Timber Ridge Drive
Virginia Beach, VA 23455 USA
(757) 464-0131; fax: (757) 464-1759

OFFICERS

Robert A. Duce, President
Kenneth Brink, President-Elect
Melbourne G. Briscoe, Secretary
David Evans, Treasurer
Margaret Leinen, Past-President

COUNSELORS

Ann Gargett
Larry Mayer
Bess Ward
Larry Atkinson
Kenneth Brink
Anthony Knap
Robert F. Anderson
Rick Spinrad

EXECUTIVE DIRECTOR

Judi Rhodes

CORPORATE/INSTITUTIONAL SPONSORS

Monterey Bay Aquarium Research Institute,
Pacific Grove, CA, USA
National Marine Fisheries Service,
Silver Spring, MD, USA
Ober, Kaler, Grimes & Shriver,
Washington, DC, USA
RD Instruments, San Diego, CA, USA
Scripps Institution of Oceanography,
La Jolla, CA, USA

OCEANOGRAPHY

CO-EDITORS

Larry P. Atkinson
Center for Coastal Physical Oceanography
Old Dominion University
Crittenton Hall
Norfolk, VA 23529
(757) 683-5558
Internet: atkinson@ccpo.odu.edu

Connie Sancetta
National Science Foundation
Ocean Sciences Division
Room 725
4201 Wilson Blvd.
Arlington, VA 22230
(703) 306-1586
Internet: csancett@nsf.gov

ASSOCIATE EDITORS

James W. Ammerman
Department of Oceanography
Texas A&M University
College Station, TX 77843 USA
(409) 845-5105

Gregg J. Brunskill
Australian Institute of Marine Science
PMB No. 3, Townsville, M.C.
Queensland 4810, Australia
(077) 789 211; FAX (077) 725 852;
Internet: g_brunskill@aims.gov.au

ASSOCIATE EDITORS (Continued)

Ellen R.M. Druffel
Department of Earth System Sciences, PSRF-207
University of California, Irvine, CA 92717
(714) 725-2116
Internet: druffel@bro.ps.uci.edu

Donald B. Olson
RSMAS
University of Miami
Miami, FL 33149 USA
(305) 361-4074
Internet: don@loquat.rsmas.miami.edu

Makoto Omori
Department of Aquatic Biosciences
Tokyo University of Fisheries
4-5-7, Konan, Minato-ku, Tokyo, Japan
(03)471-1251

Louis M. Prieur
Laboratoire de Physique et Chimie Marines
Observatoire Oceanologique de Villefranche sur Mer
BP 08 La Darse
06230 Villefranche Sur Mer, France
(33)93763739
Internet: prieur@ccrv.obs-vlfr.fr

Richard W. Spinrad
CORE
1755 Massachusetts Ave, NW Suite 800
Washington, DC 20036-2102
(202) 232-3900 x219

James Syvitski
Director, Institute of Arctic and Alpine Research
University of Colorado at Boulder
1560 30th St., Campus Box 450
Boulder, CO 80309-0450
(303) 492 7909
(303) 492 6388 (FAX)
email james.syvitski@colorado.edu

Peter Wadhams
Scott Polar Research Institute
University of Cambridge
Lensfield Road
Cambridge CB2 1ER England
223-336542
Internet: pw11@phx.cam.ac.uk

PRINTER
Lancaster Press
Lancaster, PA USA

Mark your calendar now . .

TOS 1999 Scientific Meeting "Extreme and Unexpected Phenomena"

Reno Hilton, Reno, Nevada

April 26-30.

Check the TOS web site (www.tos.org) and future mailings for program and site details.

SMALL-SCALE PLANKTONIC STRUCTURE: PERSISTENCE AND TROPHIC CONSEQUENCES

By Timothy J. Cowles, Russell A. Desiderio
and Mary-Elena Carr

MOST CONVENTIONAL sampling methods limit our ability to resolve planktonic distributions over vertical scales less than a few meters. Estimates of in situ biological rates also are limited by equipment and sampling resolution. It has been obvious to plankton researchers for decades that the uncertainties created by sampling limitations are complicated further by vertical and horizontal variability in plankton distributions (often called patchiness). Although patches of phytoplankton (usually undetected) were recognized as essential for zooplankton growth and survival (e.g., Mullin and Brooks, 1976; Dagg, 1977), the distribution, size, and concentration of phytoplankton patches have been viewed as random or stochastic (e.g., Fasham, 1978). If phytoplankton patchiness is characterized by randomness, the contribution of this variability to our estimates of phytoplankton biomass may be removed by averaging over larger scales, and samples obtained with conventional sampling equipment can be used with some confidence. On the other hand, if patchiness is nonrandom on spatial or temporal scales that are difficult to resolve with conventional methods, then conventional sampling may alias estimates of planktonic distributions and rate processes such as grazing and growth.

It is generally thought that biological structure is linked to physical processes (Denman and Powell, 1984; Mackas *et al.*, 1985; Owen, 1989) including surface waves (and wave breaking), internal waves, Langmuir circulation, horizontal

intrusions, shear instabilities, convective overturns, and salt-fingering, all of which can lead to localized intermittent vertical mixing and redistribution of biomass (Denman and Gargett, 1983; Denman and Powell, 1984; Weller and Price, 1988; Owen, 1989). Turbulence and other small-scale physical processes are proposed to constrain a wide range of biological processes, such as nutrient uptake by phytoplankton (Goldman, 1988), photosynthesis in fluctuating light fields (Marra, 1978), grazing on phytoplankton by zooplankton (Mullin and Brooks, 1976; Cowles *et al.*, 1988; Rothschild and Osborne, 1988), larval fish survivorship (Lasker, 1975), and the vertical distribution patterns of planktonic organisms, from bacteria to larval fish (Mitchell and Fuhrman, 1989; Owen, 1989; Denman and Gargett, 1988; Lasker, 1975; Bjornsen and Nielsen, 1991).

Observations of small-scale (<1 m) vertical variability in biological structure in the upper ocean began with early in situ observations of Bainbridge (1952) and the high-resolution collections of Cassie (1963) and have continued with recent centimeter-scale collections of Owen (1989), Mitchell and Fuhrman (1989), Bjornsen and Nielsen (1991), and Donaghay *et al.*, (1992). However, with the exception of some recent work (Cowles *et al.*, 1990; Donaghay *et al.*, 1992; Cowles and Desiderio, 1993) previous small-scale biological observations have lacked concurrent measurements of physical variables on the appropriate time and space scales. These recent observations confirm that any advances in understanding the response of small-scale biological structure to physical forcing require coincident measurements of physical and biological parameters over the same range of time and space scales.

In the course of developing a microstructure fluorescence sensor (Cowles *et al.*, 1990; Cowles and Desiderio, 1993; Desiderio *et al.*, 1993), we observed small-scale vertical structure of phytoplankton biomass in conjunction with fine-scale and microscale physical structure. We found that thin layers of locally enhanced phytoplankton biomass are common over the continental shelf and at open ocean locations, and that these layers are usually between 10 and 50 cm thick. As one might expect, some of these thin layers of pigment fluorescence are associated with temperature steps and/or local minima in turbulence. More surprising, however, was the finding that some individual thin layers persist as local maxima for periods of hours. Subsequent observations by our group and by others (e.g., Donaghay *et al.*, 1992) have confirmed that these sub-1-m scale local maxima can be detected across a range of coastal and oceanic locations when the appropriate high-resolution instrumentation is used.

These recent observations suggest that estimates of biological rate processes obtained by coarser-scale conventional sampling (e.g., ~5–10-m bottle spacing) may have missed the contribution of persistent sub-1-m scale structure. The common occurrence and persistence of these features suggest that it is necessary to quantify the contribution of thin layers to biological rate processes in the upper ocean. Relative to the average background concentration, thin layers of enhanced biomass may be characterized by high autotrophic growth rates, increased ingestion, growth, and reproduction by microheterotrophs, microzooplankton, and mesozooplankton, locally higher nutrient and particulate flux, and higher nutrient regeneration rates. It is likely that locally

Timothy J. Cowles and Russell A. Desiderio, College of Oceanic and Atmospheric Sciences, 104 Ocean Admin Bldg., Oregon State University, Corvallis, OR 97331-5503, USA. Mary-Elena Carr, Jet Propulsion Laboratory, 4800 Oak Grove Dr., Pasadena, CA 91101-8099, USA.

higher rates on these small-scale structures make a previously undetected contribution to carbon flux across a range of temporal and spatial scales.

In this paper we provide evidence of the existence and duration of layers in the open ocean (see Temporal Persistence of Small-Scale Features), show optical differences between nearby layers that imply persistence (see *In Situ* Characterization of Small-Scale Features), suggest a framework in which to understand the persistence or erasure of layers (see How Might Small-Scale Planktonic Features Persist?), and finally provide an assessment of the possible trophic impact of persistent layers (see Trophic Consequences of Persistent Small-Scale Structure).

Temporal Persistence of Small-Scale Features

We were intrigued to find small-scale planktonic features that persisted for hours. It seemed unlikely that physical processes would be quiescent enough to permit such persistence, and estimates of persistence times based on canonical diffusivities yield time scales of minutes, not hours. Our time-series observations suggest that 10–50-cm scale features persist over ecologically relevant time scales for planktonic organisms. Over 170 layers of particle scattering were observed to persist for at least 4–6 h in an open ocean site off the California coast (Carr *et al.*, unpublished data).

Observations with a profiling microstructure fluorometer (Cowles *et al.*, 1990; Cowles *et al.*, 1993; Desiderio *et al.*, 1993) demonstrated that the vertical patterns of phytoplankton pigment fluorescence often have local maxima within narrow layers (10–50 cm in thickness). In addition, some of these narrow local maxima were present at the onset of a time series and were still present when sampling terminated. We illustrate this phenomenon with a time series of profiles collected 100 miles off the Oregon coast. These profiles, taken ~12 min apart, revealed a variable physical structure (Fig. 1, a and b) and considerable small-scale variability in phytoplankton structure, based on the measured fluorescence (Fig. 1c; in these figures each succeeding profile is offset to show each trace more clearly). The profiles indicate internal wave displacement of ~2.2 m during the time series, which is consistent with other observations of internal wave activity for

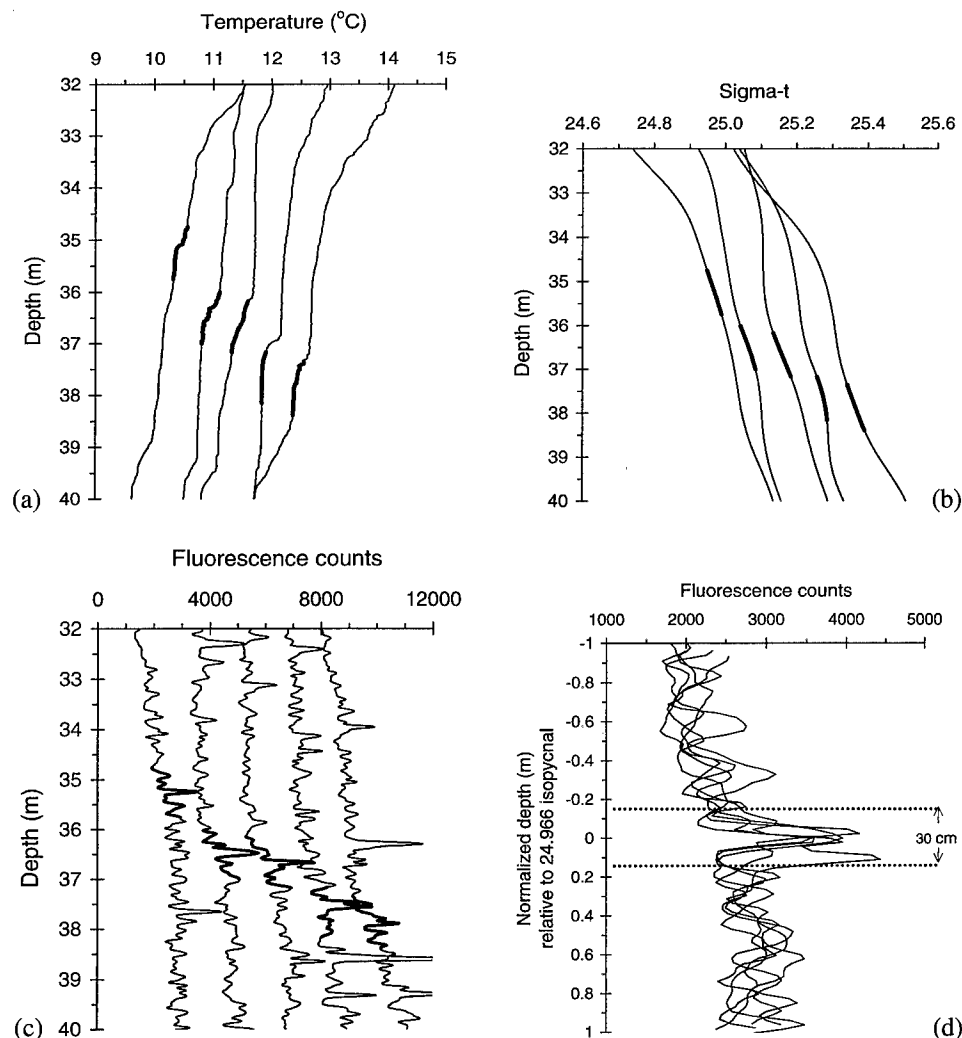


Fig. 1: Vertical detail (32–40 m) of (a) temperature, (b) sigma-t, and (c) fluorescence from five profiles spanning approximately 1 h during a cruise off the Oregon coast. The profiles in a, b, and c are offset to show each trace. In a, b, and c the 1-m segments of each profile that were centered on an isopycnal of 24.966 sigma-t units are highlighted. In d, those 1-m vertical segments of fluorescence identified in c are plotted relative to the depth of the 24.966 isopycnal (± 0.003 sigma-t units). The local maximum in fluorescence now is seen as a persistent thin layer.

this region. Some of the small-scale fluorescence maxima were associated with specific temperature or density intervals. The profiles shown in Figure 1 have a persistent phytoplankton fluorescence feature centered within 0.003 sigma-t units of the 24.966 isopycnal (Fig. 1d). The measured fluorescence of that narrow feature did not vary by more than 10% during the time-series.

Additional evidence for persistent features comes from Donaghay *et al.* (1992), who reported significant enhancements in nutrients, primary production, and meroplankton larval abundance within a thin layer in a stratified embayment. In addition, Oldham and Imberger (1992) reported 20-cm-thick layers of oxygen mi-

crostructure that persisted for hours in Australian lakes. In this issue, papers by Holliday *et al.* and Hanson and Donaghay provide additional examples of persistent small-scale features.

It is important to note that these observations of persistent small-scale structure have been made possible through advances in instrumentation that permit sampling of the upper ocean over a different range of time and space scales than could be accomplished even a decade ago. *In situ* optical instruments are particularly well-suited to reveal small-scale biological structure because these devices have high sampling rates and are compact enough to include on profiling systems.

In Situ Characterization of Small-Scale Features

We have approached the detection and characterization of persistent small-scale structure through the use of free-fall profiling systems that can carry CTDs and the new generation of biooptical instrumentation. These physical and optical tools permit us to describe individual small-scale features and to distinguish differences between nearby features. For example, while profiling the upper 100 m of the water column off the Oregon coast with a fiber-optic microstructure fluorometer (see Desiderio *et al.*, 1993), we observed spectral changes in the in situ fluorescence emission due to phycobilin pigments. These shifts of the emission peaks in the fluorescence spectra suggested a taxonomic change from cyanobacteria to cryptomonads within the thermocline that was confirmed with discrete sample collections (Cowles *et al.*, 1993).

Our present free-fall instrumentation package was developed in conjunction with Dr. J. Ronald Zaneveld of Oregon State University and has a Sea-Bird 911+CTD, two multiwavelength absorption meters (WetLabs ac-9), and a multi-excitation spectrofluorometer (WetLabs SAFIRE) as its basic configuration. Additional instruments can be added as needed. We deploy the package on a

loose data tether, with sufficient buoyancy on the package to obtain descent rates of 15–20 cm/s. These slow descent rates allow data acquisition on centimeter spatial scales and result in multiparameter characterization of small-scale features (see Hanson and Donaghay, 1998, for additional examples).

We have obtained many profiles that reveal distinct shifts in spectral absorption and spectral fluorescence properties between nearby small-scale features. For example, a series of vertical profiles from East Sound, WA, revealed several distinct layers of phytoplankton biomass (Fig. 2a). Simultaneous observations of the absorption spectra and fluorescence emission spectra indicate that the layers marked B and D in Figure 2a had different optical characteristics (the amplitudes of the signals were scaled to show spectral differences; see figure legend for details). Layer B (at 16.7 m) exhibited relatively more absorption in the violet and blue and less in the green to orange region of the spectrum than layer D (Fig. 2b), which in turn showed relatively more fluorescence emission at 450–550 nm when excited by 228-nm light (Fig. 2c). This suggests a different community composition or photoadaptive state even within close spatial proximity, providing indirect evidence that these layers have

persisted long enough for their different optical characteristics to have developed independently.

These data, and those of other investigators working with small-scale structure, indicate that the in situ observational tools are now available to fingerprint adjacent small-scale features and evaluate their differences based on physical/optical characteristics. New water sampling approaches are also being applied to assist in these comparisons and will permit rate process experiments to be conducted.

How Might Small-Scale Planktonic Features Persist?

The relative importance of small-scale planktonic layers to trophic processes will depend on the number of persistent layers and how long they persist. Both are dependent on physical and biological processes. The formation of layers, for example, could result from physical processes, such as 1) water column stratification due to solar warming, horizontal intrusions, etc., that create density gradients that might collect sinking particles (e.g., Lande and Wood, 1987; MacIntyre *et al.*, 1995), 2) locally “quiet” vertical intervals that have lower than average turbulent mixing such that local phytoplankton accumulations are not dispersed, 3) interac-

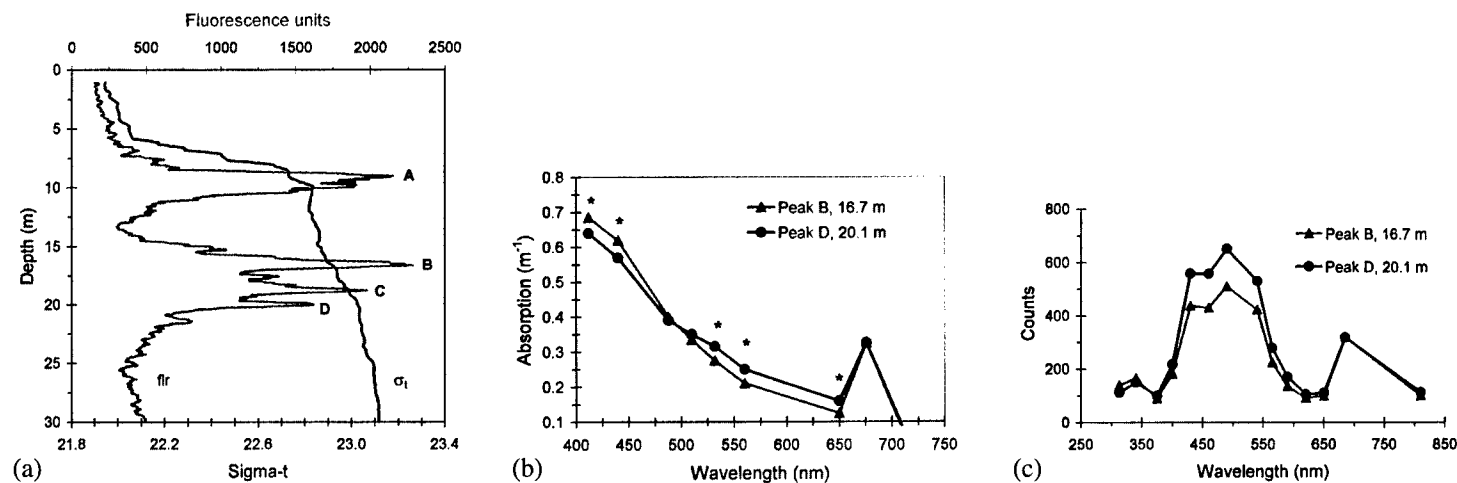


Fig. 2: (a) Characteristic profile of phytoplankton pigment fluorescence and sigma-t during a series of profiles in East Sound, WA, in the summer of 1995. Chlorophyll concentration at 10 m depth was $\sim 5 \mu\text{g l}^{-1}$. (b) Absorption spectra from peaks B and D in a, where spectra have been corrected for temperature and scattering. Each point is the mean of 10 measurements obtained within its layer from successive profiles with an ac-9. To illustrate the relative shapes of the absorption spectra, the absorption values for layer D were scaled by multiplying them by a factor of $a_{676}(B)/a_{676}(D)$. Those points at a given wavelength marked with an asterisk are significantly different at the 95% confidence level. (c) Fluorescence emission spectra from 228-nm excitation for peaks B and D. Emission values for layer D were scaled by multiplying them by a factor of $\text{emission}_{685}(B)/\text{emission}_{685}(D)$. The deeper layer at 20 m has significantly more relative emission between 450 and 550 nm than does the layer near 17 m, indicating either a relatively higher concentration of fluorescent dissolved organic material, or a relatively lower amount of absorption at the excitation wavelength by non-fluorescent moieties.

tion of vertical gradients in horizontal velocity (shear) with local stratification that could result in the horizontal dispersion (stretching) of biological distributions, like those observed by Kullenberg (1974) by injection of dye into stratified waters, and 4) interaction of internal waves and horizontal biomass gradients as proposed by Franks (1995) in his model of thin layer formation.

Layer persistence or erasure will be dependent on the interaction between the physical processes of upper ocean mixing and the biological processes of phytoplankton growth and zooplankton grazing. The intermittent occurrence and variable intensity of mixing events (e.g., Moum *et al.*, 1989) will determine the time scales of layer persistence.

The mixing environment can be characterized, in part, by the interplay of the destabilizing effect of velocity shear and the stabilizing influence of the density gradient. These two parameters provide a framework to understand whether conditions are favorable for layer persistence or not. The transition from stability to mixing is usually identified by low values (<0.25) of the Richardson number, R_i (where $R_i = N^2/s^2$, given by the ratio of the square of the Brunt-Väisälä frequency, N^2 , and the squared shear, s^2). Persistent local minima in shear and local maxima in the density gradient (represented by N^2) create regions of stability that allow thin layers to persist. Conversely, local increases in shear and/or local decreases in the density gradient can erase existing small-scale structure through shear instabilities. It is noteworthy that the most striking examples of persistent thin layers are observed in highly stratified environments (Donaghay *et al.*, 1992).

But biological factors, namely phytoplankton growth and zooplankton grazing, also will contribute to the persistence/erasure of thin layers. The balance between growth and mixing is crucial for layer persistence. Under conditions of relatively little mixing, phytoplankton growth could account for the maintenance of a thin layer of phytoplankton biomass.

Any combination of competing physical and biological processes may be present under the range of conditions experienced within the euphotic zone. The papers in this issue provide support for the view that we cannot adequately understand the role of persistent small-scale

biological/physical structure in trophic dynamics until we have a clearer picture of the contribution of thin layers to overall rate processes, and a more quantitative description of the physical and biological phase space in which we find these features.

Trophic Consequences of Persistent Small-Scale Structure

As mentioned earlier, the relative importance of persistent structure to trophic dynamics depends on the interaction of physical mixing processes, phytoplankton growth, and zooplankton grazing/growth. Now that the tools are available to characterize and evaluate locally enhanced thin layers of nutrients, phytoplankton, and microzooplankton, we need to compare these high-resolution observations with estimates of distributions and process rates obtained with conventional sampling devices.

Conventional sampling for microzooplankton grazers occurs on vertical scales of 5–10 m and typically employs 10-l Niskin bottles on a CTD/rosette system to collect discrete water samples for enumeration of microzooplankton. Each bottle spans >0.5 m, and the CTD/rosette system moves vertically during sampling due to ship motion. Therefore enumeration of a sample from this conventional sampling approach yields an estimated population size that is the average of the local minima and maxima of microzooplankton abundance over a ~ 2 -m interval. *In situ* biomass estimates of larger zooplankton (mesozooplankton $> 200 \mu\text{m}$) are usually made over vertical intervals of at least 10–25 m. The microzooplankton and mesozooplankton biomass profiles that result from this sampling approach, in conjunction with estimates of the vertical distribution of phytoplankton biomass, usually form the basis for estimates of water column grazing and secondary production (e.g., Dam *et al.*, 1993).

In contrast to coarse-scale conventional sampling, fine-scale sampling by Bjørnsen and Nielsen (1991) indicated that microzooplankton grazers can be much more aggregated (within 20–50-cm intervals) than could be discerned by conventional sampling. Laboratory experiments have shown that grazers can detect and stay within layers of food (e.g., Tesilius, 1992) and can discriminate between food items on the basis of chemical signals (Cowles *et al.*, 1988). If mi-

crograzers aggregate at this scale on their food supply in the field, and their food supply is distributed in narrow, persistent features, then the local grazing and growth rates of those grazers will be quite different than that estimated from coarser-scale sampling.

We have used these contrasting assessments of phytoplankton and microzooplankton biomass to compare estimates of the loss of phytoplankton to grazing within the euphotic zone, and to compare the individual and population growth rates for microzooplankton distributions defined by these different biomass profiles. We present here some simple calculations of grazer growth rates that help to illustrate the trophic consequences of persistent layers.

Microzooplankton grazing and growth can be modeled by a functional specific growth response for a generic ciliate (Fig. 3). This idealized growth rate function yields a doubling time of ~ 22 h at saturating food conditions [$e^r = 2$, when the growth rate (r) approaches 0.032]. We have used this response to estimate the specific growth rate for micrograzers as a function of food concentration. For example, if an assemblage of micrograzers spends 12 h d^{-1} in $75 \mu\text{g C l}^{-1}$ ($\sim 1 \mu\text{g}$ chlorophyll a l^{-1}) and 12 h d^{-1} at $15 \mu\text{g C l}^{-1}$, its daily growth will be >1.8 times larger than if it spends 24 h d^{-1} at $15 \mu\text{g C l}^{-1}$. (This estimate assumes grazing over

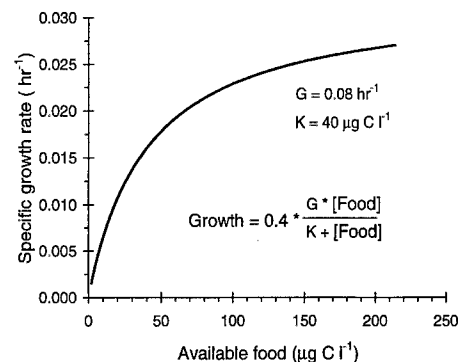


Fig. 3: Theoretical growth response of a small planktonic grazer, such as a ciliate, as a function of food availability. K [$\mu\text{g C l}^{-1}$] represents the food concentration at half saturation rate; G [h^{-1}] is the ingestion rate normalized to grazer body weight; and 0.4 represents a (typical) 40% growth efficiency (Caron and Goldman, 1990). A food concentration of $75 \mu\text{g C l}^{-1}$ roughly corresponds to $1 \mu\text{g}$ chlorophyll a l^{-1} .

a 24-h interval, but the concept is valid for grazers that have a diel feeding cycle). This represents a substantial enhancement of growth rate for grazers that spend time within persistent layers that have locally higher food concentrations.

The consequences of estimating grazer growth rates based on coarse- versus fine-scale sampling can be examined by considering the following one-dimensional model. Consider a 10-m portion of the water column that has two 0.5-m-thick layers with a phytoplankton concentration of $75 \mu\text{g C l}^{-1}$; the background concentration is $15 \mu\text{g C l}^{-1}$. If the thin layers of phytoplankton in this water column are not sampled (as might occur with conventional coarse-scale sampling), then the background food concentration would be used to estimate a specific growth rate of 0.009 h^{-1} for the grazers present (Fig. 3). If coarse-scale sampling results in water collection only at the thin layers, then the average food concentration for this 10-m interval will be overestimated. A 10-l Niskin bottle sample could intersect a 50-cm layer plus $\sim 75 \text{ cm}$ on either side of the layer, resulting in a mean phytoplankton concentration of $\sim 30 \mu\text{g C l}^{-1}$. This food concentration would yield an estimated specific growth rate of 0.014 h^{-1} . In these cases of undersampled food distributions, the estimated specific growth rates of individual grazers are independent of their vertical position due to the assumption that the food distribution is uniform.

A wider range of specific growth rates for grazers would result if the vertical distribution of thin layers of phytoplankton is resolved with fine-scale sampling; the magnitude of the mean growth rate of the grazer population then will depend on the grazer distribution. For the case in which the grazer vertical distribution is uniform, the estimated mean specific growth rate would be 0.010 h^{-1} . However, if the grazer distribution is identical to the food distribution, then the mean growth rate would be 0.013 h^{-1} , 30% more than that in the uniform grazer distribution case, and 50% more than if the thin layers of food were not sampled. And, if all of the grazers were able to congregate on the thin layers, then the specific growth rate of the population would be 0.021 h^{-1} , 110% more than the mean specific growth rate for the uniform grazer distribution case.

It is expected that the consequences of grazer aggregation on layers of enhanced food will be more important for cases in

which the background food concentration is relatively low; the functional dependence of grazer growth on food availability (Fig. 3) shows that at higher food concentrations the growth rate saturates, diminishing the growth bonus realized by aggregating grazers.

The calculations presented above indicate that the trophic impact of persistent small-scale phytoplankton structure is dependent, to a large extent, on the active and/or passive accumulation of individual grazers onto local food maxima. The degree to which grazers accumulate will determine whether persistent food layers lead to much higher population growth rates than would occur in the absence of thin layers. As shown in the paper by Holliday *et al.* (1998), new acoustic methods are now able to provide resolution of zooplankton distribution over the relevant vertical scales and will provide essential evidence for the trophic linkages between phytoplankton and zooplankton small-scale structure.

Summary

Small-scale physical, biological, and chemical processes are the dominant, and most immediately relevant, processes for planktonic organisms. The existence of persistent thin layers suggests that patchiness in vertical structure is more than ephemeral random structure, and may represent undersampled, persistent, sub-1-m scale structure. Observations of persistent fluorescence microstructure suggest that the trophic dynamics and biological rate processes of the upper water column are constrained by both fine-scale and microscale physical processes, such that local maxima in biological rate processes occur within thin layers or sheets. It is likely that conventional sampling may result in aliased resolution of these features, as well as aliased estimates of the associated rate processes, and may lead to erroneous estimates of oceanic carbon flux. The frequent occurrence of thin layers and the temporal/spatial coherence of these layers suggest that we should evaluate their contribution to upper ocean biological processes, and determine the correlation between these small-scale structures and physical processes.

Acknowledgements

The work described in this article has been supported by the Office of Naval Research and the National Science

Foundation. We are indebted to Dr. James Moum for his collaboration in the integration of a fiber-optic fluorescence sensor on his microstructure profiling system.

References

- Bainbridge, R., 1952: Underwater observations on the swimming of marine zooplankton. *J. Mar. Biol. Assoc. UK*, 31, 107–112.
- Bjornsen, P.K. and T.G. Nielsen, 1991: Decimeter scale heterogeneity in the plankton during pycnocline bloom of *Gyrodinium aureolum*. *Mar. Ecol. Prog. Ser.*, 73, 263–267.
- Caron, D.A. and J.C. Goldman, 1990: Protozoan nutrient regeneration. In: *Ecology of Marine Protozoa*. G.M. Capriulo, ed. Oxford Univ. Press, New York, 283–306.
- Cassie, R.M., 1963: Microdistribution of plankton. *Oceanogr. Mar. Biol. Ann. Rev.*, 1, 223–252.
- Cowles, T.J. and R.A. Desiderio, 1993: Resolution of biological microstructure through *in situ* fluorescence emission spectra. *Oceanography*, 6, 105–111.
- , R.A. Desiderio, J.N. Moum, M.L. Myrick, D. Garvis and S.M. Angel, 1990: Fluorescence microstructure using a laser/fiber optic profiler. *Ocean Optics X, Proc. SPIE*, 1302, 336–345.
- , R.A. Desiderio and S. Neuer, 1993: *In situ* characterization of phytoplankton assemblages using fluorescence emission spectra. *Mar. Biol.*, 115, 217–222.
- , R.J. Olson and S.W. Chisholm, 1988: Food selection by copepods: discrimination on the basis of food quality. *Mar. Biol.*, 100, 41–49.
- Dagg, M., 1977: Some effects of patchy food environments on copepods. *Limnol. Oceanogr.*, 22, 99–107.
- Dam, H.G., C.A. Miller and S.H. Janasdotir, 1993: The trophic role of mesozooplankton at 47°N , 20°W during the North Atlantic Bloom Experiment. *Deep-Sea Res. II*, 40, 197–212.
- Denman, K.L. and A.E. Gargett, 1983: Time and space scales of vertical mixing and advection of phytoplankton in the upper ocean. *Limnol. Oceanogr.*, 28, 801–815.
- and A.E. Gargett, 1988: Multiple thermoclines are barriers to vertical exchange in the subarctic Pacific during SUPER, May 1984. *J. Mar. Res.*, 46, 77–103.
- and T.M. Powell, 1984: Effects of physical processes on planktonic ecosystems in the coastal ocean. *Oceanogr. Mar. Biol. Ann. Rev.*, 22, 125–168.
- Desiderio, R.A., T.J. Cowles, J.N. Moum and M.L. Myrick, 1993: Microstructure profiles of laser induced chlorophyll fluorescence spectra: evaluation of backscatter and forward scatter fiber optic sensors. *J. Atmos. Ocean. Tech.*, 10, 209–224.
- Donaghay, P.L., H.M. Rines and J.M. Sieburth, 1992: Simultaneous sampling of fine scale biological, chemical, and physical structure in stratified waters. *Archiv. Hydrobiol. Beih.*, 36, 97–108.
- Fasham, M.J.R., 1978: The statistical and mathematical analysis of plankton patchiness. *Oceanogr. Mar. Biol. Ann. Rev.*, 16, 43–79.
- Franks, P.J.S., 1995: Thin layers of phytoplankton:

- a model of formation by near-inertial wave shear. *Deep-Sea Res.*, 42, 75–91.
- Goldman, J.C., 1988: Spatial and temporal discontinuities of biological processes in pelagic surface waters. In: *Toward a Theory of Biological and Physical Interactions in the World Ocean*. B. Rothschild, ed. Kluwer, 273–296.
- Hanson, Jr., A.K. and P.L. Donaghay, 1998: Micro to fine-scale chemical gradients and layers in vertically stratified coastal waters. *Oceanography*, 11, 10–17.
- Holliday, D.V., R.E. Pieper, C.F. Greenlaw and J.K. Dawson, 1998: Acoustical sensing of small scale vertical structure in zooplankton assemblages. *Oceanography*, 11, 18–23.
- Kullenberg, G., 1974: Investigation of small-scale vertical mixing in relation to the temperature structure in stably stratified waters. *Adv. Geophys.*, 18A, 339–351.
- Lande, R. and M. Wood, 1987: Suspension times of particles in the upper ocean. *Deep Sea Res.*, 34, 61–72.
- Lasker, R., 1975: Field criteria for survival of anchovy larvae: the relation between inshore chlorophyll maximum layers and successful first feeding. *Fish. Bull.*, 73, 453–462.
- MacIntyre, S., A.L. Alldredge and C.C. Gotschalk, 1995: Accumulation of marine snow at density discontinuities in the water column. *Limnol. Oceanogr.*, 40, 449–468.
- Mackas, D.L., K.L. Denman and M.R. Abbott, 1985: Plankton patchiness: biology in the physical vernacular. *Bull. Mar. Sci.*, 37, 652–674.
- Marra, J., 1978: Effect of short-term variations in light intensity on photosynthesis of a marine phytoplankton: a laboratory simulation study. *Mar. Biol.*, 46, 191–202.
- Mitchell, J.G. and J.A. Fuhrman, 1989: Centimeter scale vertical heterogeneity in bacteria and chlorophyll a. *Mar. Ecol. Prog. Ser.*, 54, 141–148.
- Moum, J.N., D.R. Caldwell and C.A. Paulson, 1989: Mixing in the equatorial surface layer. *J. Geophys. Res.*, 94, 2005–2021.
- Mullin, M.M. and E.R. Brooks, 1976: Some consequences of distributional heterogeneity of phytoplankton and zooplankton. *Limnol. Oceanogr.*, 21, 784–796.
- Oldham, C. and J. Imberger, 1992: Effects of hydrodynamics of oxygen transport paths in a lake. Amer. Soc. Limnol. Oceanogr. 1992 Meeting, Sante Fe, New Mexico, February 1992.
- Owen, R.W., 1989: Microscale and finescale variations of small plankton in coastal and pelagic environments. *J. Mar. Res.*, 47, 197–240.
- Rothschild, B.J. and T.R. Osborn, 1988: Small-scale turbulence and plankton contact rates. *J. Plankton Res.*, 10, 465–474.
- Tiselius, P., 1992: Behavior of *Acartia tonsa* in patchy food environments. *Limnol. Oceanogr.*, 37, 1640–1651.
- Weller, R.A. and J.F. Price, 1988: Langmuir circulation within the oceanic mixed layer. *Deep-Sea Res.*, 35, 711–747. □

MICRO- TO FINE-SCALE CHEMICAL GRADIENTS AND LAYERS IN STRATIFIED COASTAL WATERS

By Alfred K. Hanson, Jr. and Percy L. Donaghay

MODELS OF BIOGEOCHEMICAL dynamics and chemical variability in coastal waters have traditionally relied on the assumption that small-scale mixing processes are sufficiently strong and isotropic to rapidly disperse centimeter to meter scale chemical gradients and thin layered vertical structure. Although this assumption of homogeneity may be reasonable in tidally well-mixed estuaries, or within the well-mixed surface and bottom layers of some stratified systems, it may not be generally applicable to stratified coastal waters (Donaghay *et al.*, 1992). A number of naturally occurring physical, biological, and chemical processes have the potential to influence the development, maintenance, and dissipation of micro- (cm to m) to fine-scale (1 to 10 m) chemical structure in stratified coastal waters. Since micro- and fine-scale structure in temperature, salinity, and density distributions result from small-scale physical mixing processes (Osborn, 1998), it is plausible that the vertical distributions of dissolved chemicals should have similarly scaled variability. Biogeochemical activity focused within thin plankton layers (Donaghay *et al.*, 1992; Cowles and Desiderio, 1993; Cowles *et al.*, 1998) should also cause and be influenced by similarly scaled gradients in chemical concentration and reactivity. This has clearly been demonstrated for methane (Sieburth and Donaghay, 1993), mercury (Mason *et al.*, 1993), and iron (O'Sullivan *et al.*, 1997) in the oxic-anoxic transition zone of the lower basin of the Pettaquamscutt Estuary. However, field observations of micro- to fine-scale chemical variability associated with physical micro- and fine-structure

and/or thin plankton layers have been limited in more open systems both by the difficulties in sampling at these scales and by the assumption that such structures cannot persist.

Sensitive *in situ* chemical profiling techniques, with the same spatial and temporal resolution as *in situ* physical and bio-optical profiling techniques, are required to evaluate the influence of small-scale physical mixing and biological processes on chemical distributions, reaction rates and transport. We have developed an electronic profiling and sampling system (Fig. 1a) with the capability for simultaneously sampling at centimeter scales the physical, biological, chemical, and bio-optical structure of the water column. The *in situ* analytical chemical capabilities of the profiling system include electrochemical sensors for dissolved oxygen and pH and a sensitive profiling chemical analyzer (PCA; Fig. 1b) that can measure dissolved nitrite and iron(II) down to nanomolar concentration levels. Herein we will first consider the rationale for expecting micro- to fine-scale structure in nitrite and iron(II), briefly describe our technical approach, and then use high-resolution profiles collected in East Sound, WA, to illustrate the importance of such measurements to understanding chemical dynamics and impacts in stratified coastal systems.

Rationale for Nitrite and Iron(II) Fine-Structure

High-resolution measurements of dissolved nitrite and iron(II) were selected for this investigation because it was thought that their biological and chemical reactivity would lead to fine-scale chemical structure in stratified coastal waters. Nitrite and iron(II) were also chosen because their spectrophotometric determination required a limited number of reagents and had rapid

color development rates, simplifying adaptation for *in situ* vertical profiling.

Nitrite, a dynamic intermediate in the marine nitrogen cycle, is generally a trace constituent (<50 nM) in euphotic surface waters because it is both assimilated by phytoplankton and photochemically reactive (Zafiriou and True, 1979; Grasshoff and Koroleff, 1983). The accumulation of nitrite (>100–2,000 nM) in mid-depth and deeper coastal waters is thought to be controlled by the microbiological processes of nitrification (i.e., ammonia and nitrite oxidation) and denitrification (i.e., nitrate reduction), occurring within the water column and in surficial sediments (Seitzinger *et al.*, 1980; Lipschultz *et al.*, 1986).

Iron plays an essential role as a micronutrient in phytoplankton photosynthesis (Geider and La Roche, 1994). There is evidence that iron limitation may selectively influence the growth of some species of phytoplankton in coastal waters (Brand, 1991; Sunda and Huntsman, 1995). However, the complexities of the marine chemistry of iron have hindered the elucidation of its micronutrient role (Donaghay *et al.*, 1991; Wells *et al.*, 1995). Most of the iron in oxygenated coastal marine waters is present as insoluble hydrous iron(III) oxide colloids and larger particles, forms of iron that are not readily bioavailable. Dissolved iron(III) is usually present in trace (nanomolar) amounts. Dissolved iron(II) is a more soluble form of iron that is produced by microbial or chemical reduction within oxygen-depleted waters and in sub-oxic sedimentary porewaters, or by photochemical reduction within the euphotic zone (O'Sullivan *et al.*, 1991, 1997). The rate of iron(II) oxidation back to the less soluble iron(III) form is dependent on the oxidation rate constant and reactant concentrations (Millero *et al.*, 1987). The redox cycling of iron between less avail-

Alfred K. Hanson, Jr., and Percy L. Donaghay, Graduate School of Oceanography, University of Rhode Island, Narragansett, RI 02882, USA.

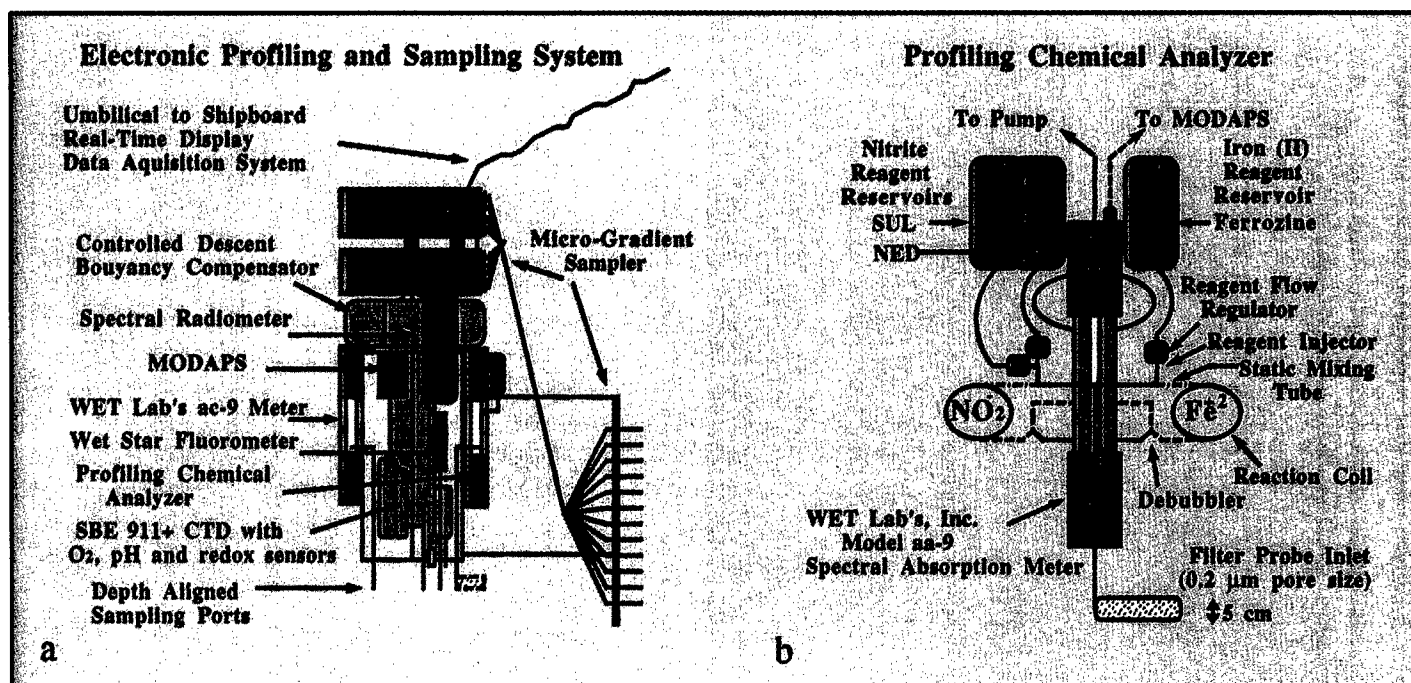


Fig. 1: Components of (a) the High-Resolution Electronic Profiling and Sampling System and (b) the Profiling Chemical Analyzer configured for dissolved nitrite and iron(II) measurements.

able forms of iron(III) and the more soluble forms of iron(II) results in elevated transient concentrations of reactive forms of iron(II) and iron(III) and can enhance the availability of iron for uptake by phytoplankton (Wells *et al.*, 1995).

The location and intensity of the expected fine-structure should vary between nitrite and iron(II) because of differences in their transient nature (i.e., oxidation or consumption half-lives), sources and sinks, and sensitivities to other factors that vary on fine-scales. For example, the relatively slow rates of microbial production and loss of nitrite (Vaccaro, 1965) should lead to weak gradients except in areas where nitrogen assimilation by intense layers of phytoplankton rapidly generate nutriclines. In contrast, the relatively rapid rates and chemical control of iron(II) oxidation by ambient pH and oxygen levels, temperature, and salinity, should lead to vertical iron(II) structure being highly sensitive to recent input events and to the fine structure in these physicochemical factors. Testing these hypotheses presented a major analytical challenge because it required measuring the concentrations of nitrite and iron(II) *in situ*, at centimeter scales over the 3–4 orders of magnitude range of concentrations (nM to μ M) expected in coastal waters. In addition, it required simultaneously measuring chlorophyll, temperature, salinity, oxygen, and pH at the same scales in order to evaluate the influence of these pa-

rameters on the chemical structure, reaction rates, and fluxes.

The PCA

The PCA is comprised of a continuous-flow, reagent-injection module connected to a dual-channel, nine wavelength, submersible spectral absorption meter (Fig. 1b). A WET Lab's model aa-9 spectral absorption and attenuation meter (Moore *et al.*, 1992) was customized to contain twin absorption channels (denoted as model aa-9). The dual-channel reagent addition module was sized (i.e., pump, tubing sizes, flowrates, etc.) to match the geometry of the optical flow cells (25-cm pathlength, 1.2 cm ID, ~25-ml void volume) of the aa-9. Seawater and reagents were drawn continuously through each channel of the PCA at 250 ml/min per channel by a gear pump located downstream. A 0.22- μ m pore size in-line filter with high-filtration surface area (Gelman maxicapsule) was fixed horizontally at the seawater inlet to the system. Reagents stored in 1.5-l plastic bags were continuously injected at constant flowrates (3–5 ml/min) into the flowing seawater. The flow rates were controlled hydrodynamically by means of adjustable restricting orifices (Dial-A-Flo, Abbott Laboratories). After flow injection, the reagents and seawater were homogeneously mixed by passage through in-line static mixing tubes. After mixing, the reagents and analytes continued to react

for 30 s during passage through the reaction coils before passing into the WET Labs aa-9 flowcells for detection.

Dissolved nitrite (NO_2^-) and iron(II) (Fe^{2+}) were determined *in situ* spectrophotometrically using classical color-forming reagents: *N*-1 naphthylethylene-diamine and sulphanilamide for nitrite (Grasshoff and Koroleff, 1983) and Ferrozine reagent for iron(II) (Stookey, 1970). Differential absorption (units = m^{-1}) measurements were utilized to determine nitrite and iron(II) using 540 and 560 nm as the respective analytical wavelengths and 650 nm as the reference wavelength. The improved optics, stable electronics, and longer pathlength of the WET Labs' model aa-9 resulted in the PCA being 10–100 times more sensitive than conventional laboratory autoanalyzers and spectrophotometers. The limits of detection for nitrite and iron(II) were 0.5 and 0.3 nM, respectively (estimated from 4 times the standard deviation of replicate blank readings). The fast data acquisition rate (5.8 Hz) of the WET Lab's aa-9 allowed >5,000 concentration readings to be acquired during a 15-min cast to 25-m depth (2 readings/cm). The PCA had the sensitivity and resolution to detect chemical gradients, at nanomolar to micromolar concentration levels, that occurred within a depth range of 10–20 cm with an instrument package drop-rate of 1–2 m/min.

The PCA was deployed as a component of a high-resolution electronic

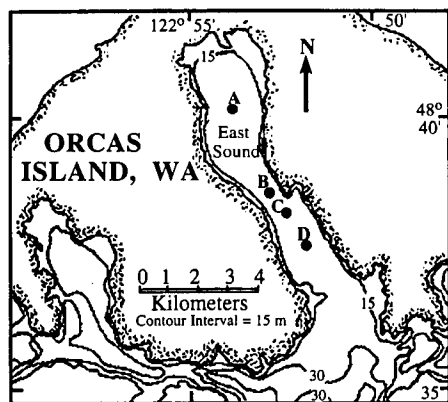


Fig. 2: Station locations and bathymetry of the coastal fjord study site, East Sound, WA.

profiling system (Fig. 1a) that included 1) a Sea-Bird Electronics, Inc., 911

plus CTD with fast response thermister, ducted flow cell, centimeter-scale resolving Digiquartz pressure sensor, and electrodes for pH, redox potential, and dissolved oxygen; 2) a WET Labs, Inc., WETStar miniature chlorophyll fluorometer; 3) a Biospherical Instruments model PUV500 spectral UV and PAR radiometer; 4) a WET Labs model ac-9 spectral absorption and attenuation meter; and 5) pump-to-surface and microgradient sampling systems. A WET Labs, Inc., Modular Ocean Data Acquisition and Power System (MODAPS) was used to acquire and time stamp data from the *in situ* instruments, then transmit the data to the surface, where they were archived in a common file and displayed in real time.

Evidence for Fine-Scale Chemical Structure in East Sound

East Sound is a shallow fjord-like basin penetrating Orcas Island, located within the San Juan Archipelago of western Washington. The basin (Fig. 2) is ~13 km long and 1–2 km wide and has a fairly uniform depth of ~30 m. A partial sill rises 10–15 m above surrounding bottom depths and extends about halfway across the southern entrance to East Sound. The physical dynamics of the primarily wind-driven circulation of East Sound are complex (Rattray, 1967). The stratified waters of East Sound, like many other seasonally stratified coastal environments, can have its vertical structure strongly modified by episodic wind events that can cause upwelling, downwelling, lateral advection, and/or

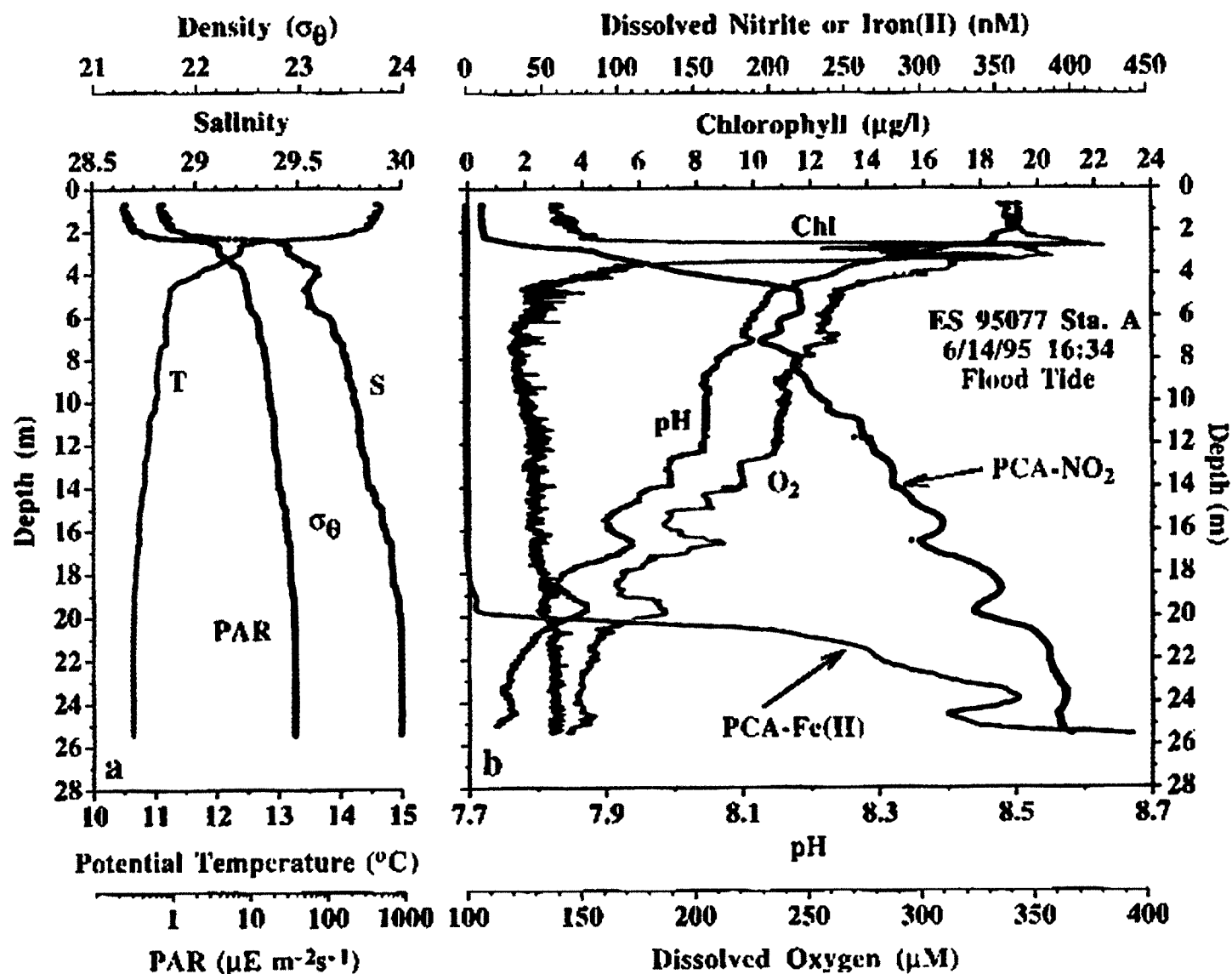


Fig. 3: Micro- to fine-scale chemical gradients associated with similarly scaled physical structures and thin chlorophyll fluorescence layers during flood tide at station A.

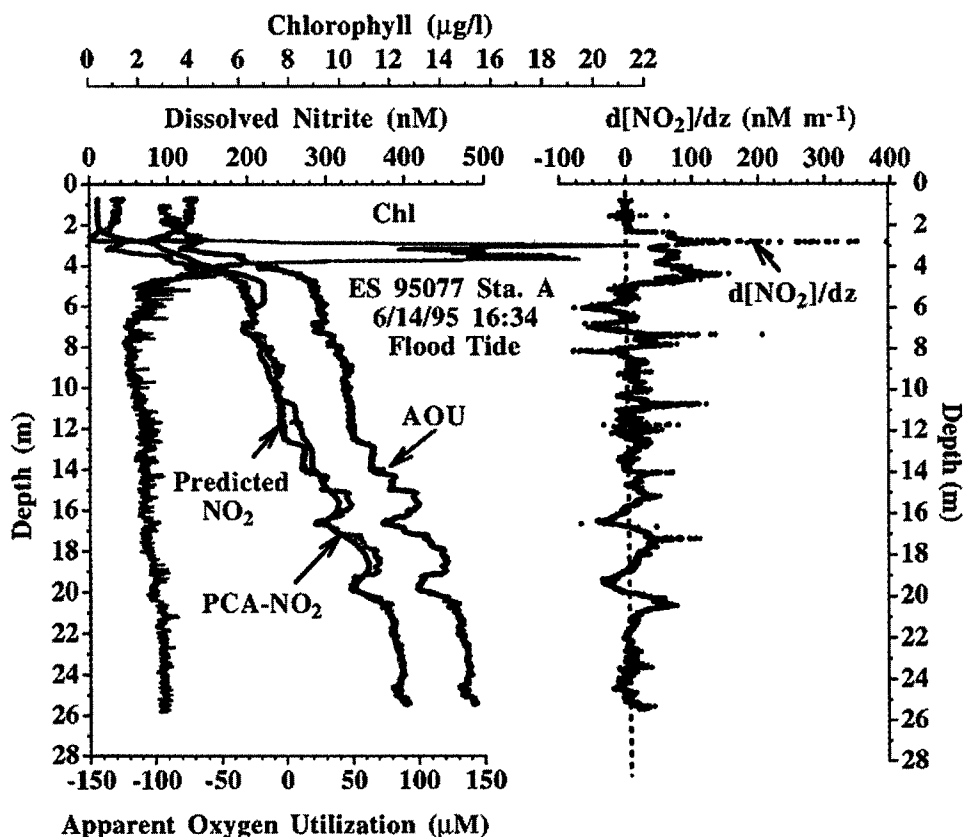


Fig. 4: Positioning of the thin chlorophyll fluorescence layer within the steep nitricline and the agreement between the fine-scale vertical distributions of AOU, nitrite, and model-predicted nitrite for the flood tide cast shown in Fig. 3.

mixed layer deepening. We have observed that such intermittent wind events can result in altered nutrient availability and lead to intense phytoplankton blooms. These blooms may be dispersed throughout the surface mixed layer and/or focused into thin layers within the pycnocline.

Vertical profiles, acquired at station A during flood tide in the late afternoon revealed considerable micro- to fine-scale structure and regions of strong gradients for temperature, salinity, density, chlorophyll a, dissolved oxygen, nitrite, iron(II), and pH (Fig. 3). The physical structure of the water column was typified by a 2-m-thick weakly stratified surface layer, a sharp pycnocline extending from ~2 to 4 m, a more gradual increase in density (with fine-scale step-structure) through the mid-depth waters, and a well-mixed bottom layer (density gradients of <0.001 $\text{sigma}_\theta \text{ m}^{-1}$). The vertical phytoplankton structure was dominated by an intense thin chlorophyll a layer positioned within the pycnocline near 3 m depth. This thin plankton layer had a maximum thickness of ~1 m and was comprised of several peaks of 10–40-cm thickness. The estimated chlorophyll con-

tents ranged from background levels of $3 \mu\text{g l}^{-1}$ to peak values $>20 \mu\text{g l}^{-1}$.

Dissolved Oxygen, pH, and Nitrite Gradients

Oxygen and pH levels were higher, and nitrite levels were lower in surface than in deeper waters (Fig. 3). Near surface levels of oxygen and pH were $340 \mu\text{M}$ and 8.51, respectively. Subsurface microscale maxima in dissolved oxygen (>340 – $381 \mu\text{M}$) were located at the same depths as maxima in chlorophyll a. The supersaturated oxygen and elevated pH values at the depth of the thin chlorophyll a layer indicate that the layer was a region of intense photosynthetic activity. Oxygen and pH levels decreased sharply below the thin plankton layer ($265 \mu\text{M O}_2$, pH 8.15 at 5 m depth), and then continued to decrease gradually toward near bottom values ($146 \mu\text{M O}_2$, pH 7.74). The nitrite profile was characterized by low surface concentrations ($\sim 10 \text{ nM}$ nitrite), a steep gradient to higher levels just below the pycnocline (220 nM NO_2^- at 5 m) and a more gradual increase to 400 nM NO_2^- near the bottom. The variations in the dissolved oxygen, pH, and nitrite profiles were highly corre-

lated (linear correlation coefficients for profiles in Fig. 3b: O_2 -pH: $r^2 = 0.974$, O_2 - NO_2^- : $r^2 = 0.960$ and pH- NO_2^- : $r^2 = 0.976$). This high degree of correspondence is attributed to the chemical stoichiometry of the photosynthetic production and organic matter remineralization reactions.

In an effort to quantify the nitrite gradient and its relationship to the thin chlorophyll a layer, we used the centimeter-scale nitrite data to calculate the nitrite concentration gradient as $d[\text{NO}_2^-]/dz$. As indicated in Fig. 4, the nitrite gradient was extremely steep ($d[\text{NO}_2^-]/dz = >300 \text{ nM NO}_2^- \text{ m}^{-1}$) at the same depth as the thin chlorophyll a layer. This supports the hypothesis that phytoplankton uptake was controlling the position and intensity of the nitrite gradient. It is also consistent with the hypothesis that the vertical position and intensity of the thin phytoplankton layer was being controlled by the position and steepness of the nutricline. Although macronutrient determinations of water samples collected from discrete depths indicated that nitrate and ammonia were extremely low in the surface waters and increased rapidly in the region of the chlorophyll a layer, these discrete samples did not have the spatial resolution needed to accurately estimate the steepness and location of peak gradients. Rigorous testing of the hypothesis would require measuring these other potentially limiting macronutrients on the same centimeter scales as the nitrite.

Distinct submeter-scaled chemical gradients were also observed for nitrite, dissolved oxygen, and pH within the mid-depth and deeper waters for this flood tide cast. Two examples are the oxygen and pH maxima and corresponding nitrite minima present near 16.5 and 20 m depth (Fig. 3b). It is unlikely that these structures are the result of locally enhanced primary production because 1) they are not associated with peaks in chlorophyll a, 2) the light levels are low (1 – $10 \mu\text{E m}^{-2} \text{ s}^{-1}$), and 3) micromolar concentration levels of nitrate (7 – $15 \mu\text{M}$) and ammonia (4 – $6 \mu\text{M}$) were found at these depths. It is possible that fine-scale maxima and minima were produced within the water column by locally elevated rates of microbial remineralization of dissolved and particulate organic matter. An alternative explanation is that the corresponding midwater oxygen and pH minima, and nitrite maxima are chemical signals that originated near the sediment-water interface (via microbial remineralization) and were horizontally transported by physical processes (i.e., isopycnal transport) to these depths at sta-

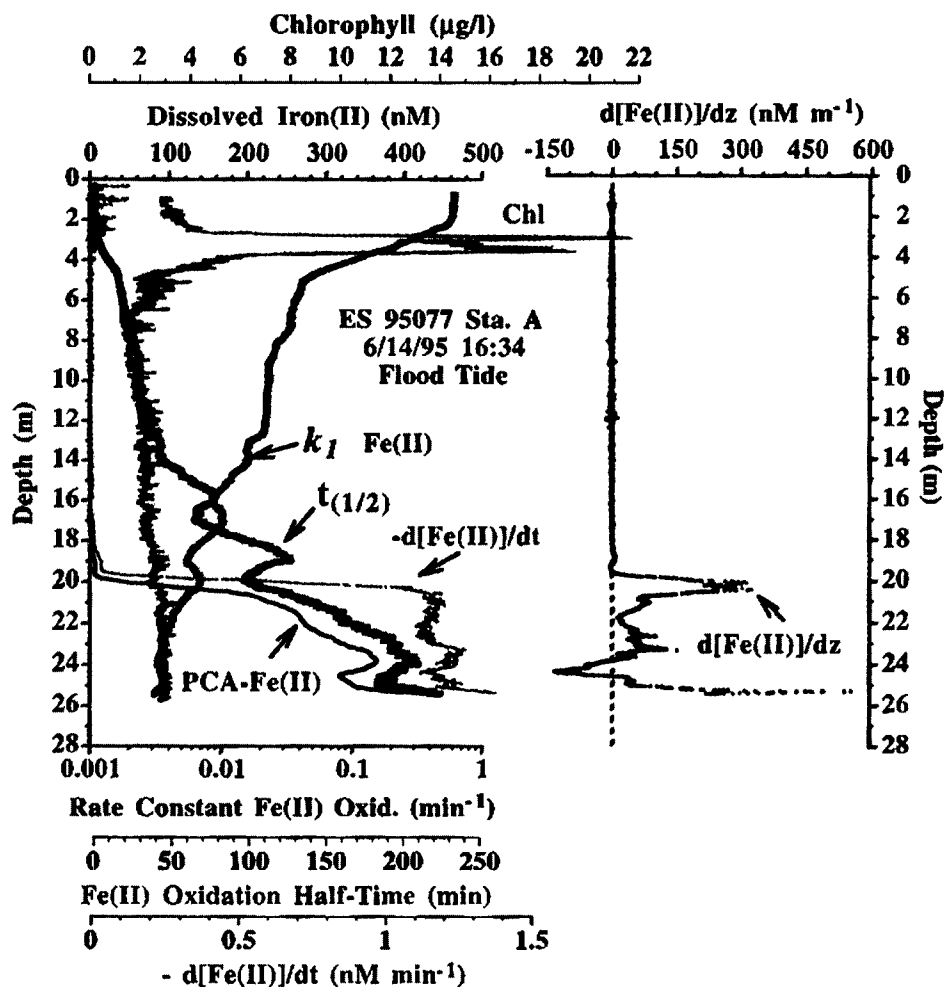


Fig. 5: Agreement between the steep iron(II) gradients detected in the bottom waters and model predictions of the vertical variability in the pseudo-first-order rate constants and half-lives for iron(II) oxidation, and the iron(II) oxidation rate for the flood tide cast shown in Fig. 3.

tion A. Although not readily discernible at the density scale shown in Fig. 3a, these mid-depth waters had characteristic density step-structures, thin (cm-scale) "sheets," with stronger gradients, separated by thicker (m-scale) "layers" with weaker or negligible gradients (Osborn and Cox, 1972; Gregg, 1975). The observed chemical fine-structure appears to be systematically related to these microscale and fine-scale physical discontinuities that Osborn (1998) attributes to localized vertical mixing and lateral intrusions, respectively. These observations are also consistent with the results of dye studies conducted in the Baltic Sea (Kullenberg, 1974, 1983). A slow rate of vertical mixing, relative to the rate of horizontal transport, may allow the chemical fine-structure to propagate along isopycnals and persist in the stratified waters.

Prediction of nitrite fine structure. If either of the remineralization explanations discussed above are correct, then the clas-

sic "Redfield model" predicts a very strong correlation in subsurface waters between nitrite concentrations and apparent oxygen utilization (AOU = theoretical O_2 solubility - observed O_2 concentration) (Redfield, 1942). This correspondence is very evident when one compares vertical profiles of AOU and PCA-nitrite (Fig. 4). To make sure that these relationships were not the result of some peculiarity of a particular cast, we collected water samples from discrete depths on two casts (10-h separation), determined nitrite concentration levels in the laboratory using standard autoanalysis methods, and then linearly regressed these data against the AOU value for the appropriate collection depth. The resulting regression, $NO_2 = 1.61(AOU) + 164.2$; $r^2 = 0.912$, was then used to predict the continuous PCA-nitrite profile for other profiler casts. Application of this linear relationship to the AOU values calculated from CTD-oxygen data from an ear-

lier profiler cast (Fig. 3b) allowed prediction of the approximate vertical position and slope of the primary nitricline and much of the fine-scale variability in the continuous nitrite profiles, which were obtained with the PCA during the earlier cast (compare predicted- NO_2 and PCA- NO_2 profiles in Fig. 4; Predicted- $NO_2 = 0.998(PCA-NO_2) - 3.18$, $r^2 = 0.974$). Such a predictive capability is a testament to the sensitivity and accuracy of the PCA instrumentation for continuous, high-resolution measurements of dissolved nitrite in coastal waters. Perhaps more importantly, these results indicate that we should expect fine structure in nitrite profiles any time lateral transport or locally enhanced microbial activity lead to fine-scale structure in the AOU.

Observed and Predicted Iron(II) Fine Structure

The vertical structure of iron(II) was quite different at station A from the nitrite structure discussed above. Dissolved iron(II) was near the detection limit of the PCA (<0.3 nM) in the upper water column, then increased rapidly at ~ 20 m to higher concentrations (up to 440 nM) in the near bottom waters. The resulting micronutrient gradient was extremely steep ($d[Fe(II)]/dz = >500$ nM $Fe(II)$ m^{-1} ; see Fig. 5). In contrast to the tight correlation of the nitrite gradient with the thin chlorophyll layer in the upper water column, this steep gradient in dissolved iron(II) was unrelated to changes in chlorophyll fluorescence. Instead, it corresponded to the top of the well-mixed bottom boundary layer, suggesting that the elevated bottom water iron(II) levels might be the result of resuspension and mixing by bottom currents during this flood-tide cast. We made no attempt to collect samples for comparative laboratory analyses of dissolved iron(II) during this study because iron(II) oxidation rates were expected to be so fast that significant losses of iron(II) would occur during sample collection and preservation [see below for a discussion of iron(II) oxidation rates]. However, replicate samples were collected from discrete depths by the pump-to-deck and microgradient sampling systems and preserved by acidification for subsequent analytical determinations of dissolved and total acid reducible iron (O'Sullivan *et al.*, 1997). Taken together, the *in situ* and laboratory results indicated that there was a substantial reservoir of iron in East Sound [ranges: 10–440 nM dissolved $Fe(II + III)$ and 50–2,929 nM

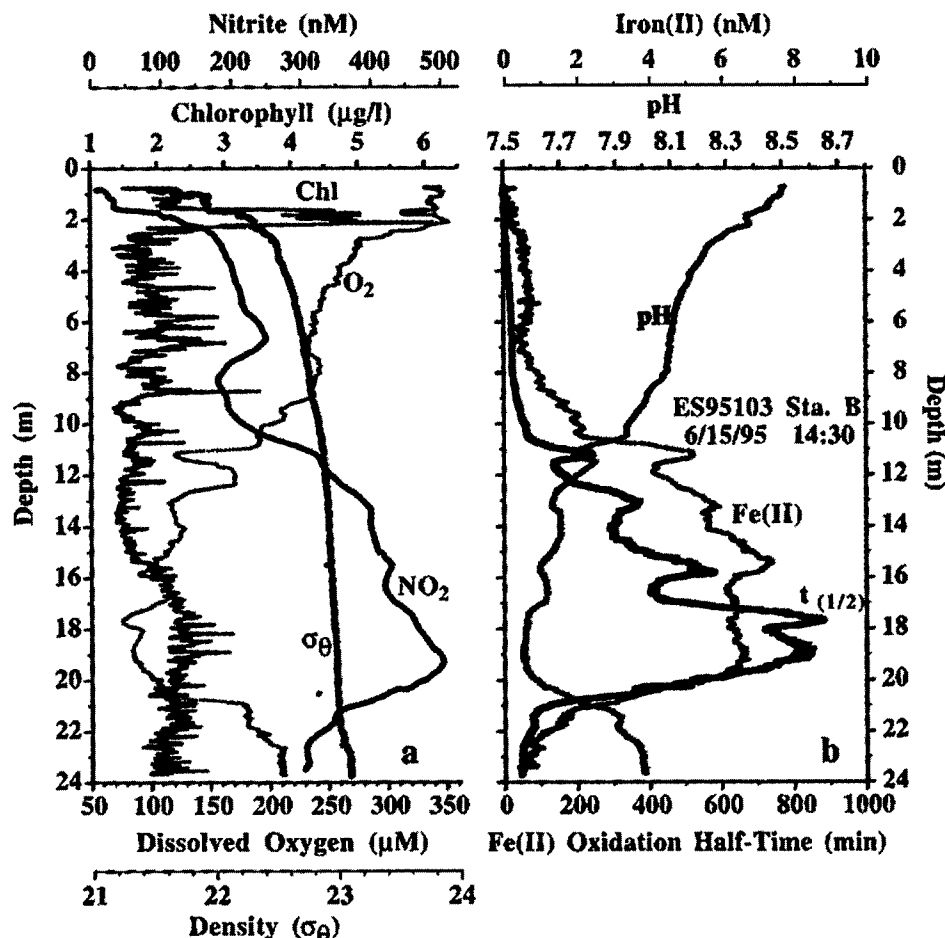


Fig. 6: Fine-scale vertical structure of physical, bio-optical, and chemical properties associated with a broad mid-depth oxygen minimum present during low tide at station B.

total Fe(II + III)], with the highest levels in the near bottom waters.

In the introduction, we hypothesized that the rapid rates and chemical control of iron(II) oxidation by ambient pH, oxygen, temperature, and salinity levels should lead to vertical iron(II) structure being highly sensitive to recent input events and to fine structure in the physicochemical factors that control the oxidation rate. If the variably elevated levels of PCA-iron(II) detected in near bottom waters was the result of a physical mixing event providing a flux of iron(II) into the overlying waters, then the iron(II) released would eventually be oxidized, transported, and accumulated as colloidal and particulate iron oxides within the mid-depth and deeper waters. The kinetics of the oxidation of iron(II) have been well studied in the laboratory, as a function of pH, dissolved oxygen, temperature, and salinity (Millero *et al.*, 1987). The pseudo-first-order rate constant, k_i , for the rate equation $-d[\text{Fe(II)}]/dt = k_i[\text{Fe(II)}]$, encompasses the effects of these four parameters

and is a first degree function of the oxygen concentration and second degree function of the pH. The effects of salinity (expressed as ionic strength: $I = 0.0199S$) and temperature ($^{\circ}\text{K}$) on the overall rate constant, k , for the rate equation $-d[\text{Fe(II)}]/dt = k[\text{Fe(II)}][\text{O}_2][\text{OH}^-]^2$ can be estimated from the relationship $\log k = 21.56 - 1545/T - 3.29I^{(1/2)} + 1.52I$. These algorithms conveniently allow the estimation of k and k_i from field data. The simultaneous measurement of all five parameters [S, T, pH, O_2 , and Fe(II)] in East Sound provided us with a unique opportunity to test the real-world applicability of this kinetic model for iron(II) oxidation, developed by Millero and co-workers, and an independent check on the validity of the Fe(II) fine-structure detected by the PCA.

The continuous salinity, temperature, oxygen, and pH data from Fig. 3 were used to estimate the vertical variability for the pseudo-first-order rate constant (k_i) for iron(II) oxidation in the East Sound water column (Fig. 5). Potential effects due to the complexation of iron(II) by organic lig-

ands or the oxidation of iron(II) by hydrogen peroxide (Millero *et al.*, 1987; Millero and Sotolongo, 1989) were ignored for these approximations. The estimated pseudo-first-order rate constant decreased systematically with depth by over two orders of magnitude for this cast. The calculated half-lives for iron(II) oxidation ($t_{(1/2)} = \ln 2 \cdot k_i^{-1}$) ranged from ~ 1 min within the well oxygenated surface waters to >200 min near the benthic boundary. If iron(II) was introduced (e.g., pore water fluxes, sediment-water interactions, or photochemical reduction) into waters characterized by slower oxidation rates (longer oxidation half-lives), then the iron(II) signal would persist for a longer time period than in the surface waters. The longer half-life estimates for iron(II) oxidation in the near bottom waters are the combined result of the cooler temperatures, reduced pH values, and lower dissolved oxygen contents. These oxidation rate estimates also suggest that there was micro- to fine-scale variability in the iron(II) oxidation potential of the stratified waters of East Sound.

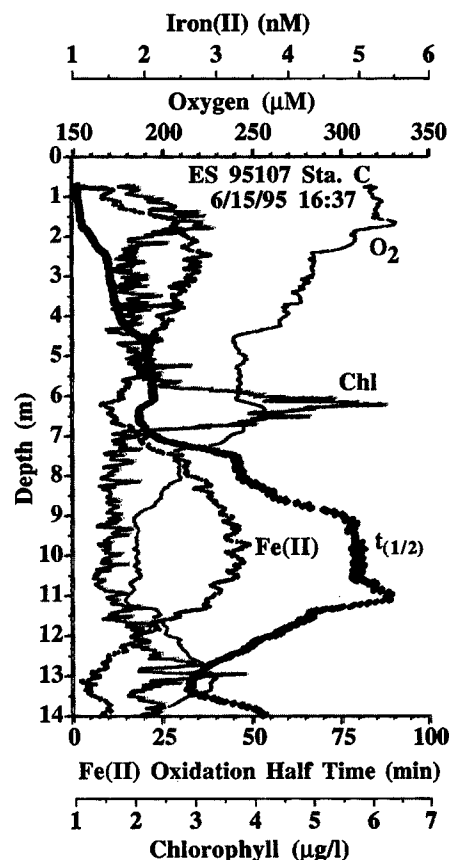


Fig. 7: Association of thin chlorophyll fluorescence layers with micro- to fine-scale gradients of oxygen, nitrite, iron(II), and model-predicted half-lives for iron(II) oxidation during flood tide at station C.

Comparison of the half-lives for iron(II) oxidation with the PCA-iron(II) distribution showed a remarkable degree of correspondence (Fig. 5). Higher concentrations of dissolved iron(II) were only detected in waters with slower iron(II) oxidation rates. The estimated oxidation rate for iron(II), $-d[\text{Fe(II)}]/dt$, was greatest (1.1–1.4 nM min⁻¹) within the iron(II)-containing waters that comprised the benthic boundary layer. The estimated oxidation rate for iron(II) increased very sharply near the top of the benthic boundary layer (~20 m) and associated steep iron(II) gradient ($d[\text{Fe(II)}]/dz = \sim 300$ nM/m), indicating that iron(II) was more effectively oxidized within this region, than in the near bottom waters containing more iron(II). Because the most likely source of the high iron(II) in the bottom waters is from sediment pore-water fluxes and tidal resuspension of sediments, it should not be surprising that another region characterized by a steep iron(II) gradient is near the sediment interface. The iron(II) fine-structure and strong gradients, detected by the PCA at this station, are predicted to be present by the underlying iron(II) oxidation kinetics.

Spatial and Temporal Variation in Fine-Scale Structure

There was considerable spatial and temporal variability in chemical compositions, predicted reaction rates, and fine-scale gradients in the waters of East Sound. This was particularly evident for a late afternoon profiler deployment at station B (Fig. 6) that was characterized by a broad mid-depth minima (12–22 m) in dissolved oxygen and pH and corresponding maxima in dissolved nitrite and iron(II). The PCA-iron(II) levels increased from subnanomolar surface values to ~7 nM within the mid-depth waters with lower oxygen contents, then declined rapidly to subnanomolar levels in deep waters. In contrast to station A, the increases in iron(II) at station B cannot be attributed to iron(II)-rich bottom waters being recently mixed upward by tidal flows. The rapid decline in iron(II) below 20 m corresponds to a rapid increase in oxygen and pH at that depth. The calculated rate constants for iron(II) oxidation indicated that the lower pH and oxygen contents within the midwater minimum extended the half-lives for iron(II) oxidation considerably (to >800 min). This not only suggests that this feature should persist for some time, but that it could be derived from an interaction with the ben-

thos (or other source) that occurred several days earlier, and then was advected as a midwater layer to this location. In addition to the steep gradients and broad iron(II) maximum, several submeter-scale maxima were also evident. As at station A, the calculated half-life for iron(II) oxidation shows submeter-scale maxima that precisely correspond to Fe(II) concentration maxima. Again, the fine-scale structure and sharp gradients are qualitatively consistent with the underlying iron oxidation kinetics.

Biological Control of Iron(II) Gradients

The chlorophyll fluorescence, oxygen, and PCA-iron(II) profiles, from a late afternoon deployment at station C (Fig. 7), demonstrate that thin plankton layers (located near 1.5, 6, and 13 m depth) can exert a similarly scaled influence on dissolved oxygen levels, and both the estimated oxidation rate and the trace concentration levels of dissolved iron(II). The fine-scale minima for estimated iron(II) oxidation half-lives can be attributed to focused photosynthetic carbon dioxide uptake (higher pH) and oxygen evolution within the thin phytoplankton layers. The corresponding minima in iron(II) concentrations may be due to locally enhanced rates for iron(II) oxidation and/or direct bioassimilation of dissolved iron(II). Conversely, the midwater (9–11 m) maximum in iron(II) corresponds both to a maximum in the expected half-life for iron(II) oxidation and to a minimum in phytoplankton chlorophyll and thus potentially lower direct bioassimilation. Iron redox cycling and phytoplankton growth appear to be closely coupled in East Sound.

Discussion

The continuous vertical profiles obtained with the high-resolution electronic profiling system and the profiling chemical analyzer in East Sound demonstrate that fine-scale chemical gradients and chemically distinct thin layers can exist in stratified coastal environments. The fine-scale gradients detected for nitrite were quantitatively related to similarly scaled gradients in apparent oxygen utilization. The fine-scale gradients detected for iron(II) were consistent with the similarly scaled gradients predicted for the pseudo-first-order rate constant for iron(II) oxidation. The mechanisms for the fine-scale structure observed in the water column included 1) focused chemical uptake or release within thin phytoplankton layers and 2) the interaction of physical mixing and

transport processes with chemical fluxes from the sediment-water interface. Isopycnal transport may be an important mechanism to supply iron and other nutrients from the benthos to high-biomass, thin plankton layers in East Sound, WA.

It is evident from the East Sound results that the vertical depth resolution of the PCA, for changes in dissolved nitrite and iron(II) concentrations, was approaching the depth-resolution of the electrochemical pH and oxygen sensors that were co-deployed with the electronic profiling system. Whereas many electrochemical sensors and some submersible chemical analyzers may have the required response times and sensitivity to detect micro- to fine-scale chemical gradients in stratified coastal waters, they generally have not been applied for that purpose (Johnson *et al.*, 1986, 1990, 1992; Taylor *et al.*, 1993; Johnson and Jannasch, 1994; Klinkhammer, 1994). The faster package descent rates that have commonly been used during coastal and offshore investigations with CTDs and submersible chemical analyzers (10–40 m min⁻¹ versus the 1–2 m min⁻¹ used in this study) have typically precluded the detection of submeter-scale variability in the water column by the submersible chemical instrumentation.

The enhanced sensitivity of the PCA for nitrite and iron(II) allowed us to document the chemical fine-structure and the presence of transient iron(II) within the water column that has passed undetected by traditional water sampling and analytical methodologies. For example, all the iron(II) fine-structure detected by the PCA in the upper portions of the East Sound water column was below the detection limit [<20 nM iron(II)] of the sampling and analytical methodology used by Murray and Gill (1978) in their earlier investigation of the geochemistry of iron in Puget Sound waters. This underscores the importance of being able to determine the concentrations of reactive chemicals at the trace levels that influence chemical and biological rates, and with sufficient resolution to define the gradients as they really occur in nature. With the high-resolution electronic profiling and PCA technologies, we now have the capability to resolve chemical gradients at the small spatial and temporal scales required to investigate the relative importance of chemical processes in the creation and maintenance of thin biologically productive layers and conversely,

the influence of such layers on chemical distributions, fluxes, and reaction rates.

Future Directions

There are important chemistry-related questions that need to be addressed concerning the dynamics of thin plankton layers. What mechanistic roles do nutrient recycling and availability play in thin plankton layer dynamics? Are episodic variations in nutrient gradients, driven by and coupled to dynamic meteorological and physical processes, critically important to the development, persistence, and behavior of thin plankton layers? How significant are the influences of thin plankton layers on the distributions of inorganic and organic chemicals and on their biologically mediated reaction rates within coastal waters? Our present difficulty in adequately answering these questions illustrates the sparseness of our chemical data on the thin plankton layers phenomena. This short-coming is partly due to the limited availability of high-resolution submersible chemical sensors and analyzers that can interface with contemporary CTD and bio-optical profiling systems. The development of a high-resolution, multinutrient profiling analyzer, would allow us to more adequately characterize the nutrient supply to high-biomass, thin plankton layers and provide the parameterization of the nutrient field that is required to develop and test predictive models for thin plankton layer behavior in coastal waters.

Acknowledgements

Funding for this research was provided by the Office of Naval Research grants N-00014-94-1-0561 to A.K. Hanson and N-00014-95-1-0225 to P.L. Donaghay. The technical assistance of Robert Griffin with PCA calibration, iron and nutrient determinations and data processing is gratefully acknowledged. We thank Casey Moore (WET Labs, Inc.), Ron Zaneveld, Jennifer Prentice, James Sullivan, and Mike Twardowski for their assistance in this work. We also thank Tim Cowles, Frank Millero, and the anonymous reviewers for their valuable comments.

References

- Brand, L.E., 1991: Minimum iron requirement of marine phytoplankton and the implications for the biogeochemical control of new production. *Limnol. Oceanogr.*, **36**, 1756-1771.
- Cowles, T.J. and R.A. Desiderio, 1993: Resolution of biological micro-structure through in situ fluorescence emission spectra. *Oceanography*, **6**, 105-111.
- Cowles, T.J., R.A. Desiderio and M.-E. Carr, 1998: *Oceanography*, **11:1**, 4-9.
- Donaghay, P.L., P.S. Liss, R.A. Duce, D.R. Kester, A.K. Hanson, T. Villareal, N.W. Tindale and D.J. Gifford, 1991: The role of episodic atmospheric nutrient inputs in the chemical, and biological dynamics of oceanic ecosystems. *Oceanography*, **4**, 62-70.
- , H.M. Rines and J.M. Sieburth, 1992: Simultaneous sampling of fine-scale biological, chemical, and physical structure in stratified waters. *Arch. Hydrobiol.*, **36**, 1-14.
- Geider, R.J. and J. La Roche, 1994: The role of iron in phytoplankton photosynthesis, and the potential for iron-limitation of primary productivity in the sea. *Photosynthesis Res.*, **39**, 275-301.
- Grasshoff, K. and F. Koroleff, 1983: Determination of nutrients. In: *Methods of Seawater Analysis*. K. Grasshoff, M. Ehrhardt and K. Kremling, eds. Verlag Chemie, Weinheim, Germany, 125-187.
- Gregg, M.C., 1975: Oceanic fine, and micro-structure. *Rev. Geophys. Space Phys.*, **13**, 586-591.
- Johnson, K.S., C.L. Beehler and C.M. Sakamoto-Arnold, 1986: A submersible flow analysis system. *Analytica Chimica Acta*, **179**, 245-257.
- , K. Coale and H.W. Jannasch, 1992: Analytical Chemistry in Oceanography. *Analytical Chem.*, **64**, 1065A-1075A.
- and H.W. Jannasch, 1994: Analytical chemistry under the sea surface: monitoring ocean chemistry *in situ*. *Naval Res. Rev.*, **3**, 4-12.
- , C.M. Sakamoto-Arnold and C.L. Beehler, 1990: Continuous determination of nitrate concentrations *in situ*. *Deep-Sea Res.*, **36**, 1407-1413.
- Klinkhammer, G.P., 1994: Fiber optics spectrometers for *in situ* measurements in the oceans: the ZAPS Probe. *Mar. Chem.*, **47**, 13-20.
- Kullenberg, G., 1974: Investigation of small-scale vertical mixing in relation to the temperature structure in stably stratified waters. *Adv. Geophysics*, **18**, 339-351.
- , 1983: Physical processes. In: *Pollutant Transfer and Transport in the Sea*. G. Kullenberg, ed. CRC Press, Boca Raton, FL, pp. 2-89.
- Lipschultz, F., S.C. Wofsy and L.E. Fox, 1986: Nitrogen metabolism of the eutrophic Delaware River ecosystem. *Limnol. Oceanogr.*, **31**, 701-716.
- Mason, R.P., W.F. Fitzgerald, J. Hurley, A.K. Hanson, Jr., P.L. Donaghay and J.M. Sieburth, 1993: Mercury biogeochemical cycling in a stratified estuary. *Limnol. Oceanogr.*, **38**, 1227-1241.
- Millero, F.J. and S. Sotolongo, 1989: The oxidation of Fe(II) with H₂O₂ in seawater. *Geochimica et Cosmochimica Acta*, **53**, 1867-1873.
- , S. Sotolongo and M. Izaguirre, 1987: The oxidation kinetics of Fe(II) in seawater. *Geochimica et Cosmochimica Acta*, **51**, 793-801.
- Moore, C., J.R.V. Zaneveld and J.C. Kitchen, 1992: Preliminary results from an *in situ* spectral absorption meter. In: *Ocean Optics XI*. G.D. Gilbert, ed. Proc. SPIE 1750, 330-337.
- Murray, J.W. and G. Gill, 1978: The geochemistry of iron in Puget Sound. *Geochimica et Cosmochimica Acta*, **42**, 9-99.
- Osborn, T.R., 1998: *Oceanography*, **11:1**, 36-43.
- and C.S. Cox, 1972: Oceanic fine-structure. *Geophys. Fluid Dyn.*, **3**, 321-345.
- O'Sullivan, D.W., A.K. Hanson, Jr. and D.R. Kester, 1997: The distribution and redox chemistry of iron in the Pettaquamscutt Estuary. *Estuarine Coastal Shelf Sci.*, **45**, 769-788.
- , A.K. Hanson, Jr., W. Miller and D.R. Kester, 1991: Measurement of Fe(II) in Equatorial Pacific Surface Seawater. *Limnol. Oceanogr.*, **36**, 1727-1741.
- Rattray, M., Jr., 1967: Some aspects of the dynamics of circulation in fjords. In: *Estuaries*. G.H. Lauff, ed. AAAS, Washington, DC., 52-62.
- Redfield, A.C., 1942: The processes determining the concentration of oxygen, phosphate, and other organic derivatives within the depths of the Atlantic Ocean. *Pap. Phys. Oceanogr. Meteor.*, **9**, 1-22.
- Seitzinger, S.P., S.W. Nixon and M.E.Q. Pilson, 1980: Denitrification and N₂O production in nearshore marine sediments. *Geochimica et Cosmochimica Acta*, **44**, 1853-1860.
- Sieburth, J.M. and P.L. Donaghay, 1993: Planktonic methane production and oxidation within the algal maximum of the pycnocline: seasonal fine-scale observations in an anoxic estuarine basin. *Mar. Ecol. Prog. Ser.*, **100**, 3-15.
- Stookey, L.L., 1970: Ferrozine—a new spectrophotometric reagent for iron. *Analytical Chem.*, **42**, 779-781.
- Sunda, W.G. and S. Huntsman, 1995: Iron uptake and growth limitation in oceanic and coastal phytoplankton. *Mar. Chem.*, **50**, 189-206.
- Taylor, C.D., B.L. Howes and K.W. Doherty, 1993: Automated instrumentation for time-series measurement of primary production and nutrient status in production-platform accessible environments. *MTS J.*, **27**, 32-44.
- Vaccaro, R.F., 1965: Inorganic nitrogen in seawater. In: *Chemical Oceanography*, Vol. 1. J.P. Riley and G. Skirrow, eds. Academic Press, London, 365-408.
- Wells, M.L., N.M. Price and K.W. Bruland, 1995: Iron chemistry in seawater and its relationship to phytoplankton: a workshop report. *Mar. Chem.*, **48**, 157-182.
- Zafriou, O.C. and M.B. True, 1979: Nitrite photolysis in seawater by sunlight. *Mar. Chem.*, **8**, 9-13. □

ACOUSTICAL SENSING OF SMALL-SCALE VERTICAL STRUCTURES IN ZOOPLANKTON ASSEMBLAGES

By D.V. Holliday, R.E. Pieper,
C.F. Greenlaw and J.K. Dawson

OBSERVATION OF AQUATIC animals in their natural environments remains a major challenge in both biological oceanography and limnology. Critical processes in feeding, reproduction, growth, and predation in small zooplankton occur at scales from fractions of millimeters up to scales that match the ambits of individuals. It is often difficult to reproduce all essential features of the marine environment in the lab, where observation of small-scale processes is more tractable than at sea. Therefore there is continuing interest in improving our ability to observe and quantify *in situ* spatial and temporal changes in the distribution and abundance of zooplankton in relation to natural physical, chemical, and other biological fields.

Making accurate measurements of spatial distributions is difficult. Conventional CTD packages, fluorometers, and acoustical sensors, when used in a "cast" mode from a ship, tend to have ~1 m vertical resolutions. The time it takes to make a measurement in relation to the "drop" rate, the necessity to pump water through some kinds of sensors, the need to acquire and average multiple samples in a quasi-random, statistically nonstationary local environment, and the coupling of the motions of the ship to the sensor all contribute to "smearing" spatial pattern in the data. These practical issues tend to reduce the spatial resolution of measurements one obtains at sea.

In many of our acoustical field studies of plankton, sea conditions and consequent uneven sampling in depth caused us, in

post-acquisition processing, to integrate over 2 m depth intervals even though the data were collected at submeter resolutions. Two meters was an empirically determined compromise between achieving as much vertical resolution as possible, while averaging enough independent measurements of scattering to obtain good estimates of the acoustical scattering power spectrum, thereby improving our estimates of abundances and sizes of zooplankters present in a given depth interval. Averaging data into 2 m depth bins has succeeded in revealing a variety of patterns and correlations between ocean physics, phytoplankton, and zooplankton distributions.

Such averaging can, however, lead to an underestimate of the intensity of structure smaller in extent than the bin interval. For example, a 10 cm thick layer of small zooplankton will appear in a 2 m average to have a peak abundance 20 times less than is actually the case, even though the total biomass reported for the interval is correct. The differences between actual distributions and apparent distributions can be ecologically important in many ways (feeding, finding a mate, etc.). Meter scale data are useful in answering some important kinds of process and distributional questions, but we should recognize that even meter scale resolution is still not adequate to allow us to quantitatively visualize the environment from the point of view of millimeter-sized organisms.

Small-Scale Scattering Structures in a Shallow Fjord

In our first example we describe small-scale vertical structure in marine zooplankton in a small fjord, West Sound, at Orcas Island in Washington State's San Juan Islands (Fig. 1). The upper end of this sound is relatively shallow, the bottom is soft mud, and the en-

tire basin is subject to relatively strong tidal forcing. Data discussed here were collected in July 1995.

We used a shore-powered, bottom-mounted, inverted (surface-facing) echo sounder to measure volume scattering strength (Sv) profiles at four frequencies (265, 420, 1,100, and 3,000 kHz) specifically selected to be sensitive to the presence of small zooplankton. Every 2 min, 24 (interleaved) scattering intensity profiles were collected at each frequency, range binned in 0.5 m intervals from 0.75 m above the bottom to 21.75 m from the transducer face (i.e., just below the surface). Ensemble averages of the 24 echoranging cycles were made, and absolute volume scattering strength profiles were computed by accounting for spreading, absorption, and various system parameters. Ensemble averages of the volume scattering strength profiles, pressure (tide), and temperature at the base of the acoustical sensor were transmitted to a shore site for real-time display and storage. Power was supplied from the shore site.

Two hours of data from this mooring will be examined. Tidal changes in water depth were measured with a pressure sensor on the up-looking sounder (Fig. 2a). Acoustical volume scattering strength profiles from the 265 kHz and 1.1 MHz sounders are illustrated in Figure 2, b and c. A thin sound-scattering layer can be seen in the 265 kHz record (Fig. 2b), at ~17 m near the start of the record. Note that height above the bottom is used rather than depth below the changing surface. When initially detected, the layer thickness was $\leq \frac{1}{2}$ m. The peak intensity (averaged over the system's half-meter range resolution) is probably underestimated. As time passed, the thickness of the layer increased to slightly more than 1 m, diffusing into a thicker, more complex structure at the time of high tide (near the

D.V. Holliday and C.F. Greenlaw, Tracor Aerospace Analysis and Applied Research Division, 4669 Murphy Canyon Road, San Diego, CA 92123, USA. R.E. Pieper and J.K. Dawson, University of Southern California, Hancock Institute for Marine Studies, 820 South Seaside Avenue, Terminal Island, CA 90731, USA.

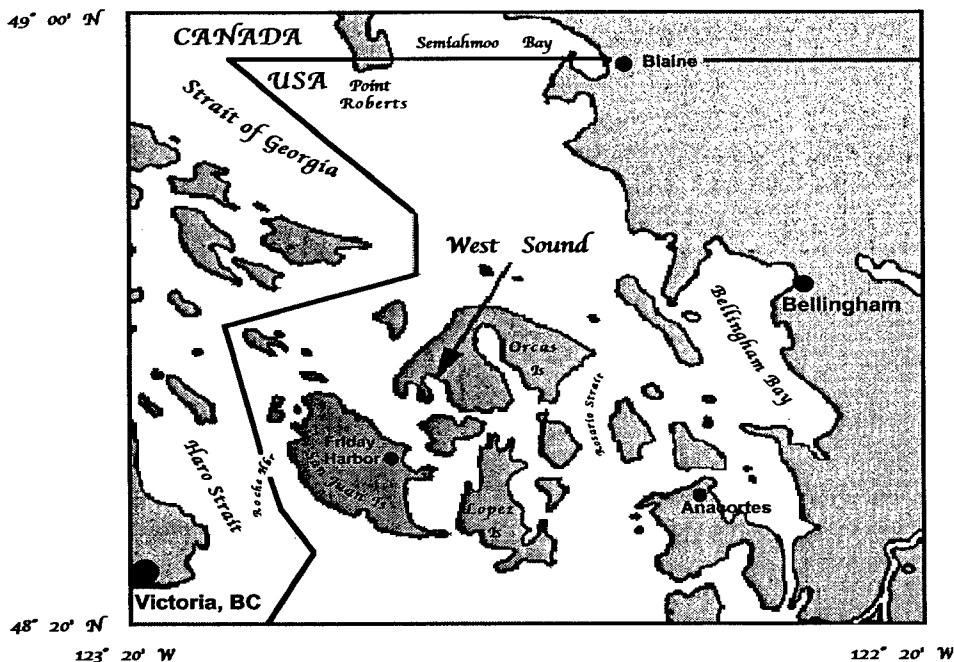


Fig. 1: A small, shallow fjord, West Sound is located in the San Juan Islands, WA, in the extreme northwestern United States.

end of the record). At 265 kHz, volume scattering strengths in the layer varied between -60 and -49 dB. The 420 kHz record (not shown) and the 1.1 MHz record (Fig. 2c) reveal similar patterns for the thin layer, with scattering at levels between -55 and -47 dB at 420 kHz and between -50 and -35 dB at 1.1 MHz.

At 1.1 MHz (Fig. 2c), sound scatterers not visible at 265 kHz (Fig. 2b) were observed as they passed over the sounder. A thin, variable intensity layer of high level scattering, limited to a couple of meters from the bottom, appears to dissipate near the end of the record (i.e., near slack water). In addition, short episodes of high scattering levels appeared early in the 1.1 MHz record, beginning in mid-column and extending to the surface. Excluding the episodes of high scattering at the beginning of the record, scattering levels just under the surface of the water were both higher and extended deeper into the water column at the end of the record than at the beginning. The wind was negligible, the area was sheltered from surface waves originating elsewhere, and there was no whitecapping or even breaking waves at the shoreline. The most likely explanations for variations in the observed scattering involve changes in the distribution of living organisms above the sounder.

In this work the sensor was deployed as an ancillary measurement tool for an acoustics program, thus the principal inter-

est was in describing variability in levels of acoustical scattering rather than in defining the underlying biological causes of the scattering. There was no opportunity to collect samples of zooplankton or fish, quantitative data on tidal velocities, velocity profiles, or CTD information. A diver participant in the project reported the following: "We would often pass through a surface layer, about a meter thick, of plankton on our dives. Zooplankton seemed to be mostly crustaceans mixed in with the phytoplankton. It often was so dense that the critters on our suits were noticeable after exiting the water" (L. Self, personal communication). Quantitative physical, optical, and acoustical measurements in East Sound, nearby on the same small island, have revealed a complex, highly stratified, multilayer, tidally driven water column (e.g., see other papers in this issue). Measurements with an acoustic doppler profiler current (ADCP) have revealed that multiple layers of the water column in East Sound are moving in different directions with attendant shear and turbulence at the layer interfaces (P. Donaghay, personal communication). We have no reason to believe that West Sound is any less complex.

Extensive side scan sonar work at 50, 100, and 500 kHz was conducted near this mooring, but only a few individual fish were observed, and fish school-like contacts were not observed during the pe-

riod illustrated. Likewise, divers reported that the abundance of medusae and ctenophores was low. Our visual observations also suggest that the numbers of medusae and ctenophores in the upper few meters at this site were very low during this data collection period.

At these high frequencies, the absorption of sound in seawater is very large (at 3 MHz, ~ 2.4 dB/m). At ranges of more than ~ 5 m above the sensor, reverberation-to-noise ratios for the 3 MHz sounder would not support an inverse calculation of the type we prefer to use, i.e., the multifrequency non-negative least squares (NNLS) method, to estimate size spectra and abundance (Holliday and Pieper, 1995). To obtain information about the size and abundances of the scatterers, a two-frequency inverse algorithm (Greenlaw, 1979; Mitson *et al.*, 1996) was employed. Ratios of volume scattering strengths were calculated by taking the difference between the (logarithmic) volume scattering strengths measured for 265 kHz and 1.1 MHz (Fig. 2d). Greenlaw (1979) pointed out that the size of the scatterer that dominates the acoustical scattering is embedded in these ratios of scattered intensity (differences in Sv). Given a few assumptions about, or *a priori* knowledge of the scatterers, then for several common marine scatterers, mathematical models exist that will allow estimation of the size and abundance of the dominant scatterer. The interested reader can find a summary of these assumptions in Holliday and Pieper (1995). Based on the frequency dependencies we observed for this layer, the diver's observations, and our experience in the fjords of the San Juan Islands, it appears that (with a few notable exceptions) small crustaceans were the dominant cause of the scattering shown in Figure 2. Although models are available for several generalized zooplankton taxonomies (copepod-like, euphausiid-like, bubble-bearing fish larvae, salp-like, etc.), most zooplankton assemblages are a mix of genera and organisms with a variety of physical shapes. When measurements at sufficient number of frequencies are available, one can sometimes successfully estimate abundance in several (shape-defined) taxonomic classes, by size within the class (Holliday, 1977). When one must work with a limited number of frequencies, it is best to choose the simplest single model that describes the shape (genera) thought, or known from direct sampling, to contribute the most energy to the acoustical scattering. For an assemblage dominated by crustaceans similar

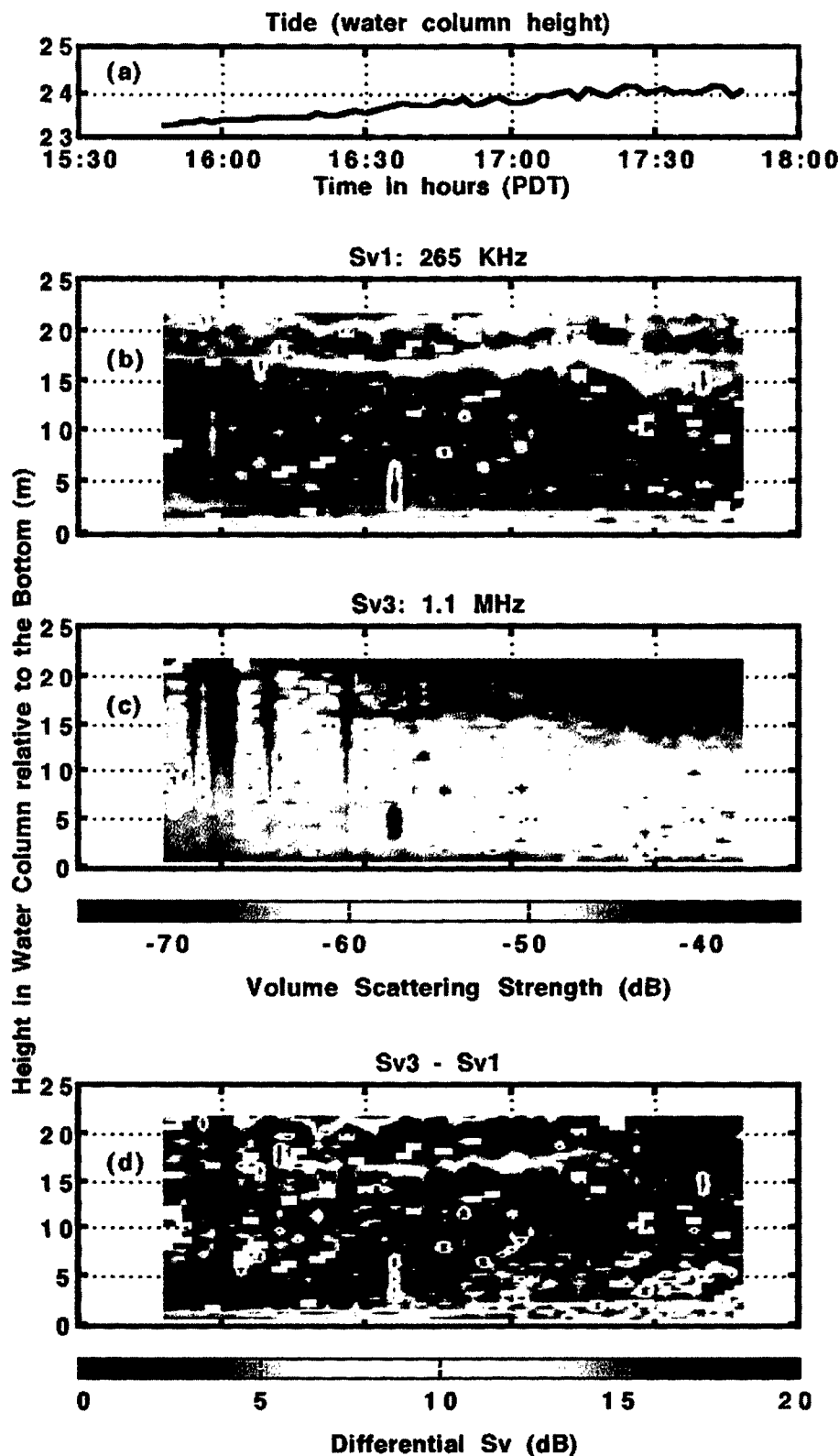


Fig. 2: Two hours of tide level data (a) are illustrated for a station in West Sound, WA, during July 1995. Acoustical scattering data, collected at 2 min intervals and in 0.25 m vertical bins are also displayed for the 265 kHz (b) and 1.1 MHz (c) channels of a four-frequency bottom mounted, up-looking echo sounder. The color legend under the 1.1 MHz data (b) also applies to the 265 kHz display (c). The sizes of the dominant scatterers, in this case mostly small crustaceans, are embedded in the difference of the logarithms of the measured volume scattering (ratios of the intensities) as illustrated in d.

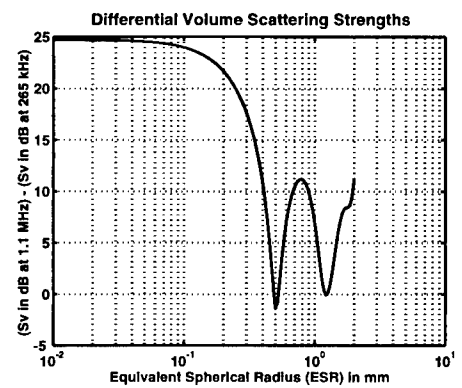


Fig. 3: The dependence of the difference of volume scattering strengths, measured in decibels (log scattering intensities), on the size of the dominant acoustical scatterers in the water column is illustrated for scatterers that follow a truncated fluid sphere scattering law.

to a calanoid copepod (roughly an ellipsoid of revolution), this is the truncated fluid sphere model (Pieper and Holliday, 1984), and this is the scattering descriptor chosen for the present analysis. The relation between the ratio of volume scattering strengths (Svs) at 265 kHz and 1.1 MHz, expressed as differential Svs versus scatterer size (ESRs) is illustrated in Figure 3. The equivalent spherical radius (ESR) is the radius of a sphere that would contain the same volume as the scatterer displaces. This model must be used with some care, because unlike the high-pass model originally used by Greenlaw, it is not monotonic with the product of scatterer size (ESR) and the wavenumber (k). One result of this nonlinear, nonmonotonic form is that there is no closed form analytical solution, therefore one must rely on numerical techniques. Another result of this functional form is the possibility that there will be multiple solutions for size for some ratios of Svs. Using different combinations of the available frequencies often allows one to resolve ambiguities in the dominant size calculated by this method.

The biomass predicted by the two-frequency algorithm (Fig. 4a) and the calculated size of the dominant scatterer (Fig. 4b) reveal that the thin layer at ~17 m consisted principally of animals with an equivalent spherical radius of ~0.3 mm. The ratio of the Svs at 420 kHz and 1.1 MHz also produced dominant size and biomass estimates that are consistent with the estimates for the layer in question, as illustrated in Figure 4. If the animals had shapes similar to calanoid copepods, this would translate to overall lengths of be-

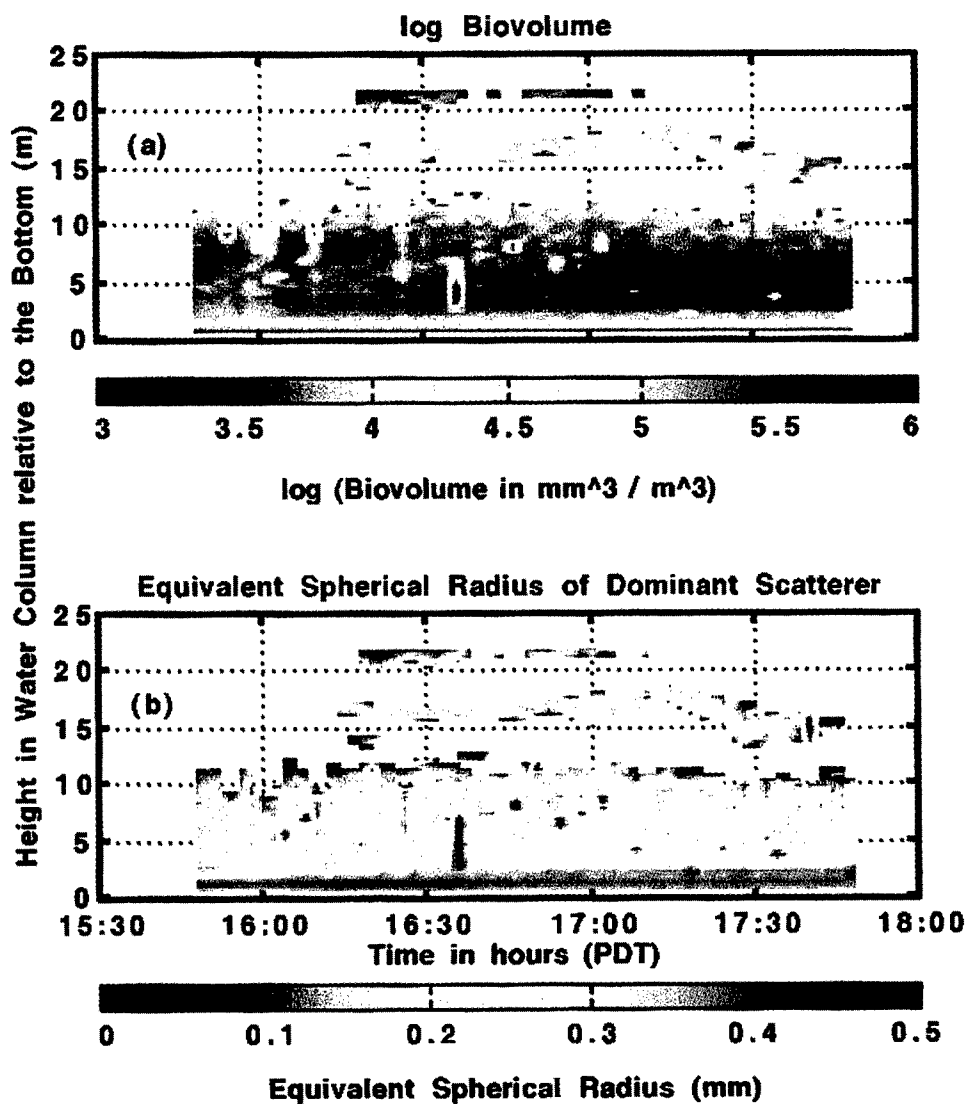


Fig. 4: Estimates of biovolume and zooplankton size are illustrated for the acoustical data displayed in Fig. 1. Blank pixels are displayed when the scattering was too low to result in a valid estimate; when the scattering ratios indicated that the truncated sphere model used for scattering from individuals was not correct; and when the scatterer size was larger than could be uniquely determined with the two-frequency inverse technique used. Examination of additional data at 420 kHz (not displayed here) revealed that most of the blank pixels in this data set were due to low numbers of small zooplankters.

tween 1.2 and 1.5 mm. Based on this size, the biovolume, a measure of biomass that is analogous to displacement volume, within the layer ranged between ~15,800 and 39,700 mm³/m³. This would correspond to a range of nominal dry weights, assuming that the layer is mostly small crustaceans, from 3,000 to 10,000 mg C/m³. Although this is a dense layer, it is not unusual. Much higher concentrations of copepods of similar sizes have been observed in even thicker layers (e.g., Alldredge *et al.*, 1984). The authors have often observed similar layers in the coastal waters of Southern California (Holliday and Pieper, 1980; Pieper and

Holliday, 1984), on the shelf off Cape Canaveral, FL (Holliday *et al.*, 1989), and in the Irish Sea (Holliday, 1993).

In addition to the thin, dense layer near 18 m, and the thin, sparsely populated layer of slightly larger animals (0.38–0.45 mm ESR) within a few meters of the bottom, there appears to be a boundary in the vicinity of 10 m (height off the bottom) that divides the water column. Above this boundary, scattering levels at 265 kHz below and above the thin midwater layer were too low to allow us to make valid size estimates with the two-frequency algorithm. In the absence of a valid estimate of the size of the scatterer, the two-frequency

algorithm returns no data for biomass. This is the reason for the absence of data in parts of the upper half of the water column in Figure 4, a and b. Small (0.12–0.2 mm ESR) plankton appear to dominate the scattering in the lower half of the water column. The biomass is diffuse but with a heterogeneous or “patchy” distribution in both abundance and size. Very near the surface, relatively high abundances of larger (~0.4–0.5 mm ESR) organisms were present for nearly 1 h in the middle of the period illustrated. There is a suggestion in the data that several high biomass concentrations or “patches” of scatterers are associated with the top of the apparent bioboundary near 10 m. Small, high biomass patches also appear to be associated with the thin midwater layer.

Plankton Layers Near the Shelf-Slope Break

Over several years we have collected numerous vertical profiles of acoustical volume scattering strength at multiple frequencies. One of our objectives was to quantify these relationships in order to gain an ability to “invert” the acoustical data, thereby estimating zooplankton biovolume spectra by size with depth (Costello *et al.*, 1989; Holliday and Pieper, 1995). While pursuing the relationship between the distribution, size and abundance of plankton, and the acoustical scattering, we have often observed profiles similar to those displayed in Figure 5. These data were collected on a narrow, shallow shelf at the north edge of the San Pedro basin near Long Beach, CA, in June 1996. The profile was made in the late afternoon, starting at 19:41 PDT. Temperature is displayed in Figure 5a, and Figure 5b is the fluorescence profile. The volume scattering spectrum is shown in Figure 5c and the biovolume-size spectrum is given in Figure 5d. The profile of total biovolume, summed over all the sizes displayed in Figure 5d, is provided in Figure 5e. The multifrequency inverse method described in Holliday and Pieper (1995) was used to map volume scattering into the plankton biovolume size–abundance profile.

Abnormally calm sea surface conditions were present during this particular cast, and we took advantage of the weather and low swell to collect a relatively high resolution profile, lowering our Tracor Acoustical Profiling System (TAPS) six-frequency sonar system at a rate of <0.04 m/s. A complete set of acoustical data are collected along with

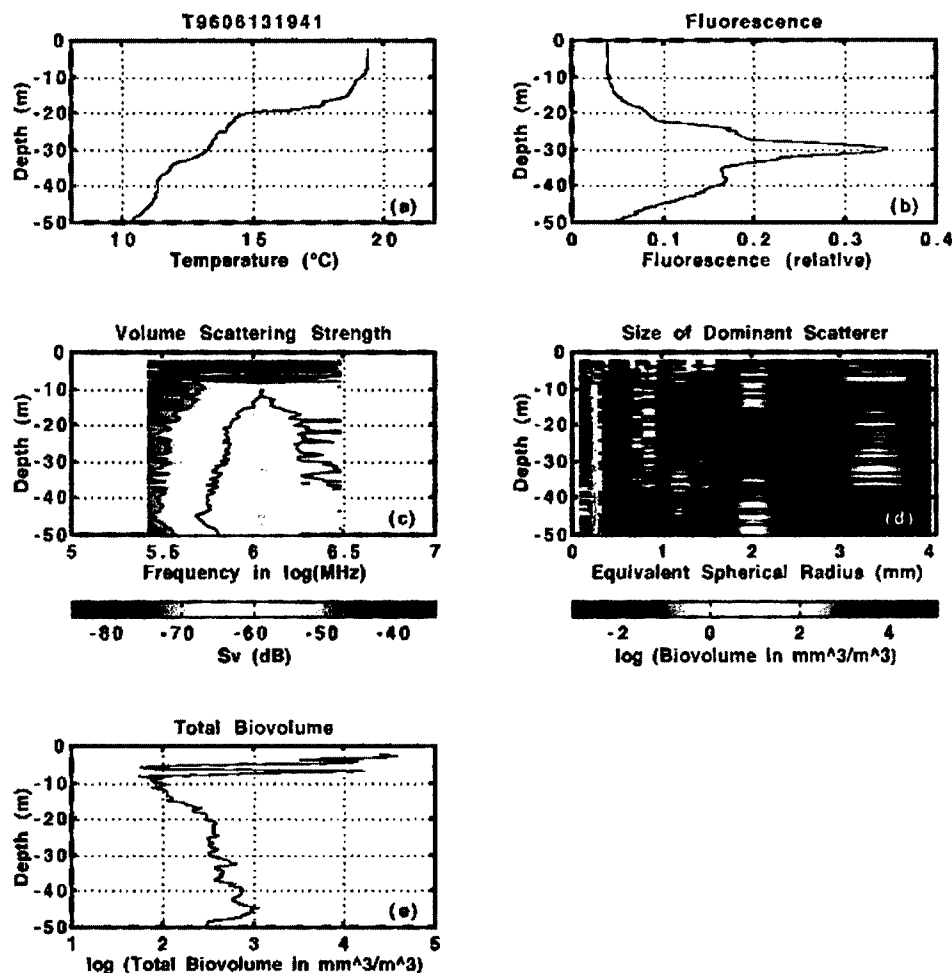


Fig. 5: Temperature (a), fluorescence (b), and volume scattering strength spectrum profile (c) are illustrated for a cast ~15 km south of Long Beach, CA, in June 1996. The calculated biomass-size spectrum profile (d) and the total biovolume profile (e) reveal that much of the biomass at this station was concentrated in three very thin layers in the upper mixed layer.

temperature by this system every 4 s. The volume scattering strengths were averaged into vertical bins of ~0.25 m.

Structure can be observed on scales from that of the basic resolution of the acoustical sensor, ~0.25 m in this instrument configuration, to scales of >100 m, the depths of the usual casts made with the instrument. The dominant structures in this particular cast were the three thin layers in the upper mixed layer. The water depth at this station was 53 m. The shallowest layer, centered at ~3.25 m, contained 63.5% of the water column biomass. A second layer, with a thickness of <0.5 m was centered at 4.25 m and contained 6.5% of the biomass. The third layer, between 6.5 and 7.5 m, represented another 8.4% of the biomass. The total water column plankton biovolume was 31,208 mm³/m². Early evening MOCNESS (Multiple Opening Closing Net En-

vironmental Sampling System) tows revealed that the copepod *Calanus pacificus* dominated the biomass. Preliminary results of the MOCNESS sampling indicated that the total biomass was higher than previously observed at this shelf location (33° 35.50' N, 118° 08.85' W) during the last 5 y of our sampling program. Larval fish and several species of euphausiid were present in small numbers relative to *Calanus*, but small crustaceans clearly dominated the plankton at this station. This represents an integrated column dry weight of 9,012 mg C/m². In addition to the exceptional intensity of the layering in the well-mixed zone, the position of the biovolume peak is notable, it being more common in this area that a zooplankton peak is associated with the chlorophyll maximum near the seasonal thermocline.

Multiple casts along transects often reveal that these small-scale structures in the

phytoplankton, based on fluorescence measurements, and in the zooplankton, from multifrequency acoustical measurements, can have horizontal extents of tens of kilometers (Holliday *et al.*, 1989; Holliday, 1993). These small-scale temperature structures are also often, but not always, associated with fluorescence maxima and with structure in profiles of optical scattering and optical transmission (Donaghay *et al.*, 1992; Cowles and Desiderio, 1993). We use the term associated, rather than correlated, for several reasons. In our observations, the acoustical estimates of zooplankton biomass (biovolume) distributions sometimes have shapes similar to the temperature gradient at such an anomaly, with the peaks of the zooplankton distributions and the maximum of the temperature gradient coinciding in depth. Both temperature gradients and small-scale turbulence can cause acoustical scattering by virtue of impedance discontinuities and variations in the sound speed of the reflected sound waves, but in our data both the levels and the spectrum of the scattering seem to best fit a model that associates peaks in zooplankton biomass with these structures. We have also observed that the strength of the acoustical scattering does not appear to be correlated with the magnitude of the gradient in the pycnocline. Often, these small steps or variations in temperature occur at boundaries of the zooplankton distribution, delimiting lower or upper bounds of particular plankton sizes or assemblages of sizes. Finally, we are cautious about making statements about correlation and coherence because the acoustical tools at hand, such as the TAPS, are working near the limit of their spatial resolution to define these structures. Nonetheless, it is clear that there are processes occurring at submeter scales that are reflected in the response of both phytoplankton and zooplankton to the physical environment.

Summary and Conclusions

In the illustrations we have provided, a substantial amount of the zooplankton biomass was concentrated in heterogeneous, small-scale structures, one form of which is a very thin layer. The biological and physical reasons for this distribution are poorly understood, but it is clear that this kind of distribution is neither unusual, nor rare, in coastal regions. This kind of distribution clearly has implications for predation by larger animals, e.g., for larval and juvenile fish. Its causes may be rooted in distributions of food,

i.e., phytoplankton, but may also be at least in part physically driven (e.g., the advantages of moderate levels of turbulence are discussed by Rothschild and Osborn 1988). To appropriately observe and understand this structure and the plankton's response, we not only require acoustical sensors with at least an order of magnitude better spatial resolution than are currently available (i.e., ~10 cm), but we also require a new protocol for deploying the sensors, one that is decoupled from the motion of a ship. Bottom-mounted systems are one solution for shallow water environments, especially if used in conjunction with ADCPs. For deeper environments, where sound absorption requires that acoustical sensors be placed near the organisms of interest, buoyancy-driven and free-fall profilers and profiling winches are attractive alternative platforms. Simply defining the distribution of the plankton at small scales, without describing their environment at similar scales is not sufficient.

For about a decade, oceanographers have been working to develop advanced sensors that can be used to examine aquatic environments faster, in more detail, and with improved spatial and temporal resolution. Some of the technologies finding applications in this quest include high-resolution imaging optics, video plankton recorders, high-frequency acoustical zooplankton sensors, optical fiber fluorometers, a variety of turbulence sensors, faster thermistors for measuring temperature, optical particle counters, multispectral optical transmissometers, and holographic cameras. Used alone, each of these technologies provides a view of only a part of the components of an ecosystem. Many ocean scientists believe measurement of fine- and microscale struc-

tures needed to describe submeter scale distribution and behavior of the animals, plants and their physical environment and their dynamic interactions ultimately will require a quantitative integration of several technologies. Individually, some of these sensor technologies have matured, and they are routinely used to examine animals and their environments on meter and submeter scales. Together, different technologies can be used either to measure different properties of the same animals in a small volume, or when they have substantially different spatial resolutions, they can be "nested," with the low-resolution system setting the spatial context for the high-resolution sensor (e.g., an optical system with a resolution of a few cubic millimeters can examine a subset of a liter of water being observed with an appropriate acoustical system). It appears to be timely to begin working on this quantitative synthesis of technologies in the hope that the result will be synergistic. This, in our opinion, although requiring a dedicated effort by multiple investigators, is one of the more promising avenues for research and development in sensors for studying plankton and its environment for the next decade.

Acknowledgements

This research was sponsored by the Office of Naval Research and by the National Science Foundation. We would like to acknowledge the invaluable assistance of R. Player, L. Howell and P. Jarrett in the conduct of the work.

References

- Allredge, A.L., B.H. Robison, A. Fleminger, J.J. Torres, J.M. King and W.M. Hamner, 1984: Direct sampling and *in situ* observation of a persistent copepod aggregation in the mesopelagic zone of the Santa Barbara Basin. *Mar. Biol.* 80, 75–81.

- Costello, J.H., R.E. Pieper and D.V. Holliday, 1989: Comparison of acoustic and pump sampling techniques for the analysis of zooplankton distributions. *J. Plankton Res.* 11, 703–709.
- Cowles, T.J. and R.A. Desiderio, 1993: Resolution of biological microstructure through *in situ* fluorescence emission spectra. *Oceanography* 6, 105–111.
- Donaghay, P.L., H.M. Rines and J.M. Sieburth, 1992: Simultaneous sampling of fine scale biological, chemical, and physical structure in stratified waters. *Arch. Hydrobiol. Beih. Ergebn. Limnol.* 36, 97–108.
- Greenlaw, C.F., 1979: Acoustical estimation of zooplankton populations. *Limnol. Oceanogr.* 24, 226–242.
- Holliday, D.V., 1977: Extracting bio-physical information from the acoustic signatures of marine organisms. In: *Oceanic Sound Scattering Prediction*, N.R. Anderson and B.J. Zahuranc, eds. Plenum Press, Marine Science Series, New York, Vol. 5, 619–624.
- , 1993: Applications of advanced acoustic technology in large marine ecosystem studies. In: *Large Marine Ecosystems: Stress, Mitigation, and Sustainability*, K. Sherman, L. Alexander and B. Gold, eds. AAAS Press, Washington, DC, Publication 92-39S, 301–319.
- and R.E. Pieper, 1980: Volume scattering strengths and zooplankton distributions at acoustic frequencies between 0.5 and 3 MHz. *J. Acoust. Soc. Am.* 67, 135–146.
- and R.E. Pieper, 1995: Bioacoustical oceanography at high frequencies. *ICES J. Mar. Sci.* 52, 279–296.
- , R.E. Pieper and G.S. Kleppel, 1989: Determination of zooplankton size and distribution with multifrequency acoustic technology. *J. Cons. Int. Explor. Mer.* 46, 52–61.
- Mitson, R.B., Y. Simard and C. Goss, 1996: Use of a two-frequency algorithm to determine size and abundance of plankton in three widely spaced locations. *ICES J. Mar. Sci.* 53, 209–215.
- Pieper, R.E. and D.V. Holliday, 1984: Acoustic measurements of zooplankton distributions in the sea. *J. Cons. Int. Explor. Mer.* 41, 226–238.
- Rothschild, B.J. and T.R. Osborn, 1988: Small-scale turbulence and planktonic contact rates. *J. Plankton Res.* 10, 465–474. □

SIMULTANEOUS IMAGING OF PHYTOPLANKTON AND ZOOPLANKTON DISTRIBUTIONS

By Jules S. Jaffe, Peter J.S. Franks
and Andrew W. Leising

UNDERSTANDING THE DYNAMICS of the relationship between phytoplankton and higher trophic levels is necessary for understanding the transfers of matter and energy through planktonic food webs. There have been several suggestions in the literature that copepods were more strongly associated with the subsurface productivity maximum than the chlorophyll maximum (Herman, 1983; Herman and Platt, 1983; Napp *et al.*, 1988). Zooplankton have been shown to respond to microscale (centimeters) patches of phytoplankton in the lab (Tiselius, 1992; Saiz *et al.*, 1993), however, except for Tiselius *et al.* (1994), who found correlations to 15 cm, there have been few data to confirm these results *in situ*. Zooplankton behavioral response to their food environment is therefore a critical factor to consider in trying to predict the relationship between phytoplankton and zooplankton in the ocean.

Testing of hypotheses regarding zooplankton-phytoplankton associations *in situ* has been difficult due to problems associated with sampling resolution. Traditional net sampling methods integrate over the small (cm to m) spatial scales relevant to exploring such relationships. Phytoplankton sampling by bottles or fluorometers generally gives spatial resolutions no finer than tens of centimeters (Bjorenson and Nielsen, 1991). Recent developments of *in situ* fluorometers have allowed observation of vertical variability to several centimeter resolution (Derenbach *et al.*, 1979; Cowles and Desiderio, 1993; Cowles *et al.*, 1993). Unfortu-

nately, similar resolution of zooplanktonic fields using noninvasive sampling techniques has been lacking due to technological constraints.

The high-resolution spectral fluorometer of Cowles (e.g., Cowles and Desiderio, 1993) has allowed observations of the microscale structure of both chlorophyll and phycoerythrin fluorescence (Cowles *et al.*, 1993). Both chlorophyll and phycoerythrin were seen to have significant variability at tens of centimeters, but the two fields were quite uncorrelated with each other. These observations raise many important questions concerning physical-biological couplings in the plankton at small scales and zooplankton foraging behavior in a patchy environment. For example, what physical and biological processes might be operating to allow formation and persistence of such thin layers or small patches of high phytoplankton biomass? What are the time and space scales of persistence of such features? Are the scales of phytoplankton patchiness the same for different taxa? And, in particular for this study, are the patches available to, or exploited by the zooplankton? The answers to such questions may alter our ideas about patchiness, production, and trophodynamics in the ocean.

To attempt to answer some of these questions, two instruments were developed: FishTV (Jaffe *et al.*, 1995) and OSST (Optical Serial Section Tomography) (Palowitch and Jaffe, 1994, 1995). FishTV uses ultrasound (445 kHz) to locate micronekton (>1 cm) in a three-dimensional (3D) volume. OSST measures laser-stimulated fluorescence over a 70 × 70 cm sheet with 0.67-cm resolution. These instruments were profiled simultaneously, imaging the same water 30

miles west of San Diego in the southern California Bight. Here we focus on the relationship between the acoustic and optical depth profiles.

Methodology

FishTV

FishTV consists of a set of eight projecting transducers and eight receiving transducers that operate at a frequency of 445 kHz. Together, the transmitters and receivers form an 8 × 8 image with a field of view of 16 × 16°, at frame rates up to 4 Hz. Data reported in this article were obtained with the system operating at a frame rate of 2 Hz. Range resolution is ~2.5 cm. In a typical deployment mode, the system images a volume that starts at a range of 2.5 m and ends at 6.3 m range, giving a volume of ~6 m³. Individual locations of targets (echo counting) can then be computed accurately if densities are <40–50 m⁻³ (see below) (Jaffe *et al.*, 1995). The system has recently been used to track several hundred targets and infer properties about the trajectories of the animals (McGehee and Jaffe, 1996).

The sonar imaging system is calibrated over its entire field of view and therefore provides values of target strengths as a function of position. To register the presence of an animal, a threshold signal-to-noise ratio of the signal was used. If a reflection exceeded this threshold for several range cells (a sonar pulse extends for several range cells), an animal was judged to be present, and its position in 3D was recorded. Because the beam patterns of the system yield large readings in the area surrounding a target, even though no animals may be present, these regions were excluded from further analysis when a target was detected. Monte Carlo simu-

Jules S. Jaffe, Peter J.S. Franks and Andrew W. Leising, Scripps Institution of Oceanography, La Jolla, CA 92093-0238, USA.

lations of the ability of the system to correctly echo-count uniformly distributed targets indicate that this effect will have no significant influence on the estimated number of targets, up to densities of 40–50 m⁻³. At higher densities the system will undercount the number of individuals. A frame consists of the 3D positions and target strength of the set of animals that were in the field of view of the sonar system over a system cycle. Frames were indexed as a function of depth, so that the optical and sonar recordings could be cross-referenced. FishTV acquires images by pulsing a transmitting array sequentially. In this deployment an entire image was collected in 0.14 s.

Several issues need to be addressed in interpreting the sonar images and, in particular, assessing whether our estimates of animal densities are absolutely accurate. The short answer is that they are not; they are most certainly an underestimate of abundance. However, if the composition of the animal population does not change appreciably over the water depth, the relative abundance as a function of depth will be accurate. For example, Stanton *et al.* (1996) have shown in a recent survey of Georges Bank that taxa of similar sizes at the site had large differences in backscatter (e.g., gastropods versus crustaceans). This led them to conclude that they could not equate volumetric backscatter strength with biomass in a simple way. In our case, vertical net tows showed no evidence of gastropods or similar animals. Crustacean zooplankton were the primary source of acoustic variability. In addition, Deamer and Martin (1995) have shown that in using a narrow band sonar system, such as FishTV, care must be taken in equating the target strength measurements

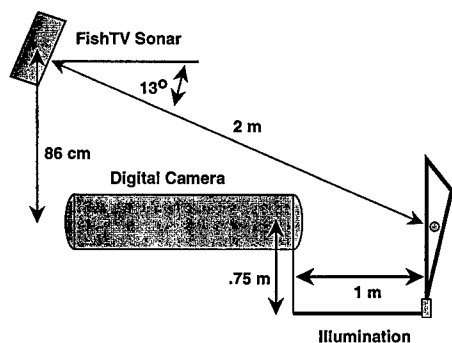


Fig. 1: A schematic diagram of the FishTV and OSST systems showing the geometric placement of the instruments.

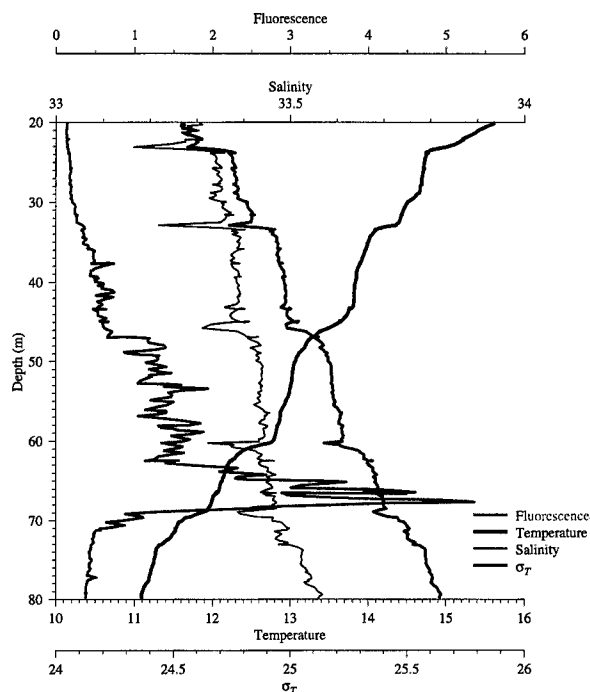


Fig. 2: A CTD/fluorometer profile taken 1 h before the simultaneous optical and sonar profiles were collected.

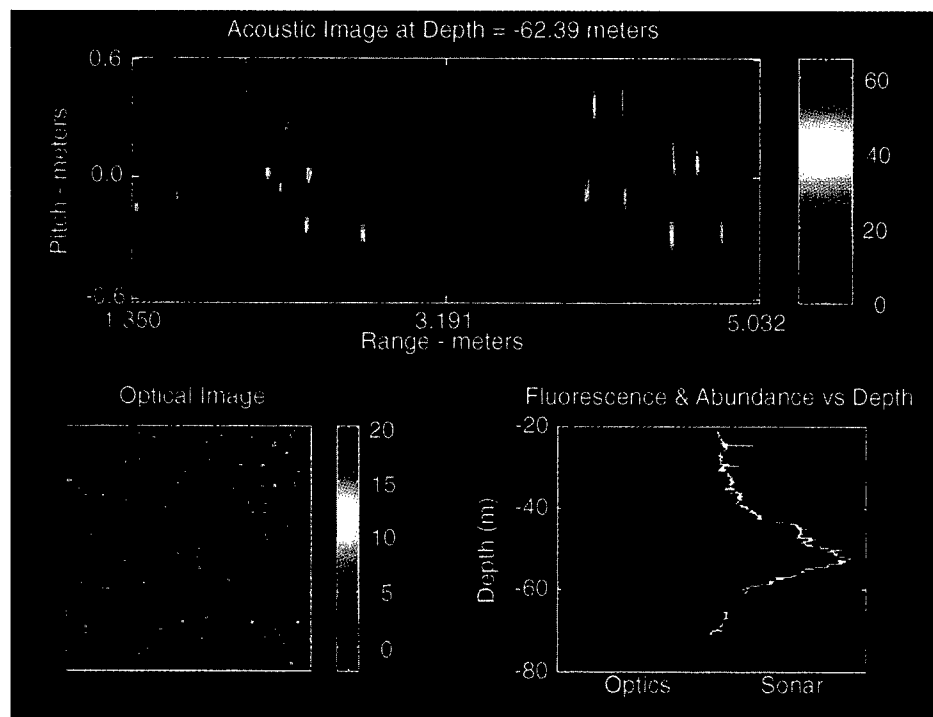


Fig. 3: Simultaneous display of sonar and optical raw data at 60 m depth: (a) a 2D image (a side-view projection) of the sonar data, (relative) target strengths of the objects are shown on the left-hand side of the frame, (b) one frame of optical data, and (c) simultaneous vertical profiles of the optical and acoustical data sets showing the location of the current frame (asterisk). Raw acoustic images were corrected for range spreading and unequal gains among transmitter-receiver pairs.

with animal size. This is because the backscatter pattern (frequency- and angle-dependent target strength) of the animals have 20–30 dB nulls that can lead to serious underestimation of animal size. Another complication is the animal orientation: animals viewed from the side reflect much more sound than those viewed head-on. Finally, our current algorithm does not perform subvoxel (voxel = 3D pixel) positional estimation, which leads to an underestimation of target strength. All of these effects tend to bias our results toward an underestimation of both animal abundance and target strengths. However, if animal orientations are not a function of depth, and the species composition is constant, our estimates are a good measure of *relative* abundance. Because species composition is likely to change as a function of depth, the target strength estimates that we derive cannot be correlated with animal size. On the other hand, the estimates of animal abundance will be valid.

Multibeam sonar systems such as FishTV allow finer resolution, or access to more resolution cells (in a given signal-to-noise level) than is possible using conventional technologies. Dual-beam systems do not allow 3D localization of acoustic targets, and both dual-beam and split-beam systems saturate at much lower animal densities than the multibeam system. This may preclude their use in many oceanic situations.

The acoustic data from a multibeam system yield information about both animal abundance and their locations through echo counting (counting of individual targets). At high animal densities, all acoustic systems will be unable to distinguish individual targets. At these densities, systems will switch from echo counting to echo integration, and no resolution of individual targets is possible. Echo counting is widely regarded as the most accurate measure of animal abundances (Stanton and Clay, 1986).

OSST

Data included in this manuscript represent the first at-sea results with the new optical imaging system. The optical system (OSST) measures laser-induced fluorescence by creating a sheet of illumination and photographing it with a very sensitive (10^{-5} lux) charge-coupled device (CCD) camera. Briefly, all lines below 520 nm of a ship-board argon ion laser were used for stimulation. The fluoresced light was then imaged with a CCD camera

(Photometrics, Tuscon AZ) with a long pass (>680 nm) filter on the lens. The laser sheet was positioned ~ 1 m in front of the camera/sonar package and aligned so that the plane of the image was parallel to the camera plane (Fig. 1). The field of view of the system was ~ 70 cm \times 70 cm over 102×102 pixels with a resolution of 0.67 cm and a frame rate of 0.9 Hz.

Combining the Instruments

The *R/V Sproul* was moored 30 miles west of San Diego in 300 m of water on 25–28 July. On the evening of 27 July, numerous vertical profiles were obtained by deploying both the FishTV and OSST systems, as well as temperature probes and a depth sensor. CTD profiles were also performed using a Sea Bird SBE19 CTD interfaced with a Wet Labs “Wet Star” fluorometer and a SeaTech 25-cm path length transmissometer. The instrument package consisting of OSST,

FishTV, and depth and temperature sensors was used to profile between 20 and 80 m. In Figures 2 and 3 addition, profiles with the CTD/fluorometer/transmissometer package were made on an hourly basis. In this article, the analysis from a set of four profiles made at 15-min intervals between 2040 and 2140 PST is presented. We estimate that registration between the sonar images and the optical images to 1 m was achieved, primarily limited by timing accuracies between the various computers that were collecting the information (future versions will resolve this issue).

The FishTV and OSST systems were both mounted on an aluminum frame that was profiled through the water column. Figure 1 shows the geometric configuration of the system that permitted the simultaneous acquisition of both the FishTV and OSST images. Of special note is that the small arm that generates

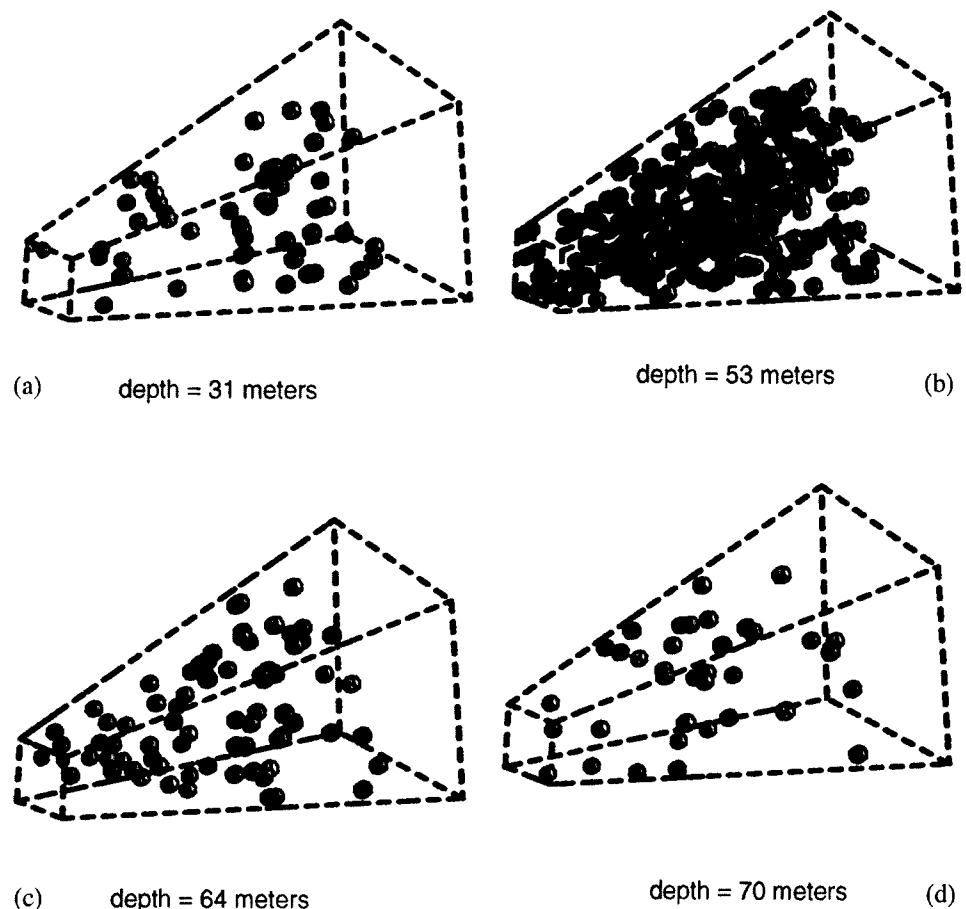


Fig. 4: Processed 3D locations of targets at depths of (a) 31 m, (b) 53 m, (c) 64 m, and (d) 70 m. The dashed line shows the volume imaged by the sonar, starting at 2.0 m and ending at 5.8 m. Targets varied between (a) -75 dB (red) and -85 dB (blue), (b) -67 dB (red) and -83 dB (blue), (c) -76 dB (red) and -83 dB (blue), and (d) -75 dB (red) and -83 dB (blue).

the laser sheet is in the acoustic shadow of the digital camera (with respect to the FishTV system). This configuration permitted an exact overlap of both the optical and acoustic images at a range of 2 m from the acoustic transducers and ~1 m away from the front of the digital camera case. The sonar was set so that targets starting at a range of 1.8 m away from the front of the sonar and ending 5.15 m away were imaged. This yielded a volume of ~3.4 m³ for the system.

Results

Data from the OSST and FishTV instruments were merged to produce profiles of chl-a fluorescence and animal abundance as a function of depth (Fig. 3). Optical data were averaged over each frame and interpolated onto 10 cm vertically spaced locations. The acoustic signal was binned by target strength; the signal plotted is the total number of hundreds of targets per 3.4 m³ with acoustic backscatter intensity greater than -85 dB (the smallest size class of targets; ~1 cm). All such acoustic data are plotted from each profile.

Vertical profiles made with the OSST and the CTD-fluorometer-transmissometer package showed similar small-scale (meters) features: a temporally persistent subsurface chlorophyll maximum layer at ~50 m (primary maximum), and a sharp (<5 m thick) transient peak centered around 60 m (secondary maximum; Fig. 3c). This secondary maximum was visible for ~8 h; calculations based on phytoplanktonic growth rates and grazing rates suggest that it was a patch that advected past our anchor site, rather than a feature that formed and dissipated *in situ* during that time. Profiles of acoustic targets showed a strong correlation with the fluorescence profiles with one major difference: there were almost no animals in the secondary (high chlorophyll, high variance) chlorophyll maximum. The numbers of animals peaked in the primary (lower chlorophyll, lower variance) maximum and decreased rapidly below.

The location of the individual targets at four depths (above the primary maximum, within the primary maximum, in the secondary maximum, and below the secondary maximum) reflect the relative absence of zooplankton from the secondary maximum (Fig. 4). These images can be compared with the corresponding optical images (Fig.

5), which show isotropic, random distributions of fluorescence down to scales of ~3 cm, with less variance than random at smaller scales. Although every effort was made to account for effects of the instrument package motion on these optical images, we cannot reject the possibility that they are an artifact of mixing by the instrument package or poor focus of the camera system. We feel it is likely, however, that these images rep-

resent the true, undisturbed state of the fluorescence microstructure, suggesting a very inhomogeneous distribution of fluorescence on microscales.

The mismatch between the fluorescence and acoustic signal is made obvious in a comparison of the four vertical profiles (Fig. 6). This mismatch is persistent over the sampling period (1 h). Target strengths in the secondary maximum are about equal to background levels (outside the fluorescence maxima). The

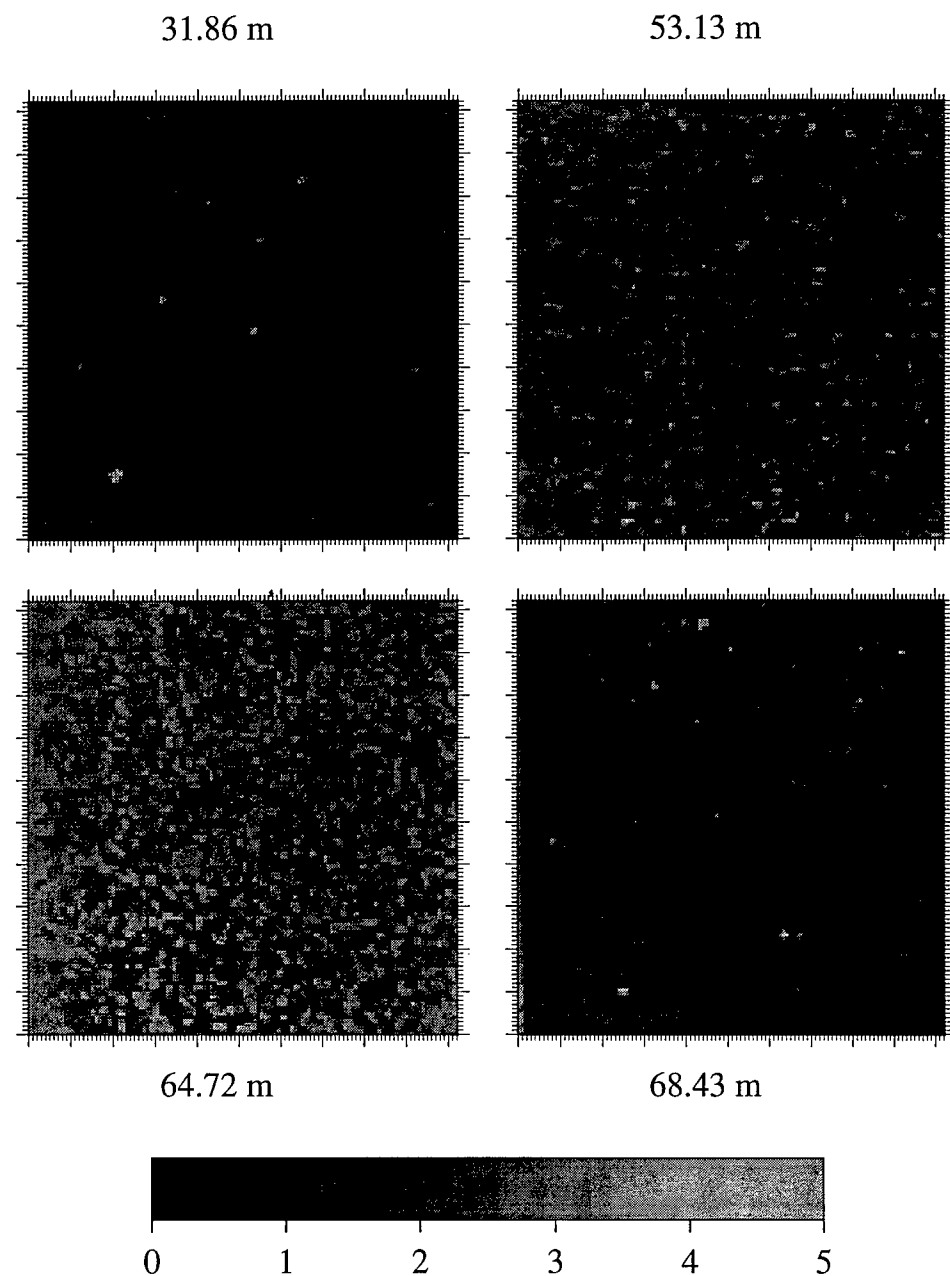


Fig. 5: Four images from the OSST, uncontaminated by ship heave. The images represent the different regions of the water column: 31.86 m is above the primary fluorescence maximum, 53.13 is in the primary fluorescence maximum, 64.72 is in the secondary maximum, and 68.43 is below the secondary maximum (see profiles in Fig. 2).

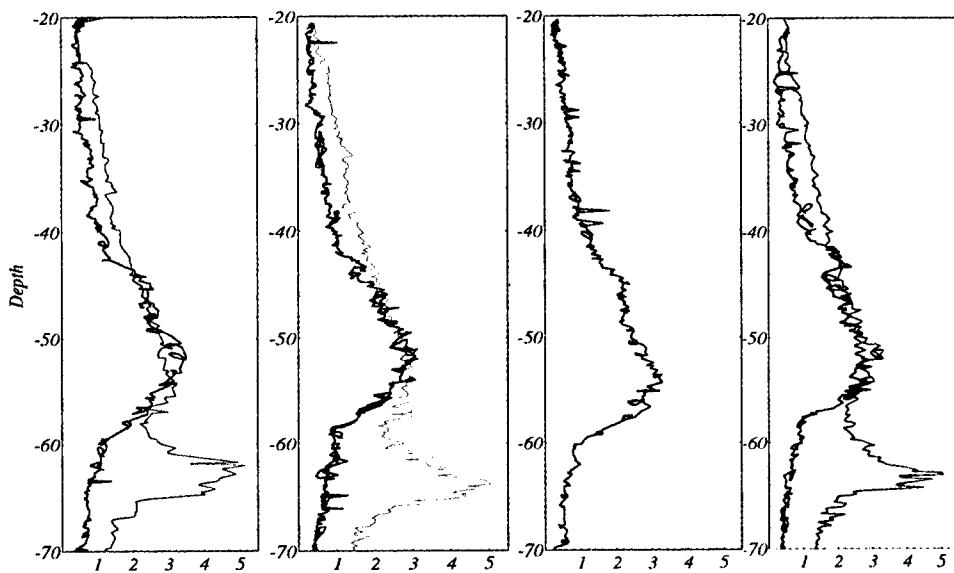


Fig. 6: A comparison of the four optical and acoustical depth profiles. The ordinate shows units in hundreds of animals/3.4 m³ for the acoustic data (in black) and units of relative fluorescence for the optical data (colored).

strong correspondence of the acoustic signal with the primary maximum is obvious in Figure 6. This is the relationship that would be predicted from a first-order model relating chlorophyll and herbivorous zooplankton.

Of the many points to consider in interpreting these data, perhaps the most important one is the effect of ship heave. Other analyses (not shown) demonstrated that small-scale observations were unaffected by the ship motions at the crest and trough of a heave cycle (4–5-s period). In addition, images where ship heave was prominent have average fluorescence values consistent with the fluorescence profile. In the case of the acoustics, because the time it took to collect an entire image was 0.14 s, and because the ship heave values were predominantly <50 cm s⁻¹ (98% of all values were <48 cm s⁻¹), the vertical translation of the platform was typically around 7 cm during the complete acquisition of a sonar image. In addition, because the image is raster scanned, the delay between adjacent beams is less than this amount. Because the beam widths of the system are only slightly more than this (6.3 cm) at 1.8-m range and substantially more (18 cm) at 5.15-m range (the furthest part of the field of view) the translation of the platform had a minor effect on the spatial patterns recorded by the FishTV.

A CTD profile taken ~1 h before the FishTV profiles (Fig. 2) shows a fairly

linear density profile with depth. The chlorophyll peaks at 50 and 65 m are each flanked by sharp gradients in temperature. These layers represent regions of high temperature gradient formed by straining of the temperature field by internal waves. The high horizontal velocities seen below 55 m (Franks and Jaffe, unpublished data) suggest that the secondary chlorophyll maximum was advecting horizontally much faster than the primary maximum (20–40 cm s⁻¹ versus 10–20 cm s⁻¹).

In addition to the sonar, optical, and CTD profiles, vertical net tows were performed with a single 50-cm diameter Bongo net with a 505-μm mesh. The results from a set of vertical hauls to various depths indicate that there was a layer of animals between 50 and 70 m. Estimates of the number of animals in the 1–10-mm size class were 40–50 m⁻³. Not surprisingly, the number of animals in the 1-cm and above class was very small due to net avoidance. The animal densities recorded by the system at the peak of acoustic reverberation were extremely high, and it is very likely that the system was undercounting the number of animals at this depth (54 m). Because of a lack of corroborating data, it is impossible to tell exactly what kind of animals were responsible for this peak of acoustic reflectivity; however, it does seem reasonable to assume that they were some type of micronekton.

Discussion

The data described in this paper represent the first at-sea results from the coupled acoustic/optical system. These data revealed surprising relationships between the small-scale distributions of phytoplankton and zooplankton. The phytoplankton showed a large amount of microscale (1–10 cm) heterogeneity. The zooplankton showed strong correlations with the “background” fluorescence (i.e., the primary, persistent subsurface fluorescence maximum) but did not show any corresponding enhancement in the most intense fluorescence peak.

One possible explanation for the high number of animal counts in the sonar images was that there was an extremely high number of smaller crustacean zooplankton, such as copepods, and that the sonar was recording a signal that was a superposition of echoes from this large number of animals. This hypothesis can be rejected by noting that the target strengths and densities of the smaller animals are not high enough to lead to the echo-intensities seen at 445 kHz. On the other hand, we cannot definitely say that only sonar reflections from micronekton were recorded, because other animals could have been present in the water column that were not sampled by our vertical net tows.

There are more questions created than answered by this first coincident, *in situ* view of fluorescence and acoustic targets in the ocean. Some of the most compelling directions for future research include measurements of smaller acoustic targets (i.e., higher frequency transducers), auxiliary sampling to test hypotheses about food quality and type, and a better understanding of the response of herbivorous zooplankton to microscale patchiness of their environment. Concurrent use of both optical and sonar imaging systems offers many potential advantages not only for *in situ* measurement of the spatial distribution and activity level of planktonic organisms but also for the “ground-truthing” of sonar systems. In a recent study, the OASIS system (Jaffe *et al.*, unpublished data) for mapping animals with sonar and simultaneous optical images of them was deployed in Saanich inlet and produced a set of data that yielded target strength information with concurrent optical animal identification. Hopefully the technology presented in this article and additional work by our

group and others will allow increased understanding of the behavioral responses of zooplankton to their environment and the importance of such dynamics in ensuring the transfer of matter and energy through the food web.

Acknowledgements

This project would not have been successful without the help of many dedicated people. Particular thanks are due to Greg Adelman and Ed Reuss, who did the bulk of the engineering on the OSST and FishTV systems. Mary Sisti cheerfully organized much of the cruise. Capt. Louis Zimm artfully piloted the *R/V R. G. Sproul*, and Tammi Koonce, Bob Wilson, and Fred Uhlmann were indispensable help in deploying the system. Alex DeRobertis and Adrienne Huston were a great help in sampling, and Dave Zawada processed much of the optical data. Thanks particularly to Eric Shulenberger, Ron Tipper, Steve Ackleson, and Jeff Simmen of the Office of Naval Research for encouraging this enterprise.

References

- Bjorenson P. K. and J. G. Nielsen, 1991: Decimeter scale heterogeneity in the plankton during a pycnocline bloom of *Gyrodinium aureolum*. *Mar. Ecol. Prog. Ser.* 73, 263-267.
- Cowles, T.J. and R.A. Desiderio, 1993: Resolution of biological microstructure through *in-situ* fluorescence emission spectra. *Oceanography*, 6, 105-111.
- , R.A. Desiderio and S. Neuer, 1993: *In situ* characterization of phytoplankton from vertical profiles of fluorescence emission spectra. *Mar. Biol.*, 115, 217-222.
- Deamer, D. and L. Martin, 1995: Zooplankton target strength: volumetric or areal dependence? *J. Acoust. Soc. Am.*, 98, 1111-1118.
- Derenbach, J.B., H. Astheimer, H.P. Hansen and H. Leach, 1979: Vertical microscale distribution of phytoplankton in relation to the thermocline. *Mar. Ecol. Prog. Ser.*, 1, 187-193.
- Herman, A.W., 1983: Vertical distribution patterns of copepods, chlorophyll, and production in north-eastern Baffin Bay. *Limnol. Oceanogr.*, 28, 709-719.
- , and T. Platt, 1983: Numerical modeling of diel carbon production and zooplankton grazing on the Scotian shelf based on observational data. *Ecol. Modeling*, 18, 55-72.
- Jaffe, J.S., M.D. Ohman and A. De Robertis, OASIS in the sea: Measurement of the acoustic reflectivity of zooplankton with concurrent optical imaging. *Deep-Sea Res.* In press.
- Jaffe, J.S., E. Reuss, D. McGehee and G. Chandran, 1995: FTV, a sonar for tracking macrozooplankton in 3-dimensions. *Deep-Sea Res.*, 42, 1495-1512.
- McGehee, D. and J.S. Jaffe, 1996: Three-dimensional swimming behavior of individual zooplankters: observations using the acoustical imaging system FishTV. *ICES J. Mar. Sci.*, 53, 363-369.
- Napp, J.M., E.R. Brooks, P. Matrai and M.M. Mullin, 1988: Vertical distribution of marine particles and grazers. II. Relation of grazer distribution to food quality and quantity. *Mar. Ecol. Prog. Ser.*, 50, 59-72.
- Palowitch, A.W. and J.S. Jaffe, 1994: Three-dimensional ocean chlorophyll distributions from underwater serial-sectioned fluorescence images. *Appl. Opt.*, 33, 3023-3033.
- , and J.S. Jaffe, 1995: Optical serial sectioned chlorophyll-a microstructure. *J. Geophys. Res.*, 100, 13,267-13,278.
- Saiz, E., P. Tiselius, P.R. Johnson, P. Verity and G.-A. Paffenhofer, 1993: Experimental records of the effects of food patchiness and predation of egg production of *Acartia tonsa*. *Limnol. Oceanogr.*, 38, 280-289.
- Stanton, T.S., D. Chu and P.H. Wiebe, 1996: Acoustic scattering characteristics of several zooplankton groups. *ICES J. Mar. Sci.*, 53, 289-295.
- , and C.S. Clay, 1986: Sonar echo statistics as a remote-sensing tool: volume and seafloor. *IEEE J. Oceanic Eng.*, OE-11, 1, 79-96.
- Tiselius, P., 1992: Behavior of *Acartia tonsa* in patchy food environments. *Limnol. Oceanogr.* 37, 1640-1651.
- , G. Nielsen and T.G. Nielsen, 1994: Microscale patchiness of plankton within a sharp pycnocline. *J. Plankton Res.*, 16, 543-554. □

ECOLOGY OF A *CHAETOCEROS SOCIALIS* LAUDER PATCH ON GEORGES BANK: DISTRIBUTION, MICROBIAL ASSOCIATIONS, AND GRAZING LOSSES

By Michael E. Sieracki, Dian J. Gifford,
Scott M. Gallager and Cabell S. Davis

THE PRESENCE OF PATCHES and layers in marine pelagic ecosystems may play an important role in providing food for higher trophic levels at concentrations high enough to support the metabolism, growth, and reproduction of the consumers. There has been a persistent enigma of average bulk water prey concentrations frequently being below that necessary for consumer growth, yet the consumer populations are observed to grow and persist (Lasker, 1975; Mullin, 1988). Concentrated patches or layers of prey organisms are not accurately sampled by traditional means such as net tows, bottle sampling, and even standard CTD and *in situ* fluorescence profiling.

The formation of a subsurface chlorophyll maximum (SCM) during the late spring and early summer in temperate waters is well established (Steele and Yentsch, 1960). This maximum is most likely caused by the combination of sinking of larger phytoplankton cells from surface waters following nutrient depletion, and the establishment of a seasonal pycnocline within the euphotic zone (Jarmart *et al.*, 1977). This combination of biological and physical factors probably controls the composition of the SCM and its vertical extent. In some cases the SCM could be vertically compressed enough to form a thin layer, on the order of several meters thick. It is likely that if such layers are common in the marine environment, consumers have adapted to

exploit this resource, and our observations, based on inadequately resolved sampling and average food concentrations over the water column, would lead to erroneous conclusions.

Chain-forming diatoms of the genera *Thalassiosira* and *Chaetoceros* often dominate the microphytoplankton on Georges Bank and in the Gulf of Maine during late spring and early summer. These organisms have been observed regularly since the survey cruises of Bigelow in the early part of this century (Bigelow, 1924). The assemblage in the Gulf of Maine can consist of >30 species of *Chaetoceros* alone (Lillick, 1940). More recent studies demonstrate that *Chaetoceros* is a dominant genera in coastal waters of the Northwest Atlantic (Marshall and Ranasinghe, 1989). These studies, using traditional methods, were designed to map large-scale features such as the entire Gulf of Maine, Georges Bank, or the coastal U.S. waters. Smaller scale features such as patches and layers of cells are not resolved. Such features are undoubtedly important from the organisms' perspective as the conditions for growth and loss due to grazing or senescence must operate at the spatial scale of the cells. New technologies, such as the video plankton recorder (VPR), permit resolution of plankton distributions *in situ* that approach biologically relevant scales (Davis *et al.*, 1992).

Chaetoceros sociales commonly occurs as chains wrapped into large, hollow spheroidal colonies (Rines and Hargraves, 1988). The colonies are large enough to be visible to the naked eye and can be easily confused with *Phaeocystis* colonies when viewed in bulk water samples without a microscope. The colonies

have been observed to contain a variety of epiphytic algae attached to their surfaces (J. Rines, personal communication).

We encountered an extremely dense and vertically compact patch of *C. socialis* colonies while making a transect with the towed video plankton recorder on the southern flank of Georges Bank in early June 1994 and 1995. It was observed again in late May 1997 using standard hydrographic methods. The patch was associated with the pycnocline located at the top of the "cold pool" (Houghton *et al.*, 1982) of water that flows in a southwest direction there along the southern flank of the Bank. The depth of the pycnocline, and associated patch, varied from 20 to 40 m in the region. The source and fate of the patch was not known. We report here our observations on the spatial structure of the patch, a previously undescribed microbial association within *C. sociales* colonies, and measurements of copepod grazing on the colonies.

Methods

The *C. socialis* patch was observed on the southern flank of Georges Bank in late May or early June of 1994, 1995, and 1997. To determine the distribution of the patch, two VPR tow-yo transects were made in 1995 (Fig. 1). The VPR methods used in this study are described in Davis *et al.* (1996). *C. sociales* was readily distinguishable in the VPR images by their shape, size, and texture (see Gallager *et al.*, 1996, Fig. 6G for example images). *Phaeocystis* colonies were seen in VPR images from other areas of the bank at different times of year, and their images had smoother outlines, smoother texture, and scattered less light

Michael E. Sieracki, Bigelow Laboratory for Ocean Sciences, W. Boothbay Harbor, ME 04575, USA. Dian J. Gifford, Graduate School of Oceanography, University of Rhode Island, Narragansett, RI, USA 02882. Scott M. Gallager and Cabell S. Davis, Woods Hole Oceanographic Institution, Woods Hole, MA, USA 02543.

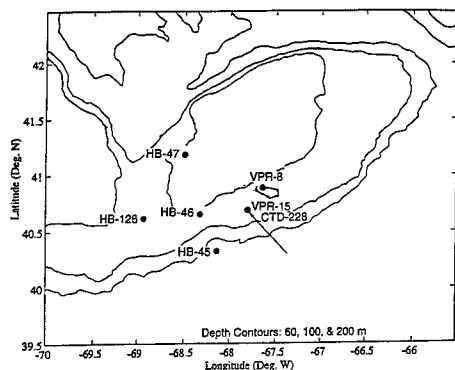


Fig. 1: The study site was on the southern flank of Georges Bank. Results are shown for two video plankton recorder transects (VPR-8 and VPR-15), and a CTD station (228) where water was collected for nutrients, chlorophyll, and plankton analyses as well as for the *Calanus* grazing experiment. Also shown are four stations (HB) sampled in 1920 by Henry Bigelow and referred to below.

than the *C. sociales* colonies. They tended to have prolate spheroid shapes, whereas the *C. sociales* colonies were more spheroidal in shape.

In 1997 colonies were collected from a station on the southern flank on 31 May in jars by scuba divers at 3-m-depth intervals through the layer of peak colony abundance. Colony counts were obtained directly from these jars by drawing multiple subsamples into the wide end of a glass 5 ml pipet and counting the colonies in it using a dissecting microscope (7.5 \times magnification) aboard ship. At least 100 colonies were counted from each depth.

In situ fluorescence, temperature, salinity, and transmissometry data were collected in addition to the video record of plankton distributions. The water column was sampled from depths of 5, 30, and 50 m using Teflon-lined Go-Flo bottles mounted on a CTD rosette. Samples were collected for analysis of major nutrients, chlorophyll, nanoplankton, and microzooplankton. Nutrients were analyzed with a Technicon Autoanalyzer-2 at the Marine Environmental Research Laboratory of the University of Rhode Island. Size fractionated chlorophyll (total, <20 and <5 μ m) was analyzed using a Turner Designs model 10 fluorometer. Nanoplankton were analyzed by fluorescence imaging cytometry (Sieracki *et al.*, 1993), and microzooplankton were preserved with 10% (v/v) acid Lugol's solution, settled into counting chambers and

Depth, m	SiO ₃ , μ M	PO ₄ , μ M	NO ₃ + NO ₂ , μ M	NO ₂ , μ M	POC, μ g L ⁻¹	Chlorophyll, μ g L ⁻¹
5	0.89	0.20	1.77	0.08	179	3.31
30	1.33	0.26	1.54	0.08	364	1.17
50	1.05	0.10	0.99	0.06	493	0.84

analyzed using a Zeiss Axiovert inverted microscope at a magnification of 200 \times .

The colony matrix proved to be extremely delicate. Colonies were found only in water that was gently siphoned out of the top of Go-Flo bottles through wide diameter silicone tubing. Samples collected from the spigot at the bottom of the bottles did not contain intact colonies, nor was the colony matrix preserved in acid Lugol's samples. Water for the copepod grazing experiment (Gifford, 1993) was siphoned gently from the top of the 30-m Go-Flo bottle. Individual female *Calanus finmarchicus* were picked live from a 333- μ m vertical net tow and added to replicate bottles containing the *in situ* assemblage including *C. sociales* colonies. Control bottles consisted of the assemblage without copepods. Bottles were wrapped in neutral density screen to recapitulate *in situ* light intensity and incubated on-deck on a plankton wheel whose temperature was maintained by flowing seawater. Bottles were harvested at times zero and 24 h and sampled for nanoplankton and microzooplankton prey as well as chlorophyll. The carbon content of individual copepods was measured using a Carlo Erba Model NA1500 elemental analyzer. Clearance rates were calculated using the equations of Frost (1972). Ingestion rates were calculated according to Marin *et al.* (1986).

Results and Discussion

Water Column Properties and Community Structure

The water column was stratified with respect to both salinity and temperature. The water temperature was 10.5°C at the surface and 6.6°C at 30 m. The fluorescence maximum and transmission minimum associated with the *C. sociales* patch were located between ~20 and 40 m. Nutrient measurements indicate that southern flank waters were relatively replete (Table 1). Silicate was somewhat depleted at the surface relative to deeper

water, but phosphate and nitrate were higher in surface waters. Similarly, chlorophyll was higher in surface water than at 30 or 50 m, suggesting that the 30 m Go-Flo bottle did not sample the maximum of the subsurface *Chaetoceros* patch. The area was hydrodynamically active due to tides and currents, and it was difficult to trigger the bottle closings within the *C. sociales* layer.

Phototrophic nanoplankton were larger and more abundant at the surface than at 30 or 50 m (Table 2). This resulted in a biomass (calculated from counting and sizing cells) at 5 m of 44 μ gC/l, double that of the biomass at 30 and 50 m. Heterotrophic nanoplankton showed a maximum in abundance at 30 m. Nanoplankton cells were smaller at this depth, so their biomass was relatively even through the water column (Table 2). Ciliate microzooplankton were more abundant by a factor of 4 in the *C. socialis* layer than in the upper water column (Table 3).

Chaetoceros sociales Distribution. The VPR#15 was an on-bank to off-bank tow that transected the *C. sociales* patch. Peak colony abundances were closely associated with the top of the subsurface chlorophyll maximum near 25 m (Fig. 2A), and the colonies persisted throughout the SCM. Colonies were correlated with *in situ* fluorescence ($r^2 = 0.80$, Fig. 2B). Colonies, although not quantified for the entire length of the tow, became more

Table 2
Population abundance, mean cell size, and biomass of phototrophic and heterotrophic nanoplankton (2–20 μ m) at CTD 228

	Depth, m	Cell Abundance, No. ml ⁻¹	Mean Cell Biovolume, μ m ³	Biomass* μ gC L ⁻¹
Phototrophs	5	3,074	65	44
	30	1,856	53	22
	50	1,816	50	20
Heterotrophs	5	1,605	65	23
	30	2,162	45	22
	50	1,319	69	20

*Calculated assuming a cell carbon density of 220 fg C μ m⁻³.

abundant farther along the tow where they caused a “white-out” of the video screen and saturated the fluorometer sensor (Fig. 3). Colony concentrations sufficient to cause the video screen to be filled are estimated to be ~2,000–3,000 per liter, so this is a minimum estimate of the peak colony concentration along this tow. *C. sociales* remained the dominant organism in the VPR images from the chlorophyll maximum depths for at least 20 km along this on-bank to off-bank track. In VPR#8 (Fig. 4) the patch was intersected at a depth of ~20 m at the southeast end of the “U”-shaped tow track. Both tows showed that the patch was narrowly compressed in the vertical, ranging in thickness from 5 to 15 m. The extent of the patch along the bank (in the approximately east-west direction) was not determined.

In 1997 direct counts of the colonies in the fluorescence maximum layer showed densities ranging from 1,900 to 3,300 per liter (Fig. 5). The peak abundance corresponded to peaks in *in situ* fluorescence and beam attenuation. It was located above the 1% light level and at a density gradient formed primarily by colder water below ~20 m.

Microscope observations of individual colonies. Live individual colonies were examined under phase and fluorescence illumination using a compound microscope (with vibration isolation) aboard ship (Fig. 6). The chlorophyll in the *C. sociales* cells appeared brightly fluorescent (Fig. 6A) and dividing cells were common in the chains. There were very few attached epiphytes (Fig. 6B) as might be seen in senescent colonies. These observations gave the impression of relatively healthy, growing diatoms. Examination of about a dozen colonies at higher magnification (40× objective), revealed the presence of several heterotrophic protistan cells near the center of each colony, or the center of each lobe of multilobed colonies (Fig. 6, C and D).

Typically there were between 2 and 10 cells, each ~6–8 μm in diameter attached to the setae of the diatom near where they converge in the colony center. The protozoans were not morphologically distinctive at this magnification. Due to the jumble of setae at the colony center it was not apparent exactly how the protozoa were attached. They did not appear to be choanoflagellates, or have distinctive cell walls or appendages. Every colony examined contained these cells, and they were only seen near the colony center. Only occasionally were other cells observed attached or associated with the colonies. A few colonies were observed to have a single pennate diatom on their periphery, as has been observed on *Phaeocystis* colonies and on the setae of a variety of diatoms, including *C. sociales* (Taylor, 1982 and references therein). Flagellates were occasionally seen swimming through a colony. diaminodiphenylindole (DAPI) staining of colonies revealed abundant, large (~1 μm) bacteria growing within the colonies on the setae. These were presumably growing on dissolved organic matter released by the diatom. These bacteria may be the food source for the heterotrophic protozoa found in the colony centers. In this case each colony may be a microbial consortia of interdependent organisms.

The observed regular pattern of a small number of similar cells located within every *C. sociales* colony suggests what may be a species-specific epi-symbiotic association. Such associations are common in tropical marine waters and in freshwater ponds and lakes (Taylor, 1982), where various ciliates, flagellates, and dinoflagellates have been observed attached to setae and cell walls of diatoms, including other species of *Chaetoceros*. To our knowledge this particular association has not been described in the literature. It is similar, however, to an observation reported by Elbrachter and Boje (1978) of the diatom *Thalas-*

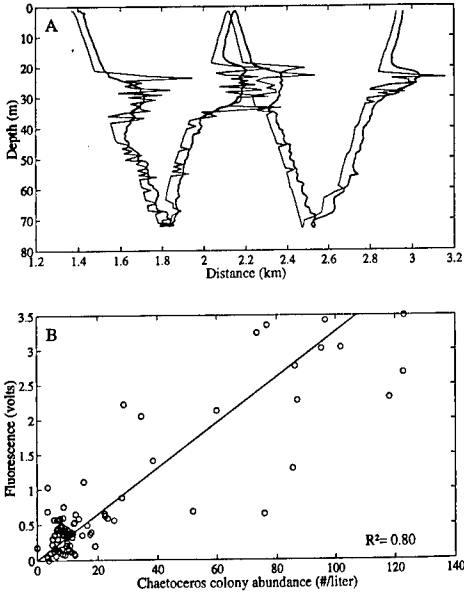


Fig. 2: (A) Vertical profiles of *C. sociales* colonies as determined from VPR images (thin line), and in situ fluorescence (thick line) from the first two tow-yos from the VPR#15 transect. Values of colony abundance and fluorescence are added to the x-variable (position). The maximum value for *Chaetoceros* colony abundance in these two tow-yos is 228 per liter. The minimum value is zero (i.e., none seen in focus in a 2-s interval). The maximum fluorescence value is 4.27 and the minimum is 0.62 (volts). (B) Linear regression of in situ fluorescence versus colony abundance. The *Chaetoceros* data have been smoothed with a low-pass filter for comparison with the fluorometry data. The minima were subtracted from all values of both fluorescence and colony abundance to yield a $y = mx$ regression model.

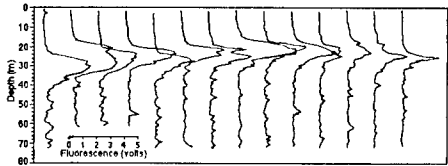


Fig. 3: Sequence of vertical profiles of in situ fluorescence taken from the beginning of VPR tow #15. These alternating up and downcasts from the first hour of the tow have been offset by equal intervals to separate the profiles and show the sharpness of the subsurface chlorophyll maxima. The distance between successive profiles is ~500 m, and the total distance shown is ~6.4 km. Note the progressive sharpening of the peak along the transect and that the sensor was saturated at the peak of the eighth profile.

Table 3
Abundance of microzooplankton (cells per liter) at CTD station 228

Depth, m	Aloricate Ciliates, 5–20 μm	Aloricate Ciliates, >20 μm	Thecate Dinoflagellates*	Mesodinium	Athecate Dinoflagellates†	Ceratium sp.
5	1,008	288	324	414	540	643
30	5,058	756	72	594	216	126
50	2,682	306	18	396	162	144

*Heterotrophic cells, mostly *Protoparidinium* sp. †Heterotrophic cells including *Gymnodinium* and *Gyrodinium* sp.

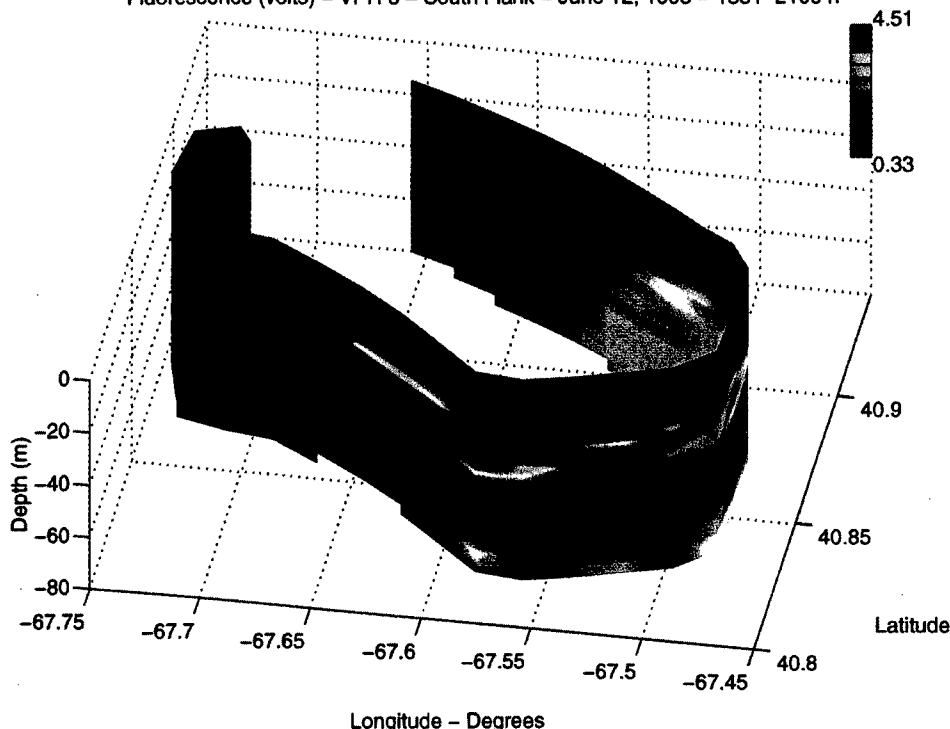


Fig. 4: Vertical section of in situ fluorescence along VPR tow #8. This section intersected the *C. socialis* patch at its southeastern end where high fluorescence was seen between ~20 and 30 m.

siosira parthenoia, which forms hollow, cylindrical colonies with threads in the center. Small protozoa were observed in the center of these colonies that were found in high numbers in the Northwest African upwelling region. In contrast to the *C. socialis*, colonies these were colonized by a diverse assemblage of eukaryotic cells, including dinoflagellates, ciliates, amoeba, and pennate diatoms, as well as bacteria. Waterbury and Caron (1987) observed this *T. parthenoia* consortium in Gulf Stream waters in the western North Atlantic.

Chlorophyll content and biomass of colonies. Individual *C. socialis* colonies contained a mean of 250 pg chlorophyll per colony (range: 120–490, $N = 45$). Phaeopigment concentration was relatively high, averaging 800 pg per colony. Using a carbon to chlorophyll ratio of 50, this would yield an average carbon content of 12.5 ngC colony⁻¹. Assuming a concentration of colonies of 2,000 L⁻¹ at its peak, that would mean the *C. socialis* patch contained up to 25 $\mu\text{gC L}^{-1}$, a biomass about equal to that of the phototrophic nanoplankton in the vicinity (Table 2).

Copepod grazing rates on *C. socialis* colonies. *Calanus finmarchicus* females

cleared 4.92 ± 4.42 (SD) ml copepod⁻¹ h⁻¹ of total chlorophyll and 6.21 ± 2.84 ml copepod⁻¹ h⁻¹ on the >20- μm fraction, which was dominated by the *C. socialis* colonies. The ingestion rate of chlorophyll is equivalent to $44.7 \mu\text{gC copepod}^{-1} \text{ day}^{-1}$, or 52.7% of copepod body carbon. The copepods cleared nanoplankton and microzooplankton at rates of 6.62 ± 7.92 and 24.03 ± 11.06 ml copepod h⁻¹, respectively, equivalent to ingestion of 2.51 and 1.39 $\mu\text{gC copepod}^{-1} \text{ day}^{-1}$. Ingestion of heterotrophic prey accounted for 3.90 $\mu\text{gC copepod}^{-1} \text{ day}^{-1}$. Total per capita ingestion of autotrophic and heterotrophic prey was 48.6 $\mu\text{gC copepod}^{-1} \text{ day}^{-1}$, equal to 57% of copepod body carbon day⁻¹, sufficient to support basic metabolism, growth, and reproduction.

Conclusions

An extensive patch of colonial *C. socialis* was observed on the southern flank of Georges Bank in June of 1994, 1995, and 1997. Bigelow (1924) described a similar patch of *C. socialis* below 20 m in the same vicinity 75 years prior (17 May 1920) “congregated in such numbers that even the coarse-meshed net came back clogged” (stations HB46 and

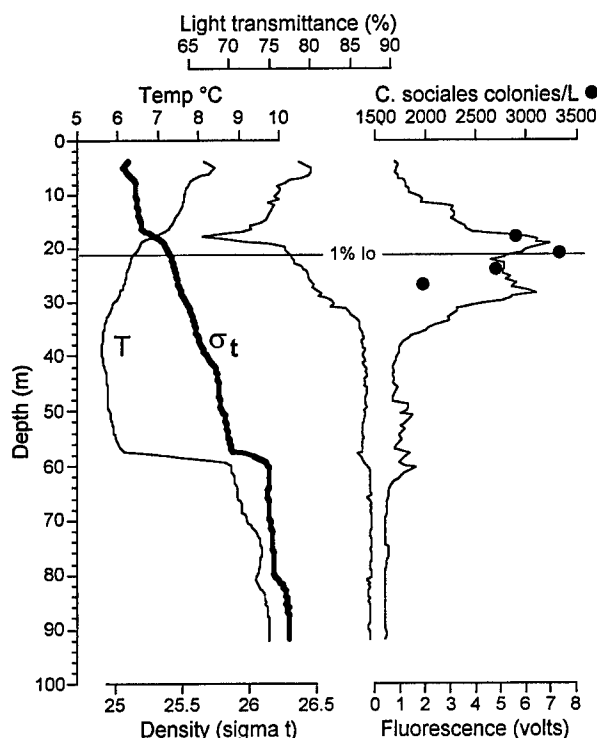


Fig. 5: Vertical profiles of temperature, density, beam attenuation, in situ fluorescence, and counts of *Chaetoceros socialis* colonies collected by scuba diving on 31 May 1997. The depth of the 1% light level is shown (1%lo). The coefficient of variation for the replicate colony counts ranged from 18 to 40%.

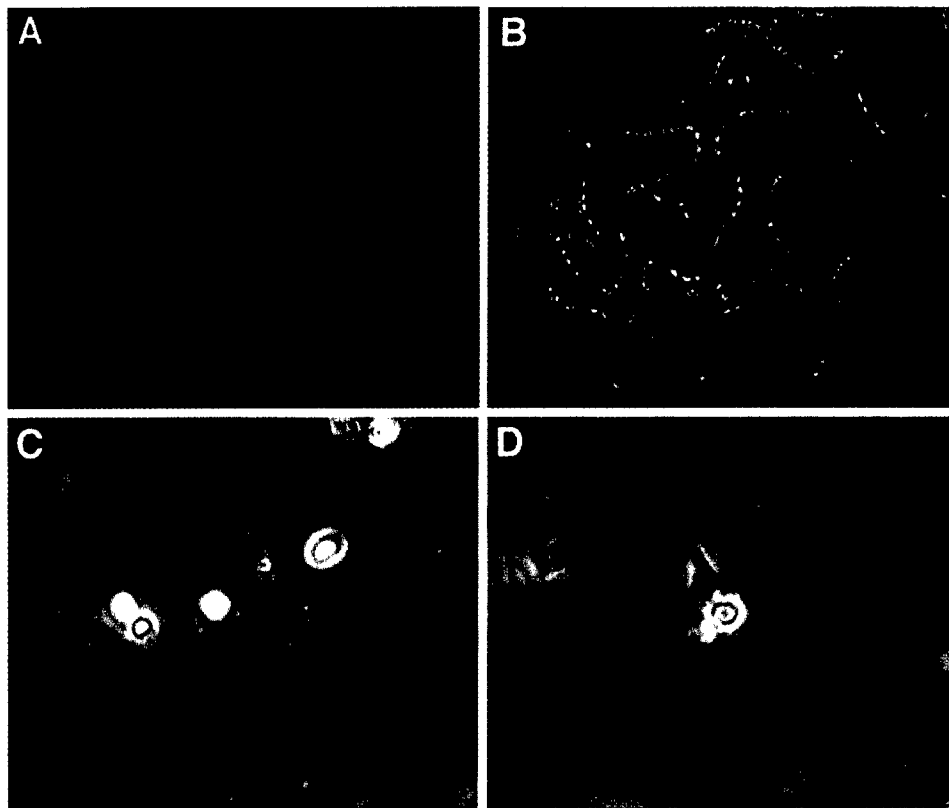


Fig. 6: Colony structure of *C. sociales* observed on the southern flank of Georges Bank. (A) Fluorescence micrograph of a colony showing its tertiary structure. (B) Transmitted phase illumination of a colony. Each colony had one or two of the larger distinctive diatom cells like that near the center of this image. (C and D) At the center of each colony, or lobe of multilobed colonies, the setae converge, and a small consortia of protozoa resides there. Between one and seven protozoan cells were observed at each center. Scale bars are 50 μm in A and B, and 10 μm in C and D.

HB128, Fig. 1). In contrast, Sears (1941) conducted a survey of the phytoplankton composition on Georges Bank from March to June and did not report the presence of *C. sociales*, indicating that there are years when it does not occur in such abundance. More continuous yearly observations would be required to determine whether the presence or absence of the patch in late spring and early summer is the more common yearly phenomenon. If it were found to occur regularly every year, the *C. sociales* patch could act as an indicator of the physical, chemical, and biological conditions necessary for its concentration on Georges Bank over time scales that are relevant to climate change effects.

Colony density in the patch was on the order of several thousands per liter. There was a distinctive consortia of protozoa and bacteria at the center of each colony, at the convergence of the diatom setae. Female *C. finmarchicus* grazed on the colonies, as evidenced by the disap-

pearance of chlorophyll in the $>20\text{-}\mu\text{m}$ fraction, and on the nano- and microzooplankton located in the layer. The observed ingestion is well in excess of the daily respiratory requirement for *C. finmarchicus* females, suggesting that the *C. sociales* patch and its associated nano- and microplankton fauna provided a concentrated food resource in the water column. This result bears on the persistent enigma of average food levels in marine pelagic ecosystems where bulk water column concentrations of prey organisms are frequently inadequate to support the metabolic needs and growth of their consumers, yet the consumer populations grow and persist (e.g., Lasker, 1975; Mullin 1988). The presence of patches and layers as a source of concentrated prey for higher order consumers may well explain this paradox. The copepod's grazing activity may also impact the patch in terms of maintaining at least its upper boundary (assuming the lower boundary is set by the pycnocline).

At the average density observed with the VPR of 450 individual *C. finmarchicus* m^{-3} , the copepods would clear 7% of the water in the patch on a daily basis. At the maximum density of 2,500 m^{-3} , 38% per day of the water would be cleared, suggesting that the impact of grazing by *C. finmarchicus* alone may significantly impact the structure and dynamics of the patch.

Acknowledgements

The research was supported by the National Science Foundation (award numbers OCE-9313678 to D.J.G., OCE-9313679 to M.E.S., OCE-9313671, and OCE-9632596 and ONR grant N00014-93-1-0602 to S.M.G. and C.S.D.). We thank E. Horgan, J.R. van Keuren, S. Plourde, P. Altalo, C. Ashjian, and A. Girard for assistance at sea, the captain and crew of the *R.V. Endeavor*, and F.J.R. Taylor for helpful discussions. US GLOBEC Contribution 94.

References

- Bigelow, H.B., 1924: Plankton of the offshore waters of the Gulf of Maine. *Bull. U.S. Bureau Fisheries*, 40, 1-509.
- Davis, C.S., S.M. Gallager and A.R. Solow, 1992: Microaggregations of oceanic plankton observed by towed video microscopy. *Science*, 257, 230-232.
- , S.M. Gallager, M. Marra and W.K. Stewart, 1996: Rapid visualization of plankton abundance and taxonomic composition using the video plankton recorder. *Deep-Sea Res. II*, 4, 1947-1970.
- Elbrachter, M. and R. Boje, 1978: On the ecological significance of *Thalassiosira partheneia* in the Northwest African upwelling area. In: *Upwelling Ecosystems*. R. Boje and M. Tonczak, eds. Springer-Verlag, Berlin, 24-31.
- Frost, B.W., 1972: Effects of size and concentration of food on feeding behavior of the planktonic copepod *Calanus pacificus*. *Limnol. Oceanogr.*, 17, 805-815.
- Gallager, S.M., C.S. Davis, A.W. Epstein, A. Solow and R.C. Beardsley, 1996: High-resolution observations of plankton spatial distributions correlated with hydrography in the Great South Channel, Georges Bank. *Deep-Sea Res. II*, 4, 1627-1663.
- Gifford, D.J., 1993: Consumption of protozoa by copepods feeding on natural assemblages. In: *Handbook of Methods in Aquatic Microbial Ecology*. P.J. Kemp, B.F. Sherr, E.B. Sherr and J.J. Cole, eds. Lewis Publishers, Boca Raton, FL, 723-729.
- Houghton, R.W., R. Schlitz, R.C. Beardsley, B. Butman and J.L. Chamberlain, 1982: The middle Atlantic Bight cold pool: evolution of the temperature structure during 1979. *J. Phys. Oceanogr.*, 12, 1019-1029.
- Jamart, B.M., D.F. Winter, K. Banse, G.C. Anderson and R.K. Lam, 1977: A theoretical study of phytoplankton growth and nutrient distri-

- bution in the Pacific Ocean of the northwest U.S. coast. *Deep-Sea Res.*, 24, 753-773.
- Lasker, R., 1975: Field criteria for the survival of anchovy larvae: the relation between inshore chlorophyll maximum layers and successful first feeding. *Fish. Bull.*, 73, 453-462.
- Lillick, L.C., 1940: Phytoplankton and planktonic protozoa of the offshore waters of the Gulf of Maine. Part II. Qualitative composition of the planktonic flora. *Trans. Amer. Phil. Soc.*, 31, 193-237.
- Marin, V., M.E. Huntley and B.W. Frost, 1986: Measuring feeding rates of pelagic herbivores: analysis of experimental design and methods. *Mar. Biol.* 93, 49-58.
- Marshall, H.G. and J.A. Ranasinghe, 1989: Phytoplankton distribution along the eastern coast of the U.S.A. VII. Mean cell concentrations and standing crop. *Cont. Shelf Res.*, 9, 153-164.
- Mullin, M.M., 1988: Production and distribution of nauplii and recruitment variability—putting the pieces together. In: *Toward a Theory on Biological-Physical Interactions in the World Ocean*. B. Rothschild, ed. Kluwer Academic Publications, Boston, MA, 297-342.
- Rines, J.E.B. and P.E. Hargraves, 1988: The *Chaetoceros* Ehrenberg (Bacillariophyceae) flora of Narragansett Bay, Rhode Island, U.S.A. *Bibliotheca Phycologica* 79, J. Cramer, Berlin.
- Sears, M., 1941: Notes on the phytoplankton on Georges Bank in 1940. *J. Mar. Res.*, 4, 247-257.
- Sieracki, M.E., P.G. Verity and D.K. Stoecker, 1993: Plankton community response to sequential silicate and nitrate depletion during the 1989 North Atlantic spring bloom. *Deep-Sea Res. II*, 40, 213-225.
- Steele, J.H. and C.S. Yentsch, 1960: The vertical distribution of chlorophyll. *J. Mar. Biol. Assoc. U.K.*, 39, 217-226.
- Taylor, F.J.R., 1982: Symbioses in marine microplankton. *Ann. Inst. Oceanogr.*, 58, 61-90.
- Waterbury, J.B. and D.A. Caron, 1987: Microbiology. In: *The Marine Environment of the U.S. Atlantic Continental Slope and Rise*. J.D. Milliman and R.W. Wright, eds. Jones and Bartlett Publishers, Boston, 140-151. □

FINESTRUCTURE, MICROSTRUCTURE, AND THIN LAYERS

By Thomas Osborn

WE ARE ALL FAMILIAR with the irregular profiles from modern, high resolution conductivity-temperature-depth profilers (commonly called CTDs) freely falling vertical profilers, and towed thermistor chains (Figs. 1 and 2). In fact sufficient resolution was available back in the 1930s with the advent of the Bathythermograph (BT) (Eckart, 1948) and even earlier through the use of the thermocouple (Schmidt, 1914; and Hacker, 1933). Figures 3 and 4 show thin layers of biological material. Fish and copepods which swim can easily form layers, but what about some of the particles which are very small, neutrally buoyant, and only swim slowly, if at all. Are their profiles related to the temperature, density, or their gradients? The easily measured profiles of temperature, salinity, density etc., carry a signature of the relevant physical processes. How much do they tell us about the formation of the biological and chemical layers?

Microstructure refers to the signatures of oceanic turbulence at scales where molecular viscosity and diffusion are important. Quantitative measurements at these scales (millimeters to centimeters) provide estimates of the cross-isopycnal diffusion rates. Finestructure is the label for larger features where the stratification limits the motion to the horizontal plane. Signatures of this stirring motion have horizontal scales substantially greater than their vertical scales. Eckart (1948) created the paradigm of stirring and mixing, which shows the significance of the predominantly horizontal flow field, and the boundary conditions, in producing these irregular vertical distributions and layers.

Thin layers are superficially like the physical finestructure features in thickness and extent. This similarity is a result of the

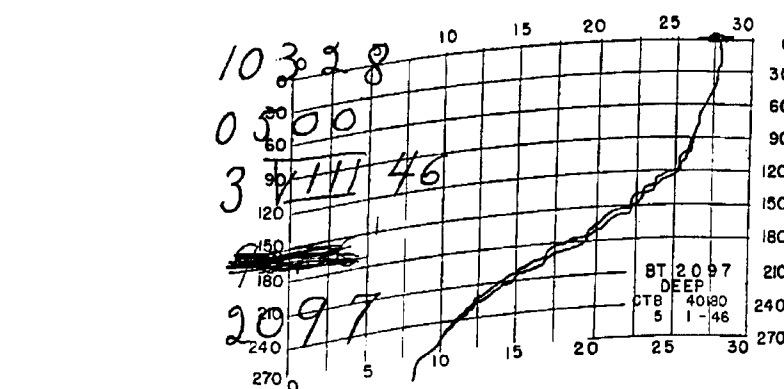


Fig. 1: Bathythermograph trace from Eckart (1948) showing temperature finestructure.

density stratification which forces most of the motion to be horizontal and makes sharp vertical gradients out of weak horizontal gradients. In fact, it is useful to consider thin layers as the biochemical equivalent of the finestructure in temperature, salinity, or density, with the caveat that the biological and chemical layers are forced by biochemical processes as well as physical processes. The biochemical processes interact and

couple with the physical processes. However, while the coupling of processes may bind the biochemical layers to temperature, salinity, or density layers, it is the vertical shear of the horizontal currents in conjunction with the horizontal gradients that have a major role in forming both thin layers and finestructure. Since the horizontal variations of biological, chemical, and physical parameters can differ significantly, there is no a

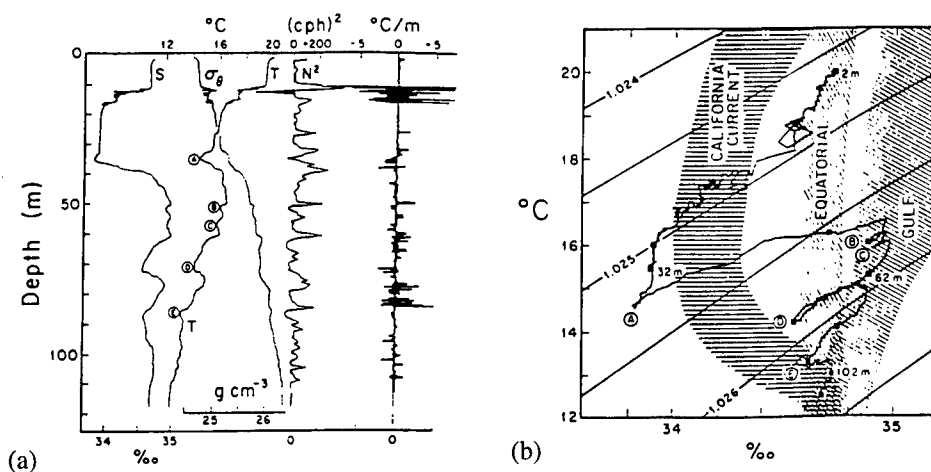


Fig. 2: (a) Temperature, salinity, and potential density averaged over 0.03 m off Cabo San Lucas showing a multitude of intrusions and finestructure features (modified figure from Gregg 1975). N^2 is averaged over ~ 0.8 m to show the finestructure in the density. The temperature gradient has not been smoothed, showing how the variance is at the microstructure scales and the finestructure is not visible without averaging. (b) T-S diagram showing the different water masses in the region that contribute to the vertical profile.

Thomas Osborn, Department of Earth and Planetary Sciences, The Johns Hopkins University, Baltimore, MD 21218-2681, USA.

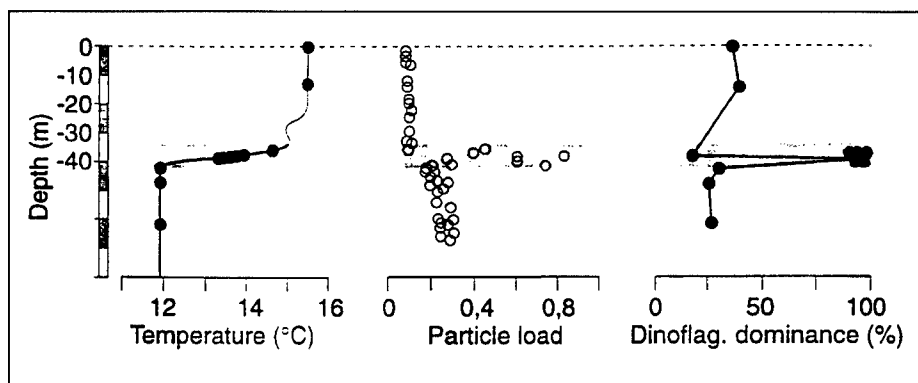


Fig. 3: Vertical profiles of La Rochelle, France, with an *in situ* particle size profiler after Gentien *et al.* (1995) showing temperature, particle load, and percentage of dinoflagellates (% total phytoplankton). The closed and open circles are the locations of water samples.

priori reason for thin layers and fine structure features to be firmly locked together. Crucial, first order, measurements include the vertical profile of the horizontal velocity with resolution at the vertical scale of the thin layers and finestructure in conjunction with the variation in horizontal and vertical distributions of the biological, chemical, and physical fields.

Carl Eckart: Stirring and Mixing

In his early and very insightful paper, Eckart related the finestructure in temperature profiles collected with a BT, to the physical processes of stirring and mixing. Stirring of the fluid is accomplished by the spatial variations of the velocity and has two effects (Fig. 5). First, it increases the interfacial area between water parcels with different characteristics, and, second, it increases the property gradients across those interfaces. Both of these effects increase the rate of transport by molecular diffusion. When molecular diffusion smoothes out all the spatial variations, the fluid becomes uniform, i.e., well mixed. Mixing is molecular diffusion removing the inhomogeneities created by the stirring.

Microstructure and Finestructure

Finestructure and microstructure are both signatures of the stirring. Microstructure is at the smallest scales, where molecular viscosity significantly affects the flow, and finestructure at larger scales where stratification is important (Gargett *et al.*, 1984).

Microstructure has scales that range from tens of centimeters downward, and the measurements are usually in terms of derivatives with respect to a spatial coor-

dinate. The variance of the derivatives is concentrated at these scales and, for the case of velocity shear, determines the energy dissipation. Also, at these small scales the effect of stratification is limited, and the flow approaches isotropy. Both the temperature and velocity microstructure measurements produce estimates of the vertical eddy diffusivity (Osborn and Cox, 1972; Osborn, 1980), which compare favorably with direct measurements (Toole *et al.*, 1994; Ledwell *et al.*, 1993). This direct and quantitative application of the microstructure measurements has probably been a major reason why so much effort has been focused on microstructure for the last 25 years.

Finestructure as a term seems to apply to any wiggle or irregularity in a temperature, salinity, or density profile that can be seen by a CTD with vertical resolution of a meter. Fedorov (1978), in the introduction to the English edition of his book, uses the term "fine stratification," and the editor, J.S. Turner, identifies the generally accepted English equivalent as "finestructure." The signatures are interpreted as layers of the water extending much further horizontally than vertically. These features can be generated *in situ* by vertical mixing, they can be the result of intrusions from adjacent water masses, or they can be the ephemeral signatures of internal waves. In any case, they are the result of relative motion in the water. The T-S diagram (a plot of temperature against salinity) is a useful tool in separating intrusive finestructure from the effects of local mixing or internal waves Ochoa (1987).

Finestructure can be identified either by looking at the property directly or at

the gradient profile (Grant *et al.*, 1961), if the gradient has been smoothed either by averaging the data or by using a sensor with limited frequency response. Full spectral resolution of the derivative reveals the microstructure scale variations that often obscure the mean trend. In Figure 2 the density profile and the N^2 profile was averaged over 0.8 m vertically and shows the finestructure, while the temperature gradient profile reveals the microstructure. Looking at finestructure with vertical gradient profiles involves an implicit averaging scale. The averaging scale is often not specified because it is "buried" in the details of the observing instrument and its role in how the data appears to the observer may not be appreciated.

Given that finestructure appears in both temperature and "averaged" gradient profiles, we must bear in mind that the two views of the same water are very different. First, an intrusion is usually thicker than its edges, at least the high gradient portion of its boundaries, so that while the temperature trace has one thick intrusion of order ≤ 10 m, the gradient profile sees two thinner boundaries, on the order of 1 m vertically. Again, Figure 2 has a nice example of a 20 m thick salinity minimum that is much less obvious from the profile of N^2 . Second, although finestructure in the temperature and its gradient arise due to spatial variations in the temperature and velocity field, we will see that the way in which these phenomena cause temperature finestructure is not the same manner by which they cause finestructure in the temperature gradient. When we compare biological and chemical thin layers to the finestructure, we must be careful to recognize the different mechanisms for generating the finestructure.

Eckart's Analysis

Eckart started from the heat equation (neglecting solar heating) written in tensor notation (i.e., summation over repeated indices) but no Reynolds' decomposition.

$$\frac{D\vartheta}{Dt} = \kappa \frac{\partial^2 \vartheta}{\partial x_i \partial x_i} \quad \text{with} \quad \frac{D}{Dt} = \frac{\partial}{\partial t} + u_i \frac{\partial}{\partial x_i} \quad (1)$$

where ϑ is the temperature, κ the molecular diffusivity for heat, i and j ($=1, 2$, or 3) are indices, x_i are the three coordinate axes ($i = 1$ is the x axis, $i = 2$ is the y

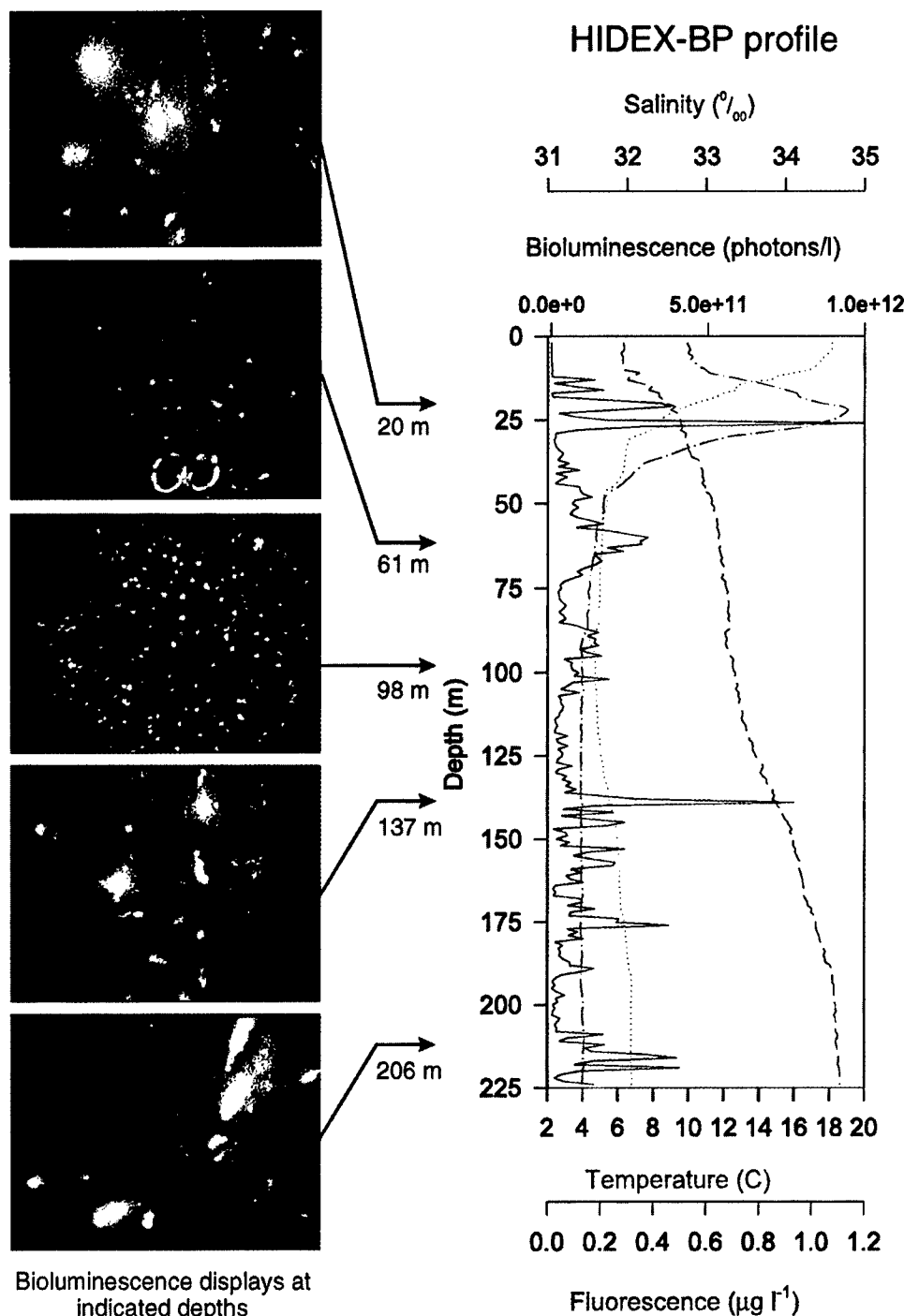


Fig. 4: Profile of bioluminescence from the Gulf of Maine (Widder, 1997). Individual video frames (1 m wide) at the indicated depths show the different displays associated with the peaks in bioluminescence. At 20 and 137 m, the picture is characteristic of copepods. At 61 and 98 m, there are dinoflagellates. At 61 m there is a lobate ctenophore and at 206 m a cydippid ctenophore.

axis, and $i = 3$ is the z axis) and u_i is the water velocity vector (whose components are u_1 , u_2 , and u_3 , which correspond to u , v , and w in regular notation).

Because of the advective term, the gradient operator and the total derivative operator do not commute, but rather:

$$\frac{\partial}{\partial x_j} \frac{D}{Dt} = \frac{D}{Dt} \frac{\partial}{\partial x_j} + \frac{\partial u_i}{\partial x_j} \frac{\partial}{\partial x_i} \quad (2)$$

and

$$\frac{D}{Dt} \frac{\partial \vartheta}{\partial x_j} = \kappa \frac{\partial}{\partial x_j} \frac{\partial^2 \vartheta}{\partial x_i^2} - \frac{\partial u_i}{\partial x_j} \frac{\partial \vartheta}{\partial x_i} \quad (3)$$

Multiplying by the gradient gives:

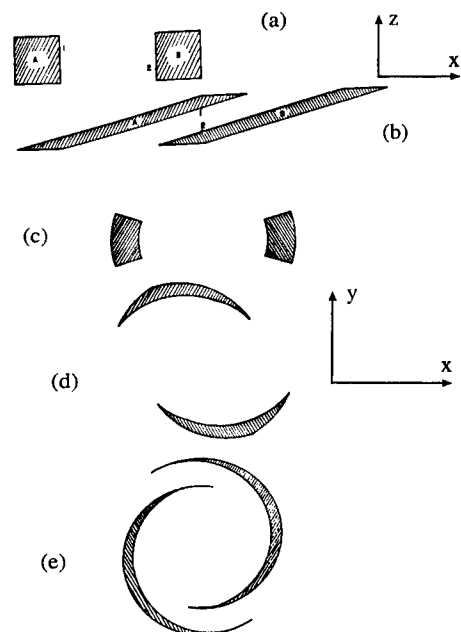


Fig. 5: Schematic after Eckart (1948) showing (a and b) the effect of a laminar, vertical shear on two adjacent water parcels. The shear converts a horizontal variation into a strong vertical difference. The stirring increases the gradient and the interfacial area between the parcels. A circular eddy (c, d, and e) can increase lateral gradients, as long as the motion is not a pure rotation. Given the stratification of the ocean, a circular eddy is likely to be horizontal and may well involve vertical shear.

$$\frac{1}{2} \frac{D}{Dt} \left(\frac{\partial \vartheta}{\partial x_j} \right)^2 = \kappa \frac{\partial}{\partial x_j} \left(\frac{\partial \vartheta}{\partial x_j} \frac{\partial^2 \vartheta}{\partial x_i \partial x_i} \right) - \kappa \left(\frac{\partial^2 \vartheta}{\partial x_i \partial x_i} \right)^2 - \frac{\partial u_i}{\partial x_j} \frac{\partial \vartheta}{\partial x_i} \frac{\partial \vartheta}{\partial x_j} \quad (4)$$

Define the following by taking integrals over a volume of fluid.

$$\begin{aligned} G^2 &= \iiint \left(\frac{\partial \vartheta}{\partial x_j} \right)^2 d\tau \\ I^2 &= \iiint \left(\frac{\partial^2 \vartheta}{\partial x_i \partial x_i} \right)^2 d\tau \\ S &= \iiint \frac{\partial u_i}{\partial x_j} \frac{\partial \vartheta}{\partial x_i} \frac{\partial \vartheta}{\partial x_j} d\tau \end{aligned} \quad (5)$$

G^2 and I^2 cannot be negative quantities.

As we follow that volume of fluid along its path, the following equation holds:

$$\frac{1}{2} \frac{d}{dt} G^2 = \iint_{\text{boundary}} \hat{n} \cdot \nabla \vartheta \frac{D\vartheta}{Dt} d\sigma - \kappa I^2 - S \quad (6)$$

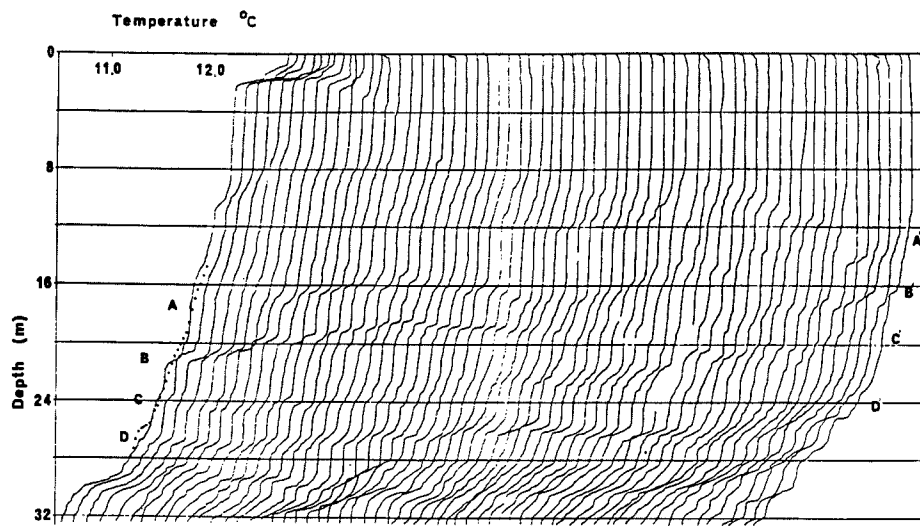


Fig. 6: From Lazier (1973) showing the time variability of the finestructure due to internal waves. The profiles of temperature versus depth have a common depth axis, but each successive profile is displaced to the right by 0.108°C . The dotted line at the left represents the average profile over the 12 h of observation.

where \hat{r} is an outward pointing, unit vector at the boundary.

The magnitude of the gradient can change for three reasons: 1) heat flux and temperature change on the boundary, 2) molecular diffusion, and 3) spatial variations in the motion.

Because κ and I^2 are both positive quantities, molecular diffusion cannot increase the magnitude of the gradient. Thus, aside from a combination of a heat flux and temperature change at the boundary, the magnitude of the gradient can only increase due to motion. Interestingly enough, vorticity is not required.

Because,

$$\frac{\partial u_i}{\partial x_j} = \frac{1}{2} \left\{ \frac{\partial u_i}{\partial x_j} + \frac{\partial u_j}{\partial x_i} \right\} + \frac{1}{2} \left\{ \frac{\partial u_i}{\partial x_j} - \frac{\partial u_j}{\partial x_i} \right\} \quad (7)$$

and the second term, which is half the vorticity, is antisymmetric while the rest of the integrand is symmetric:

$$S = \frac{1}{2} \iiint \left\{ \frac{\partial u_i}{\partial x_j} + \frac{\partial u_j}{\partial x_i} \right\} \frac{\partial \vartheta}{\partial x_i} \frac{\partial \vartheta}{\partial x_j} d\tau. \quad (8)$$

Following that derivation, Eckart used a simple example.

At $t = 0$, $\vartheta = ax + bz + c$, and there is only horizontal motion in the x direction.

$$\frac{\partial \vartheta}{\partial t} + u(z) \frac{\partial \vartheta}{\partial x} = \kappa \nabla^2 \vartheta \quad (9)$$

If we start from a situation like Figure 5, with large enough spatial scale that molecular effects are negligible initially, then the solution to the above equation and boundary conditions is:

$$\vartheta \equiv \vartheta_0 = a[x - u(z)t] + bz + c$$

and

$$\frac{\partial \vartheta}{\partial z} = b - at \frac{\partial u}{\partial z}. \quad (10)$$

For a while the magnitude of the vertical component of the temperature gradient can increase or decrease, depending on values of a , b , and $\partial u/\partial z$, but eventually the time-dependent term will dominate and the magnitude of the gradient will increase. As the stirring continues and the gradient becomes stronger, the importance of the molecular diffusivity term increases and will, eventually, have to be taken into account. Then the balance will include the destruction of gradient variance by molecular diffusion. Eckart points out that there is no general proof that the magnitude of the gradient will always increase continually, noting that a velocity that oscillates in time would produce a gradient that oscillates in time. A prescient foreshadowing of the reversible finestructure caused by internal waves seen in Figure 6 from Lazier (1973).

The derivation of Eckart's shows that the velocity field and the boundary conditions generate the structure in both the temperature and the temperature gradient profiles. The same derivation also applies to a nonreactive chemical compound, including salinity, the only change being to replace the thermal diffusivity by the appropriate chemical diffusivity. Now we see why in frontal regions the salinity and temperature profiles, and especially their finestructure, don't track each other (e.g., Fig. 2). The T-S relation is a melange of different water types, another way of saying the boundary conditions and horizontal gradients are different for temperature and salinity. Thus, the stirring of velocity field produces different results. An injected patch of dye with a different initial distribution from either the temperature or salinity would also evolve a profile and finestructure that differed from the temperature, salinity, and their gradients. Kullenberg's (1974) experiments show the time development of such dye patches and the effects of shear in creating finestructure layers.

It is important to note that the intrusion of a layer into a vertical profile can occur due to the vertical shear over an extended vertical region rather than advection of just the "intruding layer." Intrusions can appear because of shear, not just by the interleaving of adjacent water bodies. The shear produces layers from what were previously horizontal differences. Given the large amount of velocity shear and the spatial heterogeneity of the coastal ocean, it is not surprising that there is structure in the physical and biological parameters. Intrusions that cross isopycnals (Gregg and McKenzie, 1979) can also arise from shear in a stratified region with large horizontal gradients.

Thin Layer Generation

It is necessary to differentiate between biological thin layers and chemical thin layers composed of reactive compounds. Organisms obey a conservation equation similar to the heat equation but with sources and sinks due to biological processes. They have the possibility of motion relative to the water but lack the molecular diffusion term. Reactive chemical elements also satisfy a slightly different conservation equa-

tion allowing for chemical reactions as well as molecular diffusion (Eckart, 1940). For the sake of simplicity, we will consider the biological layer with the concentration specified as $n = n(x, y, z, t)$ in units of numbers per unit volume. There is summation over the repeated subscripts.

$$\frac{\partial n}{\partial t} + \frac{\partial}{\partial x_i} (nV_i) = \gamma \quad (11)$$

The velocity of the organisms is $V_i = V_i(x, y, z, t)$ (absolute velocity in space, not relative to the water), and γ , is the net rate of production of the species. The velocity of the species relative to the flow is

$$v_i = V_i - u_i. \quad (12)$$

Here u_i is the water velocity, the same meaning as in the earlier derivation. The relative motion can arise from swimming, sinking/rising due to buoyancy differences, slippage relative to the flow due to inertia, or the effects of finite size leading to relative motion.

The flux of particles relative to the water is

$$J_i = (nv_i). \quad (13)$$

γ can be written as the sum of two terms, the cell division (birth) rate and the mortality rate. These are frequently written as proportional to the local concentration, although there is no requirement that the factors of proportionality are constant in time or space. Let's define the local production rate of cells = $\mu \cdot n$, and the local mortality rate of cells = $m \cdot n$.

Rearranging and using the equation of continuity $\partial u_i / \partial x_i = 0$.

$$\frac{Dn}{Dt} = \mu \cdot n - m \cdot n - \frac{\partial J_i}{\partial x_i} \quad (14)$$

There is biological generation and disappearance of organisms, and their motion relative to the water can be convergent or divergent, i.e., $\partial J_i / \partial x_i \neq 0$. Both of these mechanisms lead to local increases or decreases in concentration while following the same patch of water. The only way to have a large group of some species in a given parcel of water is for them to have grown there or to have moved relative to the water. In terms of Eckart's picture of the initial conditions in Figure 5a, that state could be generated by growth

and/or aggregation. There is no diffusion of the organisms due to the potentially turbulent water motion because, as in the previous derivation of Eckart, there has been no decomposition of the flow into a "mean and fluctuating part." Therefore, following the flow means tracking the original water parcel no matter how convoluted it becomes. Advection can change the concentration at a fixed location, but it does not change the concentration in a given parcel of water.

The reference frame of a stationary observer, a mooring, a specific vertical profile, or a fixed sampling grid, is on the Eulerian reference frame. Then the time rate of change of the concentration at the fixed point is the partial derivative with respect to time, which in expanded form is:

$$\frac{\partial n}{\partial t} = \mu \cdot n - m \cdot n - \frac{\partial J_x}{\partial x} - \frac{\partial J_y}{\partial y} - \frac{\partial J_z}{\partial z} - u \frac{\partial n}{\partial x} - v \frac{\partial n}{\partial y} - w \frac{\partial n}{\partial z} \quad (15)$$

The fixed observer is measuring $\partial n / \partial t$ and the advective term, $-u(\partial n / \partial x) - v(\partial n / \partial y) - w(\partial n / \partial z)$, appears to be a "source" of organisms. The profiles in Figures 3 and 4 are in the framework of a fixed observer. The thin layers seen there may have grown *in situ*, be due to aggregation from relative motion, or may be due to the lateral intrusion of water already containing high concentrations of those particles. This lateral intrusion can be accomplished by a sheared flow as shown by Eckart's schematics in Figure 5. A thin layer could also be produced by the erosion of a thicker layer (this would be an advective effect, the carrying away of water and particles) through predation or some other form of enhanced mortality rate. As well, physical processes affect birth rate, mortality, and relative motion. The coupling of physical processes back into biological rates and activities means that μ , m , and the J 's are all functions of position and time, as well as the history of the organism and its environment.

Discussion and Conclusions

Compare equation (15) to the equivalent version of equation (1) and equation (3) written explicitly for the vertical component of the temperature gradient.

$$\frac{\partial \theta}{\partial t} = \kappa \left(\frac{\partial^2 \theta}{\partial x^2} + \frac{\partial^2 \theta}{\partial y^2} + \frac{\partial^2 \theta}{\partial z^2} \right) - u \frac{\partial \theta}{\partial x} - v \frac{\partial \theta}{\partial y} - w \frac{\partial \theta}{\partial z} \quad (16)$$

and

$$\begin{aligned} \frac{\partial}{\partial t} \left(\frac{\partial \theta}{\partial z} \right) &= \kappa \left[\frac{\partial^2 \left(\frac{\partial \theta}{\partial z} \right)}{\partial x^2} + \frac{\partial^2 \left(\frac{\partial \theta}{\partial z} \right)}{\partial y^2} + \frac{\partial^2 \left(\frac{\partial \theta}{\partial z} \right)}{\partial z^2} \right] \\ &\quad - \frac{\partial u}{\partial z} \frac{\partial \theta}{\partial x} - \frac{\partial v}{\partial z} \frac{\partial \theta}{\partial y} - \frac{\partial w}{\partial z} \frac{\partial \theta}{\partial z} \\ &\quad - u \frac{\partial}{\partial x} \left(\frac{\partial \theta}{\partial z} \right) - v \frac{\partial}{\partial y} \left(\frac{\partial \theta}{\partial z} \right) - w \frac{\partial}{\partial z} \left(\frac{\partial \theta}{\partial z} \right) \quad (17) \end{aligned}$$

The temperature changes because of molecular diffusion and advection while the vertical component of the temperature gradient has comparable terms plus the additional one due to the shearing of the velocity. The equation for the time development of the density of organisms (Eq. 15) looks much like the temperature equation, without molecular diffusion, but with the addition of birth, mortality, and relative motion. Thus the distribution of temperature, salinity, their gradients, and biological concentrations are all strongly affected by the local, time-dependent, velocity distribution as well as the large scale sources and sinks for temporal and spatial variability (e.g., fronts, river discharge, storms). It is appropriate to think of thin layers as "biological finestructure" because there is the strong role of the advection, but we must also bear in mind the dissimilar aspects of the source and sink terms.

All three equations contain advection. The temperature and temperature gradient equations also contain a molecular diffusion term. There is no term comparable with molecular diffusion in the particle equation because there is no requirement for the biological concentration to diffuse at the molecular level. However, the equation for biological concentrations contains a divergence term, $\partial J_i / \partial x_i$, which has a similar mathematical form to the heat flux but with no constraint that the flux be down gradient because the biological term involves behavior. The temperature gradient equation contains terms involving products of the velocity and temperature derivatives. These terms can generate or remove finestructure.

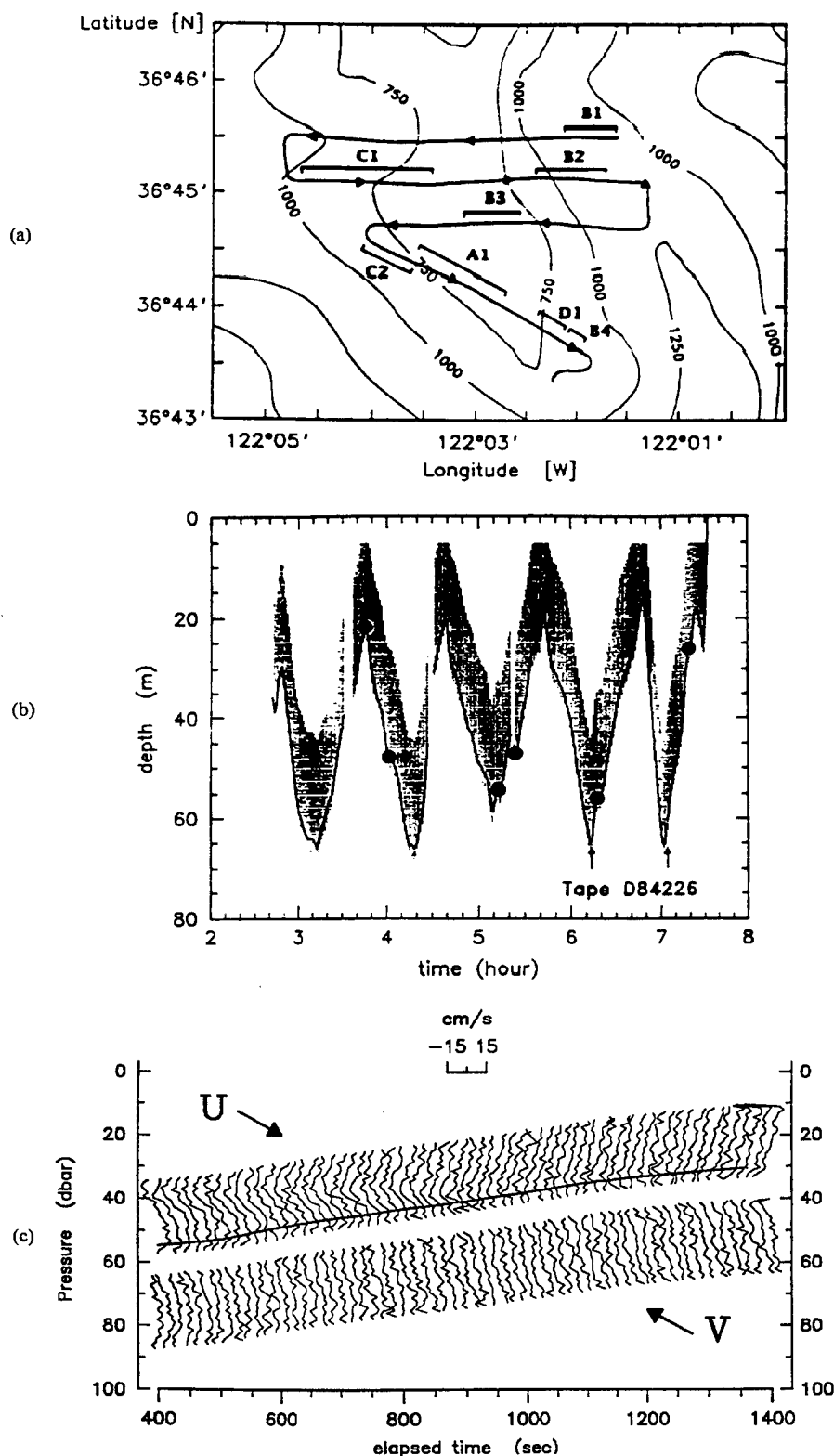


Fig. 7: (a) Track pattern of the submarine Dolphin in Monterey Bay. The labeled brackets refer to different shear layers. (b) Pressure profile during the dive. The filled circles correspond to changes in heading shown in a. The shaded region indicates the range of the acoustic Doppler profiler. (c) Time series of 15-s average velocity profiles with a 1-m vertical sample interval, for the rising portion of the southeastward leg in a. The horizontal axis is elapsed time. U is along the axis of the submarine, and V is perpendicular to the axis of the vessel. The U profiles are plotted at the correct depth, whereas the V profiles have been shifted down 30 m for clarity of the display. Note the extensive shear apparent in the U velocity component from the start of the record to time 950 s (from Itsweire et al., 1989). This shear layer is labeled C2 in a.

The particle equation contains birth and mortality, which do not appear in the temperature gradient equation. Because these terms represent a source/sink in the interior of the volume of the fluid, they are mathematically similar to the terms for the generation/destruction of finestructure by shear in the temperature gradient equation. Again, however, they have a large behavioral component and are not just a signature of the physical processes. As well, the source/sink need not be spatially co-located with the generation of temperature gradient finestructure.

Because the effect of the advection depends on the velocity field and the distribution of the concentration (temperature, salinity, density, or particles), there is no *a priori* reason why the temperature/salinity/density finestructure or their gradient finestructure should line up with the finestructure of biological layers. Some alignment is inevitable because both are subject to the same velocity field, which is dominantly horizontal. But the fact that the physical and biological/chemical parameters are layered does not mean that the layers actually coincide. It is even more difficult to see why a nonswimming organism (or a chemical species) would align with the gradient finestructure, because there are significantly different source terms for the different features. Detailed resolution of the shear versus depth with resolution comparable with, or better than, the scales of the thin layers and finestructure is crucial.

The preceding analyses avoided the question of "turbulent diffusion" and the possible destruction of finestructure and thin layers by turbulent mixing. Such an analysis is possible (Donaghay and Osborn, 1997). It produces additional divergence terms (arising from the advective terms) in equation (15), which would spread the layer, depending on the spatial distribution of the turbulence relative to the layer or finestructure. Turbulent diffusion can be incorporated into equations (16) and (17) by increasing the molecular diffusivity. However, that analysis is pushing the theoretical framework because the motion that produces the microstructure and finestructure is the turbulent mixing. When we consider all these processes, there is no longer the separation of scale necessary for the Reynolds decomposition into mean and fluctuating

parts. Work on thin layers and fine-structure brings us into the temporal and spatial scales where the streakiness of the horizontal stretching and the cross-isopycnal (essentially/almost vertical) transport by the turbulence are active and interactive. Again, we are asking, how does the velocity field interact with the vertical and horizontal distribution of the other parameters in the water column?

If, as Eckart's paradigm suggests, shear is the forcing for much finestructure and thin layers, where does it come from? Two important sources are tidal currents and inertial currents. In coastal waters, these motions are sheared and rotate their direction with time, which makes it unlikely that they produce reversible finestructure. Itsweire and Osborne (1988) and Itsweire *et al.* (1989) observed layers ≥ 10 m thick where the shear exceeded 10^{-2} s^{-1} , and rotated in the horizontal plane at the local inertial frequency (Fig. 7). In such a flow, points that start initially with only a vertical separation of 10 m, will be 1 km apart horizontally in just 3 hours. Those shear layers were probably some form of near-inertial motion, and therefore the shear propagated vertically and horizontally. As such, it could generate finestructure features at different depths as it moved through the water column. Information about the spatial and temporal distribution of the vertical velocity shear in the water column at the vertical scales of thin layers and finestructure is difficult to procure. Ship-mounted acoustic doppler current profilers (ADCPs) with sufficient resolution for those shear layers haven't had sufficient range to reach below the upper layer. Surface waves induce significant vertical displacement of the vessel. Moorings give a time series but don't show the spatial distribution. Technological developments are improving the situation, but the measurements are still sparse.

If we consider the index of papers in the *Journal of Physical Oceanography* since its inception, the relative dearth of papers on finestructure compared with microstructure is striking. I would suggest this situation is due to the combination of observational difficulty and the lack of a quantitative structure for the application of the results. I know from personal experience that it is much easier to make and operate one mi-

crostructure instrument than to produce and operate simultaneously several finestructure profilers. Thermistor chains, which give beautiful two-dimensional cuts through the ocean, are also very difficult to produce, calibrate, and operate (Mack, 1989).

Thin layers and finestructure are difficult to sample and resolve, given their three-dimensional and highly time-dependent nature. A good description of thin layers is needed. We need to have a good three-dimensional description and to compare and contrast measurements of the fine-scale physical processes at the same time in order to ascertain the spatial distributions and the interrelationships between the biological fields, the physical/chemical fields, the local advection, and turbulence. This is a first step in identifying the processes and interactions. What are the temporal and spatial scales?

1) *Vertical scales.* How thin are the layers? Although this question is easy to ask and seems appropriate for descriptive purposes, great care must be taken that it is approached in an appropriate context. One of the early questions about finestructure was how thin do the layers become. The answer is that the layers become thinner and thinner as you look more closely, but the dynamics also become different. Somewhere below the 1-m vertical scale, the phenomena becomes small-scale turbulence and not the lateral layers with aspect ratio on the order of 1,000 that were being studied. One is easily sucked down this path because it is the same measurement (usually temperature gradient), and so you naturally think it is the same process as one goes to finer and finer scales.

2) *Horizontal scales.* How far do thin layers extend? Are they continuous, or do they have holes or are just broken into quasi-continuous patches? What are the growth and mortality rates? How are the distributions related to the density profile, the temperature profile, finestructure features, and the occurrence of turbulence?

3) *Time scales.* How long do they last? Are they related to tidal and inertial processes. How quickly do they form? Short time scales (in a Lagrangian framework) suggest aggregation over growth.

4) *Stratification.* How are thin layers related to the density surfaces? Do they cross density surfaces? Are some thin

layers examples of the accumulation of particles at density interfaces?

The fascinating measurements by Kulenberg (1974) show the variability of the signatures from the spreading and layering of dye patches. Due to the passive nature of the dye, this variability arises from physical processes alone. When biological processes combine and interact with this situation, there will be strong coupling between the physical, biological, and chemical processes. Turbulence affects organisms directly through their survival rates, reproduction rates, feeding rates, and predation rates. Internal waves and convection in the upper layer affect the light history and growth of phytoplankton by advecting them into, and out of, favorable environments. When looking at the dynamics of thin layers, it will be important to relate the growth and mortality of the organisms to the basic physical parameters. These include not just temperature, light, and nutrients, but also local turbulence levels and history, local shear, and internal wave activity, as well as the mean circulation. The coupling of biological and physical processes will be rich.

Acknowledgements

This paper would have been impossible without the insight provided in Carl Eckart's original paper, which has been read and appreciated by much of the oceanography community for many years. Figures were kindly provided by E. Widder of Harbor Branch Oceanographic Institution, M. Gregg of the Applied Physics Laboratory, University of Washington, and P. Gentien of IFREMER. Support was provided by the Office of Naval Research Codes 322BC and 322PO.

References

- Donaghay, P.L. and T.R. Osborn, 1997: Toward a theory of biological-physical control of harmful algal bloom dynamics and impacts, *Limnol. Oceanogr.*, 42, 1283-1296.
- Eckart, C. 1940: The thermodynamics of irreversible processes II. Fluid mixtures. *Physical Rev.*, 58, 269-275.
- , 1948: An analysis of the stirring and mixing processes in incompressible fluids. *J. Mar. Res.*, 7, 265-275.
- Fedorov, K.N., 1978: *The Thermohaline Finestructure of the Ocean*. Pergamon Press, Oxford.
- Gargett, A.E., T.R. Osborn and P.W. Nasmith, 1984: Local isotropy and the decay of turbulence in a stratified fluid. *J. Fluid Mech.*, 144, 231-280.
- Gentien, P., M. Lunven, M. Lehaitre, and J.L. Duvent, 1995: *In situ* depth profiling of particle sizes. *Deep-Sea Res.*, 42, 1297-1312.

- Grant, H.L., R.W. Stewart and A. Mollet, 1961: Horizontal coherence of oceanic temperature structure. *J. Fluid Mech.*, 12, 241–263.
- Gregg, M.C., 1975: Microstructure and intrusions in the California current. *J. Phys. Oceanogr.*, 5, 253–278.
- Gregg, M.G. and J.H. McKenzie, 1979: Thermohaline intrusions lie across isopycnals. *Nature*, 280, 310–311.
- Hacker, W., 1933: Sichttiefe, Warmegang und Durchlüftung in Hochgebirgsseen. *Geogr. Jber, aus Ost.*, 16, 88–105.
- Itsweire, E.C. and T.R. Osborn, 1988: Microstructure and vertical velocity shear distribution in Monterey Bay. In: *Small-Scale Turbulence and Mixing in the Ocean*. J.C.J. Nihoul and B.M. Jamart, eds. Elsevier, Amsterdam, 46, 219–228.
- Itsweire, E.C., T.R. Osborn and T.P. Stanton, 1989: Horizontal distribution and characteristics of shear layers in the seasonal thermocline. *J. Phys. Oceanogr.*, 19, 301–320.
- Kullenberg, G., 1974: Investigation of small-scale vertical mixing in relation to the temperature structure in stably stratified waters. *Adv. Geophys.*, 18A, 339–351.
- Lazier, J.R.N., 1973: Temporal changes in some fresh water temperature structures. *J. Phys. Oceanogr.*, 3, 226–229.
- Ledwell, J.R., A.J. Watson and C.S. Law, 1993: Evidence for slow mixing across the pycnocline from an open ocean tracer-release experiment. *Nature*, 364, 701–703.
- Mack, S.A., 1989: Towed-chain measurements of ocean microstructure. *J. Phys. Oceanogr.*, 19, 1108–1129.
- Ochoa, J., 1987: Two limiting types of oceanic finestructure. *J. Phys. Oceanogr.*, 17, 1539–1545.
- Osborn, T.R. and C.S. Cox, 1972: Oceanic fine structure. *Geophys. Fluid Dyn.*, 3, 321–345.
- Schmidt, W., 1914: Ein einfaches Temperaturlot. *Z. Instrumentenkunde*, 34, 328.
- Toole, J.M., K.L. Polzin and R.W. Schmitt, 1994: Estimates of diapycnal mixing in the abyssal ocean. *Science*, 264, 1120–1123.
- Widder, E.A., 1997: Bioluminescence. *Sea Tech.*, 38, 33–39. □

A MODEL FOR THE REFLECTANCE OF THIN LAYERS, FRONTS, AND INTERNAL WAVES AND ITS INVERSION

By J. Ronald V. Zaneveld
and W. Scott Pegau

THE INTERPLAY OF physical and biogeochemical processes in the ocean can result in well-defined vertical gradients and maxima in biological properties. When these gradients and maxima exist near the sea surface, it is possible to use satellite or airborne remote sensing to infer physical structure of thin layers, fronts, and internal waves within the ocean. The necessary conditions for this application of remote sensing are tied to the Inherent Optical Properties (IOP) of the water and to the local concentration (layers) of particles within the optical viewing range of remote sensing systems. In this paper, we use a two-stream radiative transfer model to demonstrate that discrete layers of particles (usually phytoplankton) can provide sufficient remotely sensed reflectance to resolve associated subsurface physical features such as the depth of specific layers of optical materials, depth and position of frontal boundaries, and the wavelength and amplitude of near-surface internal waves. This inversion of remotely sensed optical properties to obtain information on physical structure depends on the association of in-water biological, optical, and physical structure (for specific examples, see other articles in this issue).

To understand when the conditions are right for such a visualization of physical properties via biooptical remote sensing, we need to look at the vertical structure of the optical properties in relation to the physical properties. The IOP (Preisendorfer, 1976) govern the radiative transfer in the ocean. They are not directly dependent on the external lighting conditions. These IOP are due to particulate matter, dissolved substances, and water itself. Of these three, it is the particulate matter, primarily the

phytoplankton, that determine the near-surface vertical structure of the IOP. The IOP are the absorption coefficient $a(\lambda, z)$, the beam attenuation coefficient $c(\lambda, z)$, and the volume scattering function $\beta(\theta, \lambda, z)$ (for definitions see Jerlov, 1976; Gordon *et al.*, 1979), where λ is the wavelength of light, z is the depth, and θ is the scattering angle. The scattering coefficient $b(\lambda, z)$ is the integral over all directions of the volume scattering function, and the attenuation coefficient is the sum of the absorption and scattering coefficients, so that in practice only the absorption coefficient and the volume scattering function need to be known to describe the behavior of radiance in a medium, if we ignore the usually minor contributions of polarization, inelastic scattering, and internal sources.

The diffuse or irradiance reflectance R at a depth z is defined as the ratio of the upwelling irradiance E_u and the downwelling irradiance E_d . Hence $R(z) = E_u(z)/E_d(z)$. This parameter has been extensively modeled (for example Gordon *et al.*, 1988; Morel, 1988; Gordon, 1989; Morel and Gentili, 1991), primarily because of its ease of measurement since the irradiance sensor does not require absolute calibration. Remote sensing satellites sense radiance rather than irradiance, so that the models were subsequently modified to look at the ratio of the upwelling radiance L_u and the downwelling irradiance (Zaneveld, 1982, 1995; Gordon *et al.*, 1988; Gordon, 1992; Morel and Gentili, 1993). The ratio $R_{rs}(z) = L_u(z)/E_d(z)$ as used in the later papers is often called the remote sensing reflectance. Instrumentation was also developed to measure the upwelling radiance spectrum.

In this paper we develop a simple model to study under what circumstances features like the slopes of fronts, amplitudes of internal waves, and thicknesses of thin layers can be determined from remote

sensing. Forward radiative transfer models are available (e.g., Mobley *et al.*, 1993) for the determination of reflectance in stratified optical systems. Calculating the reflectance for an arbitrary vertical optical structure is thus possible. We are interested here in developing an inversion scheme, which requires a simpler two-stream model. These simpler models calculate the fluxes in the upward and downward directions only. Full radiative transfer modeling is less well suited to this task than two-stream models because the results of the full radiative transfer models cannot be mathematically inverted without first fitting empirical models to the results. Because of their simple mathematical structure, two-stream models lend themselves well to the inversion task. On the other hand, results are only approximate, and careful attention must be paid to the conditions under which they can be applied.

A Two-Stream Model for Physical Structure

To model the reflectance for various optical stratifications due to physical structure, we employ a simple two-stream model such as that used by Philpot and Ackleson (1981), Philpot (1987, 1989), Maritorena *et al.* (1994), and others to study the effect of bottom albedo on the remotely sensed reflectance. These approaches all have common two-stream assumptions (Preisendorfer, 1976); it is assumed that there is some backscattering parameter $B(z)$ that characterizes the redirection of light upward, and that there is some attenuation coefficient $g(z)$ that characterizes the round trip attenuation from the surface to a given depth z and back. The paper by Maritorena *et al.* (1994) provides an excellent discussion of the errors resulting from these assumptions. It should be noted that the diffuse reflectance and the remote sensing reflectance can be modeled by the same mathematical

J. Ronald V. Zaneveld and W. Scott Pegau,
College of Oceanic and Atmospheric Sciences,
Ocean. Admin. Bldg. 104, Oregon State University,
Corvallis, OR 97331, USA.

formalism, but the values of the parameters must be changed.

We will divide the water column into N homogeneous layers. The value of the IOP in each layer will be determined by the desired vertical distribution of optical properties. In accordance with the simple model we will assume that each layer has a diffuse attenuation coefficient $g(z)$ that describes the round trip attenuation of the upwelling and downwelling irradiance through the layer. We will also assume that the irradiance reflects according to some backscattering coefficient $B(z)$. With the above very simple notation, one can write:

$$E_u(0^-) = E_d(0^-) + \int_0^\infty B(z) e^{-2\tau_g(z)} dz, \quad (1)$$

where

$$\tau_g(z) = \int_0^z g(z\pi) dz\pi. \quad (2)$$

$E_u(0^-)$ and $E_d(0^-)$ are the upwelling and downwelling irradiances just below the surface, and the parameters $B(z)$ and $g(z)$ are apparent optical properties because they depend both on the inherent optical properties and the radiance distribution. The integrals can be broken down into sums over a number of depth intervals if the $B(z)$ and $g(z)$ parameters are assumed to be constant in each depth interval. The n th interval covers depths from z_n to z_{n+1} , with $\Delta z_n = z_{n+1} - z_n$, and has optical properties of B_n and g_n . Substitution into equation (1) and integration then yields:

$$\begin{aligned} R(0^-) &= \frac{E_u(0^-)}{E_d(0^-)} = \sum_{n=1}^N \int_{z_n}^{z_{n+1}} B_n \\ &\times \exp\left(-2 \int_0^{z_n} g(z') dz'\right) \\ &\times \exp\left(-2g_n \int_{z_n}^{z_{n+1}} dz'\right) \\ &= \sum_{n=1}^N \left\{ \frac{B_n}{2g_n} [1 - \exp(-2g_n \Delta z_n)] \right. \\ &\quad \left. \times \exp\left(-\sum_{i=1}^{n-1} 2g_i \Delta z_i\right) \right\} \quad (3) \end{aligned}$$

We note that the term

$$T_n^2 = \exp\left(-\sum_{i=1}^{n-1} 2g_i \Delta z_i\right) \quad (4)$$

is the attenuation of light to the top of the n th layer and back to the surface. The reflectivity of layer n if it were at the surface would be:

$$R_{sn} = \frac{B_n}{2g_n} [1 - \exp(-2g_n \Delta z_n)]. \quad (5)$$

Equation (3) can then be simply rewritten as:

$$R(0^-) = \sum_{n=1}^N (T_n^2 R_{sn}) \quad (6)$$

If the layer in equation (5) were infinitely thick, the reflectance would be:

$$R_{\infty n} = \frac{B_n}{2g_n}. \quad (7)$$

Equation 7 is important because it allows us to measure or calculate the ratio of the parameters B_n and g_n for given IOP and surface radiance distribution.

With this notation we can rewrite equation (6) as:

$$R(0^-) = \sum_{n=1}^N R_{\infty n} (T_n^2 - T_{n+1}^2). \quad (8)$$

The formulations in equations (6) and (7) can also include the bottom. In those cases the reflectance for the deepest layer, $R_{\infty N}$, is simply the bottom albedo.

Combining equations (7) and (3) for two layers, with the second layer being optically infinitely deep, we obtain:

$$R(0^-) = R_{\infty 1} [1 - \exp(-2g_1 \Delta z_1)] + R_{\infty 2} \exp(-2g_1 \Delta z_1). \quad (9)$$

Depending on the thickness of the first layer, Δz_1 , the reflectance can vary from $R_{\infty 1}$ to $R_{\infty 2}$. If we now look at the N layered model, but only vary the thickness of the first layer, we can deduce from equation (3) that:

$$\begin{aligned} R(0^-) &= R_{\infty 1} [1 - \exp(-2g_1 \Delta z_1)] \\ &\quad + \exp(-2g_1 \Delta z_1) \\ &\quad \times \sum_{n=2}^N \left\{ \frac{B_n}{2g_n} [1 - \exp(-2g_n \Delta z_n)] \right. \\ &\quad \left. \times \exp\left(-\sum_{i=2}^{n-1} 2g_i \Delta z_i\right) \right\}. \quad (10) \end{aligned}$$

By setting

$$R_{2N} = \sum_{n=2}^N \left\{ \frac{B_n}{2g_n} [1 - \exp(-2g_n \Delta z_n)] \times \exp\left(-\sum_{i=2}^{n-1} 2g_i \Delta z_i\right) \right\}, \quad (11)$$

We then get that:

$$R(0^-) = R_{\infty 1} [1 - \exp(-2g_1 \Delta z_1)] + R_{2N} \exp(-2g_1 \Delta z_1), \quad (12)$$

so that by comparison with equation (9) it is seen that the entire structure of layers 2 through N can be considered to be a single layer (layer $2N$) as far as the dependence of the irradiance reflectance on a changing thickness of the first layer is concerned. Layer $2N$ is infinitely deep. Solving for the optical depth of the first layer gives:

$$g_1 \Delta z_1 = -0.5 \ln \left[\frac{R(0^-) - R_{\infty 1}}{R_{2N} - R_{\infty 1}} \right]. \quad (13)$$

Equation (13) shows that if we can measure $R_{\infty 1}$ and R_{2N} , we can determine the variable optical depth of the first layer, $\Delta z_1 g_1$, if $R(0^-)$ is measured as a function of location. This concept is critical to what follows. If we have a stratified ocean in which a layer of varying thickness with homogeneous properties overlies the remainder of the ocean, which can contain any number of layers, we can then determine the optical thickness of the first layer, $g_1 \Delta z_1$, provided the optical properties of the first layer do not covary with the optical properties of the layers below it. To do so, we must be able to measure the reflectance of the first layer where it is optically infinitely deep ($R_{\infty 1}$), and the reflectance of the combination of the second through N th layer in a location where the first layer does not exist (R_{2N}). With the above equations in hand, a number of geometries can be resolved.

Reflectance of Physical Features

Thin Layers

Generation mechanisms of the thin layers are discussed elsewhere in this volume. The high concentration of biological materials in these layers results in increases in the scattering and absorption characteristics in these layers. Thin layers are usually present offshore

of coastal upwelling fronts and at the bottom of the mixed layer. This was observed by Zaneveld and Pak (1979), who discussed "optical amplification" of physical features. At the time, only beam attenuation could be measured in a continuous vertical profile. Recent advances in instrumentation (Moore *et al.*, 1992; Zaneveld *et al.*, 1994) now allow us to determine the spectral absorption, attenuation (and hence scattering) coefficients in a continuous vertical profile at the same time, and space scales as the physical parameters. By means of filtering the intake of the flow-through *in situ* instrumentation, it is even possible to separate the effects due to dissolved and particulate components. It is, of course, this instrumental advance that has sparked the current interest in the interaction of the biology, physics, and optics of thin layers.

We can model a thin layer as one in which the inherent optical properties are much larger than in the water immediately above and beneath it. Equation (3) would thus apply. From equations (3) and (12) we see that the influence of the thin layer on the reflectance depends exponentially on its depth and on the reflectance of the thin layer if it were infinitely thick and at the surface (as expressed in Eq. 7). From equation (13) we see that we can only invert for the depth of the thin layer if R_{2N} is known, or we can solve for the optical properties via R_{2N} if the depth is known.

Fronts

At oceanic fronts the physical structure is usually accompanied by strong gradients in optical properties (Zaneveld and Pak, 1979). The front is modeled as a wedge of homogeneous watermass 1 overlying stratified watermass 2. Figure 1 shows the structure of the hypothetical front. Referring to equation (12), watermass 1 would have a reflectance of $R_{\infty 1}$, if it were infinitely deep, and watermass 2 would have a reflectance of R_{2N} . Note that watermass 2 does not need to be vertically homogeneous. If locations are known where the pure watermasses occur, $R_{\infty 1}$ and R_{2N} can be measured at those locations. Such a location is found for watermass 1 at a distance from the front where the upper layer is thick enough to have become optically infinitely deep. It can be

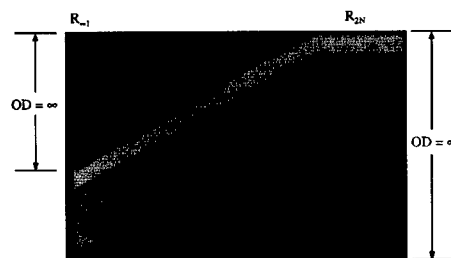


Fig. 1: Structure of a hypothetical front. Watermass 1 is physically homogeneous. At some distance from the front, the optical depth (OD) of watermass 1 becomes infinitely large. The reflectance $R_{\infty 1}$ is measured here. The reflectance of the stratified watermass 2 is measured at the other side of the front. For further details, see the text.

shown that when watermass 1 overrides stratified watermass 2 and forces it to subside, the layers are stretched so that they become thinner perpendicular to the boundary of the two watermasses, but retain the same thickness in the vertical direction. The R_{2N} that is valid when the layers 2 through N has horizontal boundaries is thus also valid for inclined boundaries.

The vertical structure of a front can then be determined from optical remote sensing using the following approach. The reflectance is measured on either side of the front at a location where the reflectance has become constant as a function of distance from the front. This determines parameters $R_{\infty 1}$ and R_{2N} in equation (13). The reflectance is then measured as a function of location across the front. Equation (13) is then applied to determine the optical depth at each location. The actual depth can then be determined if g_1 is known. Maritorena *et al.* (1994) have shown that g_1 is 1.01 to 1.33 times greater than the downward diffuse attenuation coefficient K_d (which in turn is a few percent different from the total diffuse attenuation coefficient). Fairly good algorithms for the determination of $K(490)$ from remote sensing exist (Austin, 1981), thus at the "pure" watermass 1 location the $K(490)$ of the overriding watermass 1 can be determined. With the use of relations between g and K as in Maritorena *et al.* (1994), it is then possible to determine the depth of the interface using equation (13).

Sloping Bottoms

It is interesting to note that the same procedure can be applied to a watermass of varying depth overlying a bottom. In that case R_{2N} is the bottom albedo, and equation (13) can be used to derive bottom depth by the same approach. This method was used by Philpot and Ackleson (1981) to experimentally determine bottom depth using a known bottom albedo. A similar approach was used by Maritorena *et al.* (1994). It does not appear to have been recognized that R_{2N} and hence the albedo can be determined remotely in very shallow water. If the nature of the bottom and therefore the albedo does not change, the bathymetry can be determined entirely by passive remote sensing using an approach very similar to that for fronts, without any *a priori* knowledge of the bottom albedo. In the bottom case we should measure the reflectance in very shallow water close to shore. This will be reflectance R_{2N} . The layer 2N thus consists of a thin layer of water and the bottom. Physically homogeneous watermass 1 overlies this layer, and its thickness constitutes the bathymetry. The thickness of watermass 1 and the bathymetry are then determined in an identical way to that described above. The key here is that no *a priori* knowledge of the bottom albedo is necessary. The only requirement is that for accurate bathymetry the albedo must not change. This method could be of use in inaccessible areas. Tidal range can also be determined in this way.

Internal Waves

It is quite common for internal waves to occur at density interfaces. In that case internal waves will continuously change the depth of a layer, which will modify the reflectance. Such an event was observed at East Sound where the ocean color was seen to change from light whitish green to dark green with a periodicity of minutes. Unfortunately, no time series record was obtained. With the use of equation (12), the dependence of the irradiance reflectance on an internal wave can readily be modeled. Substituting

$$\Delta z_1(t, x) = z_2 + A \cos(\omega t + kx), \quad (14)$$

where A is the amplitude, ω the frequency, and k the wavenumber of the in-

ternal wave, into equation (12), leads to the desired relationship:

$$R(0^-, t, x) = R_{\infty 1} \times (1 - \exp\{-2g_1[z_2 + A \cos(\omega t + kx)]\}) + R_{2N} \exp\{-2g_1[z_2 + A \cos(\omega t + kx)]\}. \quad (15)$$

Because the amplitude appears in the exponent, there can be a considerable nonlinear influence on the reflectance at the surface.

Inversion of the internal wave case is interesting because in this case the layer 2N does not occur at the surface, in contrast to the frontal case. The amplitude of the internal wave can still be solved for, however, because the reflectance R_{2N} does not need to be known, as will be demonstrated. We take layer 2N to consist of the water mass structure from the top of the interface on which the wave rides, downward to infinity. At location, x_1 , where the wave is closest to the surface, the depth of the density and optical interface on which the internal wave rides is $z_2 - A$, and the reflectance is $R(x_1)$. At location x_2 , where the wave is furthest from the surface, the depth of the internal wave is $z_2 + A$, and the reflectance is $R(x_2)$. Applying equation (13) at x_1 and x_2 and subtracting then gives:

$$[(z_2 + A) - (z_2 - A)]g_1 = -0.5 \ln \left[\frac{R(x_2) - R_{\infty 1}}{R_{2N} - R_{\infty 1}} \right] + 0.5 \ln \left[\frac{R(x_1) - R_{\infty 1}}{R_{2N} - R_{\infty 1}} \right],$$

or

$$2Ag_1 = -0.5 \ln \left[\frac{R(x_2) - R_{\infty 1}}{R(x_1) - R_{\infty 1}} \right]. \quad (16)$$

The optical amplitude of the internal wave can thus be determined, and the actual amplitude can be approximated if g_1 can be determined via the diffuse attenuation coefficient K .

Discussion

The applicability of the inversion is by no means universal and is dependent on several factors. The difference in the reflectances of the water masses, as in equation (13), must be large enough to obtain meaningful results. Different remote sensing instruments have vastly different sensitivities in terms of determining the reflectances. The error in determining the reflectances greatly influences the ability to invert. Finally, the parameter g_1 must be determined to obtain the actual depth. An excellent discussion on the dependence of this parameter on external lighting conditions and the IOP can be found in Maritorena *et al.* (1994). As stated above, they concluded that $K < g_1 < 1.32 K$. This parameter alone can thus lead to a 15% error if we assume that $g_1 = 1.16 K$.

Further work is needed to test the approach outlined above using satellite or aircraft optical remote sensing. At present, satellites typically have pixel sizes on the order of 1 km, so that they could only be used for the largest scale features. Aircraft remote sensing would thus be more appropriate for the optical detection of physical features. It would be useful to determine the optical and physical structure of the ocean during remote sensing in order to assess the viability of the approach.

Acknowledgement

This work was supported by the Environmental Optics branch of the Office of Naval Research and the Ocean Biology/Biogeochemistry program of the National Aeronautics and Space Administration.

References

- Austin, R.W., 1981: Remote sensing of the diffuse attenuation coefficient of ocean water. In: *Proceedings of the 29th Symposium of the AGARD Electromagnetic Wave Propagation Panel*. 18-1 to 18-9.
- Gordon, H.R., R.C. Smith and J.R.V. Zaneveld, 1979: Introduction to ocean optics. In: *Ocean Optics VI*, Proc. SPIE 208, 14-55.
- , 1989: Dependence of the diffuse reflectance of natural waters on the sun angle. *Limnol. Oceanogr.*, 34, 1484-1489.

- , O.B. Brown, R.H. Evans, J.W. Brown, R.C. Smith, K.S. Baker and D.K. Clark, 1988: A semi-analytic radiance model of ocean color. *J. Geophys. Res.*, 93D, 10,909-10,924.
- , 1992: Diffuse reflectance of the ocean: influence of nonuniform pigment profile. *Appl. Opt.*, 31, 2116-2129.
- Jerlov, N.G., 1976: *Marine Optics*. Elsevier Oceanography Series, vol. 14. Elsevier, Amsterdam, 231 pp.
- Maritorena, S., A. Morel and B. Gentili, 1994: Diffuse reflectance of oceanic shallow waters: influence of water depth and albedo. *Limnol. Oceanogr.*, 39, 1689-1703.
- Mobley, C.D., B. Gentili, H.R. Gordon, Z. Jin, G.W. Kattawar, A. Morel, P. Reinersman, K. Stamnes and R.H. Stavn, 1993: Comparison of numerical models for computing underwater lightfields. *Appl. Opt.*, 32, 7484-7504.
- Moore, C., J.R.V. Zaneveld and J.C. Kitchen, 1992: Preliminary results from an *in situ* spectral absorption meter. In: *Ocean Optics XI*. G.D. Gilbert, ed. Proc. SPIE 1750, 330-337.
- Morel, A., 1988: Optical modeling of upper ocean in relation to its biogenous matter content (case 1 waters). *J. Geophys. Res.*, 93, 749-768.
- and B. Gentili, 1991: Diffuse reflectance of oceanic waters: its dependence on sun angle as influenced by the molecular scattering contribution. *Appl. Opt.*, 30, 4427-4438.
- and B. Gentili, 1993: Diffuse reflectance of oceanic waters. II. Bidirectional aspects. *Appl. Opt.*, 32, 6864-6879.
- Philpot, W.D., 1987: Radiative transfer in stratified waters: a single-scattering approximation for irradiance. *Appl. Opt.*, 26, 4123-4132.
- , 1989: Bathymetric mapping with passive multispectral imagery. *Appl. Opt.*, 28, 1569-1578.
- and S. Ackleson, 1981: Remote sensing of optically shallow, vertically inhomogeneous waters: a mathematical model. *NASA Conference Publication 2188, Proceedings from Chesapeake Bay Plume Study Superflux 1980*, Williamsburg, VA.
- Preisendorfer, R.W., 1976: *Hydrologic Optics* (in 6 volumes). Dept. of Commerce, NOAA.
- Zaneveld, J.R.V., 1982: Remotely sensed reflectance and its dependence on vertical structure: a theoretical derivation. *Appl. Opt.*, 21, 4146-4150.
- , 1995: A theoretical derivation of the dependence of the remotely sensed reflectance on the inherent optical properties. *J. Geophys. Res.*, 100, 13,135-13,142.
- , J.C. Kitchen and C.C. Moore, 1994: Scattering error correction of reflecting tube absorption meters. In: *Ocean Optics XII*. S. Ackleson, ed. Proc. SPIE vol. 2258, 44-55.
- and H. Pak, 1979: Optical and particulate properties at oceanic fronts. *J. Geophys. Res.*, 4, 7781-7790. □

EFFECTS OF A THIN LAYER ON REFLECTANCE AND REMOTE-SENSING REFLECTANCE

By A.A. Petrenko, J.R.V. Zaneveld,
W.S. Pegau, A.H. Barnard
and C.D. Mobley

OPTICAL REMOTE SENSING using satellites holds the promise of determining biological and optical properties globally. Much research has been carried out on the inversion of the spectral radiance signals detected by satellite. However, almost all inversion algorithms are based on the assumption of a homogeneous ocean. How do thin layers of particulate matter affect the reflectance of the ocean? A thin layer exhibits increases in absorption and scattering parameters (inherent optical properties, IOPs) (Preisendorfer, 1961) compared with surrounding waters. These increases are due primarily to phytoplankton and in a lesser degree to dissolved organic matter.

It is intuitive that the deeper a thin layer is in the ocean, the smaller its influence on the reflectance at the surface. It is also intuitive that the thinner the layer, the less change in reflectance. It is perhaps not as obvious that, under certain circumstances, the thin layer can have no overall effect on the reflectance even if its absorption and scattering coefficients are an order of magnitude larger than the coefficients of the surrounding water. In effect, the layer may be invisible to remote sensing, even though it has significantly higher inherent optical properties than the surrounding water. This paper will address these issues and provide some examples of the effect of an idealized thin layer on reflectance.

Algorithms have been developed to derive the concentration of chlorophyll in

the ocean from surface irradiance reflectance (R) or remote-sensing reflectance (R_{rs}). Such algorithms were based on the assumption that reflectance of a stratified ocean was equal to the reflectance of a homogeneous ocean with a phytoplankton concentration equivalent to the depth-weighted average of the real phytoplankton concentration profile (Gordon and Clark, 1980). This was later proved to be true only when the absorption coefficient (a), the scattering coefficient (b), and the chlorophyll concentration all covary with depth (Gordon, 1992). Thin layers could affect R and R_{rs} if their IOPs do not covary with depth.

Elsewhere in this volume, Zaneveld and Pegau (1998, this issue) have shown a simple two-flow model for the reflectance of a stratified ocean. Their equation (8) explains the phenomena mentioned above. The ocean is assumed to consist of N layers. Each layer is characterized by its "inherent reflectance" defined as the reflectance it would have if the layer were infinitely thick. The contribution of the layer to the overall reflectance of the ocean depends on the inherent reflectance of the layer weighted by factors proportional to the depth and thickness of the layer. A deeper, thinner layer contributes less to changes in R than a shallow, thick layer. However, equation (8) in Zaneveld and Pegau also shows that, if all layers have the same inherent reflectance, the reflectance of that stratified ocean is indistinguishable from the reflectance of a homogeneous ocean. The inherent reflectance does not necessarily change if the IOPs change in absolute value. The inherent reflectance is often expressed as $0.33 b_b/a$ (Morel and Prieur, 1977), where b_b is the backscattering coefficient. If b_b/a is constant, then even a layer with very high IOP can have the same inherent re-

fectance as one with low IOP. If we were to insert a thin layer in a homogeneous ocean, the layer would influence the reflectance at the surface only if its inherent reflectance was different than the reflectance of the water it replaced.

We will illustrate these effects with some examples based on *in situ* measurements. A thin layer, observed in East Sound, Orcas Island, WA, was characterized by locally higher IOPs. The observed thin layer had significant vertical structure within it (Fig. 1). The IOPs did not covary with depth; the scattering to absorption ratio fluctuated significantly both in the thin layer compared with the rest of the water column and within this layer. To estimate how reflectances depend on the depth and thickness of this observed thin layer, it was decided to model this feature with an idealized thin layer. The inherent optical properties of the idealized thin layer were chosen on the basis of the optical properties measured *in situ*. R and R_{rs} were evaluated using the Hydrolight numerical radiative transfer model (Mobley, 1994). Changes of R and R_{rs} in the presence of the thin layer were compared with a homogeneous water column. The depth and thickness of the idealized thin layer were then varied in order to estimate their influence on R and R_{rs} .

Methods

Absorption and scattering coefficients were derived from *in situ* measurements collected with an absorption and attenuation meter at nine wavelengths (ac-9; WETLabs, Inc). The measurements were taken on 1 June 1996 in East Sound, a fjord on Orcas Island, WA in Northern Puget Sound (Hanson and Donaghay, 1998, this issue). Values of absorption and scattering of the idealized thin layer

A.A. Petrenko, Dept. of Ecology, 300 Desmond Dr., PO Box 47710, Olympia, WA 98504-7710, USA. Present address: LOB-UMR 6535, Centre d'Océanologie de Marseille, Campus de Luminy, 13288, Marseille-Cedex 09, France. J.R.V. Zaneveld, W.S. Pegau, A.H. Barnard, COAS, 104 Admin. Bldg., Oregon State University, Corvallis, OR 97331, USA. C.D. Mobley, Sequoia Scientific, 9725 SE 36th St., Suite 308, Mercer Island, WA 98040, USA.

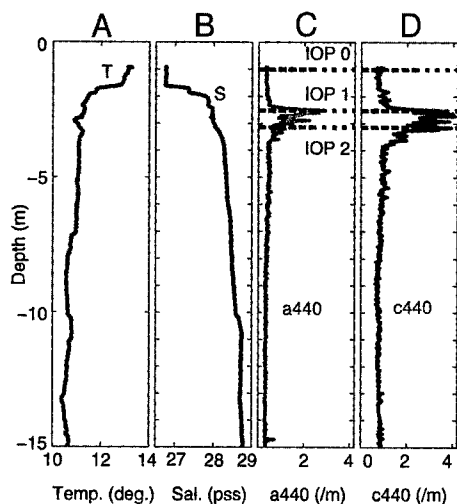


Fig. 1: Vertical profiles of (A) temperature, (B) salinity, (C) absorption, and (D) beam attenuation coefficients at 440 nm. IOP 0 corresponds to the measurements taken around 1 m, IOP 1 to those collected in the shallower part of the thin layer, and IOP 2 to those collected in the deeper part of the feature.

were represented by the average values obtained within the *in situ* thin layer. Two extreme cases could be distinguished within the observed thin layer: 1) a low ratio of scattering to absorption ($b/a = 0.11$) at 2.5 m (IOP 1) and 2) a high ratio of scattering to absorption ($b/a = 4.45$) at 3.1 m (IOP 2; Figs. 1 and 2). For the water column outside the thin layer, the average values of the absorption and scattering coefficients around 1 m depth were used (IOP 0; Fig. 1). The average measured spectral values of a and b of these three cases (IOPs 0, 1, and 2) were splined over the visible spectra every 10 nm. Basic boundary conditions were applied to force the spline functions; the a values were equal to the pure water value at 700 nm, and the b values were chosen at 400 and 700 nm by linear extrapolation (Fig. 2, A and B). A Raleigh phase function was used for the scattering due to the pure water, and an average of three Petzold phase functions (Petzold, 1972; Mobley *et al.*, 1993) was used for the particulate scattering. The ratio of backscattering to absorption (b_b/a), ($i = 0, 1$, and 2) was calculated for the three basic IOP cases using the b_b/b ratios for the Petzold volume scattering function. (b_b/a)₂ was higher than (b_b/a)₀ and (b_b/a)₁ throughout the visible spectrum; (b_b/a)₁ was lower (higher) than (b_b/a)₀ for wave-

lengths shorter (longer) than 600 nm (Fig. 2C).

R and R_{rs} were estimated with the Hydrolight numerical radiative transfer model (Mobley, 1994). We used the following set of assumptions in the model: horizontally homogeneous ocean, real sky radiance distribution, sun at 45° from the zenith, plane air-water interface (no wind), and no internal sources of light. For this study, the model was run with different permutations: varying the IOPs of the thin layer (IOPs 1 or 2), the thickness of the thin layer (10 cm to 1 m), and its position in the water column (surface to 19–20 m depth). In all cases, the rest of the water column was homogeneous (IOP 0) and infinitely deep.

Results

When a thin layer of IOP 1 is added to the homogeneous (IOP 0) water column, the reflectance is referred to as $R_{01}(i, j)$, where i indicates the depth of the top of the thin layer (in meters) and j indicates the thickness of the thin layer (in meters). R for the homogeneous water column of IOP 0 is designated as R_0 .

Idealized Thin Layer of 1-m Thickness

Spectral variability of R and R_{rs} . We examined the influence of the b_b/a ratio on R and R_{rs} . When the thin layer was located at the surface, $R_{01}(0,1)$ (i.e., reflectance with a 1-m thick layer of IOP 1 at the surface) and $R_{02}(0,1)$ were distinctly different from R_0 (Fig. 3). Large changes in reflectances were due to the presence of the thin layer. Spectrally, $R_{01}(0,1)$ ranged from 9 to 600% of R_0 . $R_{02}(0,1)$ was higher than R_0 throughout

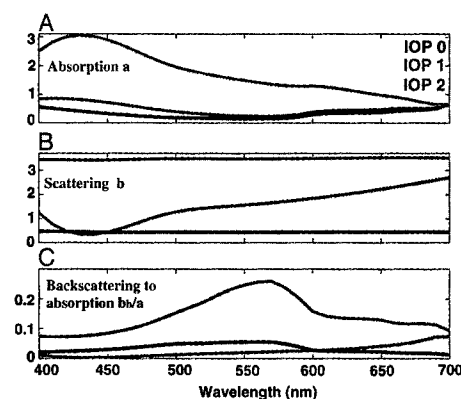


Fig. 2: Spectra of (A) absorption coefficient, (B) scattering coefficient, and (C) b_b/a . The color convention in the figures is black for IOP 0, blue for IOP 1, and red for IOP 2.

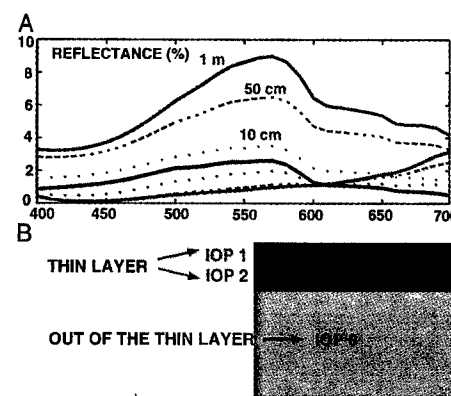


Fig. 3: Spectra of (A) R , (B) R_{rs} in percent. Solid lines are for R_0 (black), $R_{01}(0,1)$ (blue), and $R_{02}(0,1)$ (red); dashdot lines for $R_{01}(0,0.5)$ (blue) and $R_{02}(0,0.5)$ (red); and dotted lines for $R_{01}(0,0.1)$ (blue) and $R_{02}(0,0.1)$ (red).

the visible spectrum (Fig. 3), ranging from 290 to 800% of R_0 . R_0 , $R_{01}(0,1)$, and $R_{02}(0,1)$ exhibited spectral shapes similar to the shapes of their respective b_b/a ratios (Figs. 2C and 3). The spectral variability of R_{rs} was qualitatively identical to that of R in the three cases.

Variability of R and R_{rs} due to the vertical position of the thin layer. When the thin layer was deeper, R was closer to R_0 (Fig. 4). For all wavelengths (only shown here for 410, 440, 520, and 550 nm), R increased (decreased) exponentially to the homogeneous case R_0 , the deeper the thin layer of IOP 1 (IOP 2) was located (Fig. 4). R_{rs} followed the same trend as R (data not plotted). The convergence of R_{rs} to R_{rs0} occurred when the thin layer was located at a deeper depth than that for which R converged to R_0 . This implies that R_{rs} was more sensitive to the presence of deep thin layers than R .

Surface Thin Layer of Varying Thickness

While the thin layer was maintained at the surface, its thickness was diminished from 1 m to 50 and 10 cm. The spectral shapes of both R and R_{rs} for the 50-cm layer were similar to those for the 1-m thick layer (Fig. 3). $R_{01}(0,0.5)$ ranged from 11 to 476% of R_0 . $R_{01}(0,0.5)$ was lower than R_0 until 600 nm and higher than R_0 at longer wavelengths. $R_{02}(0,0.5)$ was higher than R_0 throughout the visible spectrum (Fig. 3), with a range of 232–631% of R_0 . Both $R_{01}(0,0.5)$ and $R_{02}(0,0.5)$ still mirrored the shape of the b_b/a relation of their respective thin layer (Fig. 2C). For a 10-cm-thick layer, the R spectra converged toward R_0 (Fig. 3).

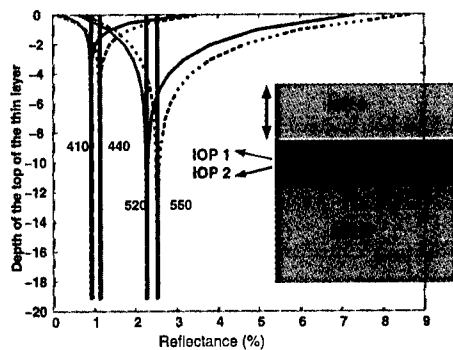


Fig. 4: Vertical profiles of R in percent, at four wavelengths 401, 440, 520, and 550 nm, versus the depth at which the top of the thin layer is located (solid black lines for IOP 0, blue lines for IOP 1, and red lines for IOP 2 results). R_0 results (black lines) are constant with depth since the thin layer is absent in these cases.

$R_{01}(0,0.1)$ was 43–214% of R_0 , and $R_{02}(0,0.1)$ was 133–260% of R_0 . We observed the same pattern for R_{rs} .

Discussion

As discussed earlier in the paper, the contribution of a thin layer to the overall reflectance depends on the contrast of its inherent reflectance with that of the surrounding water. Indeed, percent changes in R and R_{rs} increased with increased absolute value of $(b_b/a)_{\text{thin layer}} - (b_b/a)_{\text{surrounding water}}$ and decreased the thinner the layers were and/or the deeper they were located. We can conclude that changes in reflectance depend to the first order on the changes in b_b/a , the optical thickness of the layer, and the depth of the layer.

Our simplified approach to this analysis did not include the effects of Raman scattering or fluorescence on reflectance. We chose the Petzold averaged phase

function as a good approximation for the coastal waters of East Sound. It is possible that other phase functions could improve our estimates (see Mobley and Stramski 1997; Stramski and Mobley 1997), but these phase functions require detailed knowledge of species and size distributions of the particulate matter. We also ignored the effects of bubbles since we were assuming no wind, and we did not incorporate bottom effects or changing sun angle into our calculations. Any of these factors could alter the details of our modeling analysis, but would not alter the general conclusions we have presented.

In all cases of thin layers reviewed for this study, the shallower portion of the feature had lower backscattering to absorption ratio than the deeper part of the thin layer for wavelengths shorter than 550 nm. Our results indicate that this type of thin layer will result in reduced reflectances and remote-sensing reflectances at short wavelengths. The presence of such thin layers will also impact the interpretation of ocean color algorithms based on reflectance ratios. It was also found that R_{rs} was more sensitive to the presence of a deep thin layer than R . R and R_{rs} differ by their numerator. This result indicates that the numerator of R_{rs} , the water-leaving zenith radiance just above the surface (Mobley 1994), captures more upwelling light for deep layers than the numerator of R , the upwelling irradiance. This depth sensitivity of remotely sensed reflectance may result in an erroneous estimation of the chlorophyll concentration and the vertical structure of the water column and will need to be examined carefully in remote-sensing applications.

Acknowledgements

This study was funded by Office of Naval Research Environmental Optics Program, which also supported the development of Hydrolight. We thank Dariusz Stramski and Juli Berwald for their help, and Russ Desiderio for his review of the manuscript.

References

- Gordon, H.R., 1992: Diffuse reflectance of the ocean: influence of nonuniform phytoplankton pigment profile. *Appl. Opt.*, 31, 2116–2129.
- and D.K. Clark, 1980: Remote-sensing optical properties of a stratified ocean: an improved interpretation. *Appl. Opt.*, 19, 3428–3430.
- Hanson, A.K. and P.L. Donaghay, 1998: Micro- to fine-scale chemical gradients and layers in stratified coastal waters. *Oceanography*, 11, 10–17.
- Mobley, C.D., 1994: *Light and Water: Radiative Transfer in Natural Waters*. Academic, New York.
- , B. Gentili, H.R. Gordon, Z. Jin, G.W. Kattawar, A. Morel, P. Reinersman, K. Stamnes and R.H. Stavn, 1993: Comparison of numerical models for computing underwater light fields. *Appl. Opt.*, 32, 7484–7505.
- and D. Stramski, 1997: Effects of microbial particles on oceanic optics: Methodology for radiative transfer modeling and example situations. *Limnol. Oceanogr.*, 42, 550–560.
- Morel, A. and L. Prieur, 1977: Analysis of variations in ocean color. *Limnol. Oceanogr.*, 22, 709–722.
- Petzold, T.J., 1972: Volume scattering functions for selected ocean waters. Scripps Institution of Oceanography, La Jolla, Report SIO Ref. 72–78.
- Preisendorfer, R.W., 1961: Application of radiative transfer theory to light measurements in the sea. *Int. Geophys. Geod. Monogr.*, 10, 11–29.
- Stramski, D. and C.D. Mobley, 1997: Effects of microbial particles on oceanic optics: a database of single-particle optical properties. *Limnol. Oceanogr.*, 42, 538–549.
- Zaneveld, J.R.V. and W.S. Pegau, 1998: A model for the reflectance of thin layers, fronts, and internal waves and its inversion. *Oceanography*, 11, 44–47. □

A QUANTITATIVE LITTORAL CLASSIFICATION SYSTEM

By A. Brandt, J. Calman
and J.R. Rottier

A GENERAL APPROACH for quantitative classification of littoral sites has been developed. The approach uses dimensionless parameters to describe the processes in a specific area of physics (e.g., ocean physics, meteorology, acoustics, etc.) and in a particular coastal geographic configuration (e.g., shelves, straits, enclosed seas, rivers, etc.). As a first application, a littoral classification system has been developed to describe the physical oceanographic processes on coastal continental shelves. This system incorporates four dimensionless parameters to describe the large-scale ocean features that characterize specific coastal regions: eddies, upwelling, currents, and stratification. Seven diverse worldwide sites have been compared using these classification parameters, illustrating their differences and similarities. This classification system is then used to address a specific coastal issue: the dispersion of a point discharge in the surface layer.

Events in both the civil and military sectors during recent years have resulted in increased interest in the littoral, including diverse and important topics such as the viability of coastal ecosystems, prediction of hurricane tracks, the effects of climate change on water levels, and sensor and weapon performance for naval operations in littoral waters (e.g., Davis VI, 1995; Warrick *et al.*, 1996). To address these issues an understanding of the littoral ocean environment is needed. The littoral, however, presents additional complexities compared with the open ocean, because of the large space-time variability of the submesoscale physical, biological, and optical properties of the

water column and the site-specific nature of the coastal geometry and topography. As a result, littoral modeling and design efforts inherently tend to be site specific.

Nevertheless, littoral sites do have some attributes in common. A littoral classification scheme based on the parameters that describe the key physical processes would allow quantitative comparison among sites and for extrapolation of data and models to sites that have not been studied by identifying analogous sites where data are available. Such a classification scheme would also provide a basis for assessing the performance of naval systems [antisubmarine warfare (ASW) techniques, weapons, etc.] and for the design of data collection scenarios appropriate to sites that are not readily accessible.

To date, attempts to classify littoral areas have generally employed qualitative comparisons. The only published quantitative classification scheme was developed for estuaries. The initial classification of estuarine types was developed by Pritchard (1955, 1989), who classified estuaries into highly stratified, weakly stratified, and partially mixed categories. This was extended and made quantitative by Hansen and Rattray (1965) and Jay and Smith (1988), who used a two-parameter system derived from the theoretical relationships for the estuarine salt balance.

The classification framework presented herein follows the general philosophy employed in the development of the estuarine classification scheme. It utilizes the fundamental equations governing littoral processes as a basis for determining the classification parameters, appropriate to particular littoral configurations, i.e., coastal shelves, enclosed seas, straits, etc. As envisioned, this general approach could be used to derive a classification scheme for any

class of littoral processes, i.e., physical, acoustic, meteorological, etc.

Littoral Classification—A Quantitative Approach

Differences in geometry, topography, and the physical processes at littoral sites tend to make each site unique when observed at a sufficient level of detail. To identify the underlying similarities among sites, one must, in a sense, "step back" to a level of abstraction that allows the various sites to exhibit commonalities, while ignoring the details. The degree of abstraction, however, must not be too great or everything will tend to look the same (e.g., all coasts have a shelf break), and the classification would be of little use. Moreover, to be useful for more than just general statements of site similarities, the scheme must provide quantitative estimates of the characterizing parameters.

Based on these general requirements, there are three basic criteria that a viable classification scheme must meet:

1. The classification parameters must represent the key governing processes.
2. The parameters must quantitatively parameterize these processes.
3. The parameters must involve only readily available, site-specific data.

Identification of the governing processes is key to obtaining a useful classification scheme; however, there is no general procedure for identifying these parameters that will apply in all situations. For a specific type of coastal region and a specific class of physical processes, such as in the case of the estuarine classification, it is possible to use a well-defined system of equations to derive the appropriate quantitative parameters (dimensionless groups). For other more general situations, such as for classifying the physical oceanographic processes on coastal continental

A. Brandt, J. Calman, J.R. Rottier, The Johns Hopkins University Applied Physics Laboratory, Laurel, MD 20723, USA.

shelves (as discussed subsequently), the plethora of differing processes (i.e., tidal motions, upwelling, shelf break fronts, etc.) precludes the use of any one set of equations. Thus a more heuristic approach for the determination of the key processes is employed. It involves identification of the parameters that result from the forces driving the system, which in turn govern the more detailed (small-scale) phenomena. Additionally, if the scheme is to be useful in a practical sense, these parameters should depend only on data readily available from the current databases (criterion 3 listed previously).

There are a wide range of phenomena of potential interest in littoral areas, e.g., physical, acoustic, biological, atmospheric, etc., each of which encompass a range of dynamic processes. Also, there are many different types of coastal geographical configurations (CGC), shelves, straits, enclosed seas, rivers, etc.; each having its own characteristics and key parameters. It follows that a littoral classification scheme would have to be specific to each phenomenology-CGC combination. Development of a specific classification scheme thus involves initially choosing a phenomenology, CGC combination, from which the quantitative dimensionless groups can be identified. This process is schematically shown in Figure 1, left side. The general approach for further use of the classification scheme for specific applications is depicted on the right of Figure 1 and involves weighting of the classification parameters in a manner appropriate to the specific application. This general approach will be employed to derive a coastal shelf classification scheme in this paper.

A Littoral Classification for Physical Processes on Coastal Continental Shelves

Acknowledging the wide range of physical processes extant in coastal shelf regions (cf., Csanady, 1982; Hsu, 1988), we adopt a heuristic approach to determine the appropriate classification parameters. The approach followed starts with identifying the driving forces and boundary conditions that drive the processes on the coastal shelf, as shown in Figure 2. Next the dynamic processes found in the coastal ocean are categorized as large-scale features that are

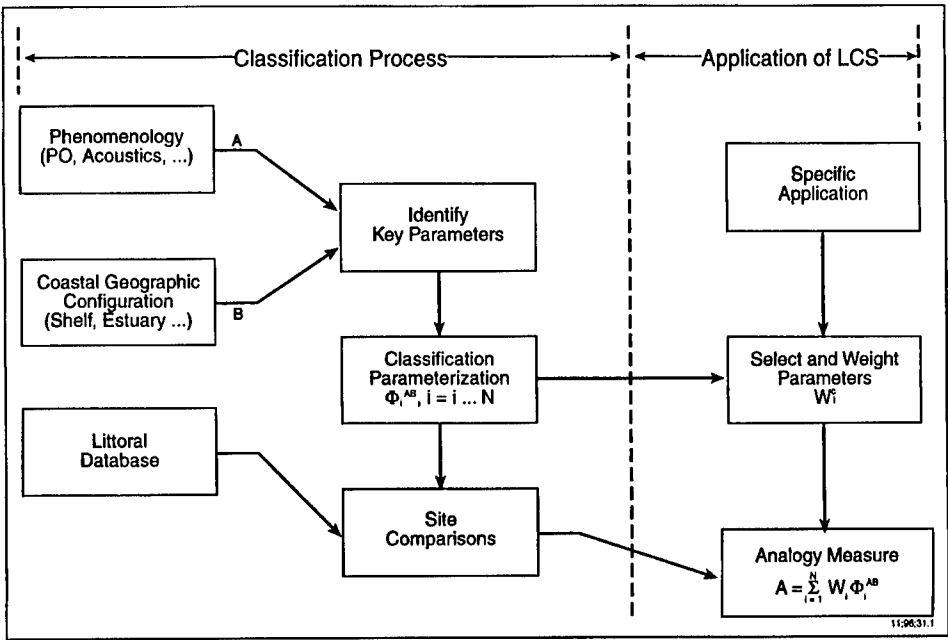


Fig. 1: Littoral classification approach.

generally uniform over the whole of a specific coastal region and small-scale features that can be highly variable in time and/or space within that region. Our assessment of these features, based on a review and classification of the known physical processes (cf., Phillips, 1977; Csanady, 1982, 1990; Pedlosky, 1987; Huyer, 1990), indicates that there are four primary, large-scale physical processes in the coastal/littoral ocean:

eddies, upwelling, currents, and stratification (as indicated in Fig. 2). These large-scale features can be used to characterize the coastal region and provide the appropriate level of abstraction for our classification scheme. This admittedly heuristic assumption is the basis for our approach, the viability of which will be determined from the outcome, i.e., the ability to derive appropriate dimensionless parameters that allow site

Driving Forces & Boundary Conditions	Large Scale Features	Local, Small-Scale Processes (Partial List)
<ul style="list-style-type: none"> Shelf width (L_s), slope Inertial forcing (R_o) Wind stress (τ), friction velocity (\underline{u}_*) Ocean circulation (\underline{u}_o) Tidal Forcing, currents (\underline{u}_T) Surface heat flux River outflows Topography Coastal contour 	<ul style="list-style-type: none"> Coastal eddies, scale Upwelling (w_u) Coastal currents (\underline{u}) Stratification (N) 	<ul style="list-style-type: none"> Cross-shelf currents Coastal jets and filaments Fronts: <ul style="list-style-type: none"> Shelf Break Tidal Mixing: <ul style="list-style-type: none"> Surface Layer Internal Bottom BL Internal waves Optical clarity

Fig. 2: Coastal shelf processes.

comparisons, particularly for specific applications.

In general, the nature and intensity of the small-scale processes are governed by the large-scale processes whose parameterization (developed subsequently) provides a basis for their assessment. As indicated in Figure 2, the boundary and driving forces are related to the large-scale features and represent the basic parameters that can be calculated from the available databases. The two geological boundary conditions, topography and coastal contour (shoreline), do not enter directly but serve to define the boundaries of specific coastal shelf regions. The coastal shelf may have to be segmented to account for significant variations in the geological boundaries, as was necessary along the Korean coast in the site classification that follows.

To derive an appropriate parameterization for the four large-scale processes, we utilize the basic scaling relationships derivable from the accepted, classical oceanographic models. Consider first the coastal eddy scale. When the equations of motion for geophysical flows in a rotating frame are cast in dimensionless form, the key dimensionless parameter that arises is the Rossby number, Ro . Related to Ro is the Rossby radius of deformation, or simply the Rossby radius, L_R , that arises from the geostrophic balance (Gill, 1982; Pedlosky, 1987)

$$L_R = c/(2\Omega \sin \phi) \quad (1)$$

where $c = (g'h)^{1/2}$ is an interfacial wave speed (assuming that there is a baroclinic, two-layer flow), h is the thickness of the upper layer, $g' \equiv g\Delta\rho/\rho_0$, g is the gravitational constant, $\Delta\rho$ is the density difference between the layers, ρ_0 is the mean, reference density, and ϕ is the latitude. The Rossby radius characterizes the scale of motion, induced by the earth's rotation, which for coastal regimes can be compared with the local horizontal scale, the shelf width, L_S as

$$\Phi_L = L_R/L_S \quad (2)$$

This parameter indicates whether or not the large-scale motions are confined to the shelf region. It depends on the local shelf width and stratification as well as the latitude of the area of interest; $\Phi_L < 1$ indicating a wide shelf and $\Phi_L > 1$ indicating a narrow shelf. The coastal eddy scale, Φ_L , will be used as the parameterization for coastal eddies for purposes of littoral

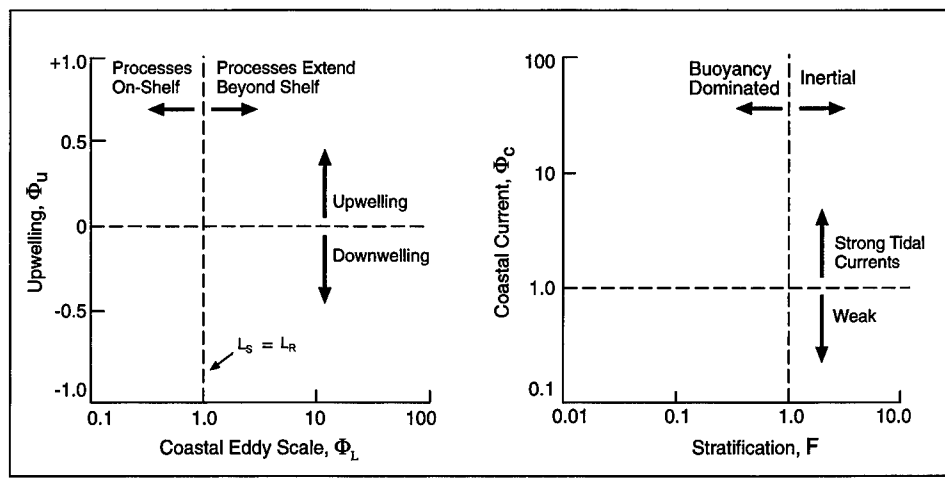


Fig. 3: Coastal shelf classification.

classification. This parameter (along with the other three, described as follows), is shown schematically in Figure 3, where the physical significance of the parameter ranges are also indicated.

Upwelling in coastal regions can result from several processes, including offshore Ekman transport resulting from wind stress and Coriolis acceleration, density discontinuities at the shelf break front, etc. (Huyer, 1990). To parameterize upwelling for this classification scheme, we utilize the simple, two-layer upwelling solution derived by Gill (1982), for the case of two-dimensional (no variation in the along-shore direction) baroclinic flow due to wind forcing. Gill's solution yields time-dependent relationships for the upper layer off-shore current speed, the interfacial depth, and the steady along-shore current speed. For the present application, we chose as a metric for the degree of upwelling the rate of change of the interfacial depth at the coast (the maximum value), i.e., the vertical upwelling velocity

$$W_u = dh/dt = \tau/\rho_0 (g'h)^{1/2} = (\tau/\rho_0)c \quad (3)$$

where τ is the along-shore surface wind stress. Using the conventional representation for τ in terms of the friction velocity, u_*

$$|\tau/\rho_0| = u_*^2 = C_D |U_{10}| U_{10} \quad (4)$$

where U_{10} is the surface wind speed, conventionally measured at the 10-m height, and C_D is the drag coefficient taken as constant at the typical value of $C_D = 0.001$ (Geernaert, 1990). The ratio of the

upwelling velocity to the interfacial wave speed, c , that is characteristic of the two-layer geometry, yields the littoral upwelling parameter

$$\Phi_U = u_*^2/c^2 \quad (5)$$

Φ_U serves as an indicator of the degree of upwelling that can be expected at a particular site as determined from the stratification (through c) and the wind speed and direction, U_{10} . Upwelling versus downwelling conditions are determined from the direction of U_{10} and the coastal orientation, i.e., a northward wind on an east coast in the northern hemisphere will cause upwelling due to Ekman transport (Gill, 1982).

The third parameter is related to the along-shore coastal current. Tidal effects impose a variable, periodic current, U_T , that adds to the mean current, U , resulting from the wind stress and large-scale (deep water) circulation patterns. If U_T is taken as the maximum tidal current over a tidal cycle, then the ratio

$$\Phi_C = U_T/U \quad (6)$$

indicates the relative contributions of the short-term (~semidiurnal) tidal flows and the long-term (e.g., monthly average) coastal currents.

To represent the fourth parameter, the stratification, we use a bulk Froude number defined as

$$F = \Delta U/N h_i \quad (7)$$

where ΔU is the difference between the upper and lower layer current speeds, and h_i is the thickness of the interface between the upper and lower layers and

$$N = (-g\Delta\rho/\rho_0 \Delta z)^{1/2}$$

$$= (-g'/h_i)^{1/2} \quad (8)$$

is the buoyancy frequency. The Froude number results from the equations of motion for a stratified flow as the dimensionless parameter that represents the balance between the inertial and buoyancy forces (cf., Phillips, 1977). The stratification in most coastal regions can be reasonably represented as a two-layer system, so that F represents the degree to which the water column is stratified. Large values of F indicate that inertial forces (shear) dominates over buoyancy and that the stratification is weak, as is typical in the winter in the coastal ocean. Conversely small F indicates large buoyancy forces, i.e., strong stratification typical of summer conditions.

Figure 3 illustrates the significance of the four parameters that characterize the physical processes on coastal shelf regions: Φ_L , Φ_U , Φ_C , and F . These four parameters are mutually independent so the pairing of the parameters as shown in Figure 3 is arbitrary. The numerical scales for each of the parameters shown in Figure 3 represent the ranges anticipated for worldwide coastal shelf regions.

Coastal Shelf Comparisons

The four classification parameters can be used to represent the key coastal shelf processes. The quantities necessary to compute values for each of these parameters at specific sites are readily obtainable from data base compilations and the research literature, although they may be hard to obtain for certain remote or "protected" sites. In general, all the necessary parameters (such as the interface thickness, h_i) may not be directly specified in the available databases; however, they can be computed from the available data [e.g., h_i can be determined from standard conductivity, temperature, depth (CTD) profiles].

To illustrate the coastal shelf classification, data from seven sites have been collected and used to compute values of the four classification parameters. The locations of these sites are shown in Figure 4. Data for two U.S. sites, California and Gulf of Alaska, are available on a monthly average basis, whereas for the Washington State and foreign sites, only seasonally averaged data were readily available. (Data sources used include

Landry and Hickey, 1989; Thomson, 1981; Oceanographic Atlas of Korean Waters, 1987; Master Oceanography Observations Data Set, 1994; U.S. Navy Marine Climatic Atlas of the World, 1977; Tide Tables 1994, Central and Western Pacific Ocean and Indian Ocean, 1993; Lenz, 1995; Lenz and Chapman, 1989; S. Tarbell, 1995.)

Figure 5 shows the data from these seven sites in the form of classification diagrams. From these diagrams we can make several general observations regarding these sites. First, it is apparent from the values of the stratification parameter (Fig. 5b) that all of these coastal sites are influenced by stratification, i.e., $F < 1$. The strongest effects of stratification were found to occur in the months of June and August at the Alaska and CODE (Southern California) sites, respectively. (Note that the seasonal averages for the foreign sites may obscure some of the stronger effects.) Weak stratification is indicated for the winter in the Korea-East 1 coastal segment and for all but the summer months at the Yellow Sea site. The latter is to be expected as this region is rather shallow, having a very wide shelf, as can be seen from the value of the coastal eddy/shelf width parameter, Φ_L , Figure 5a. The Yellow Sea (effectively a very wide shelf) also has a significantly larger coastal current parameter value as compared with the

other sites, due to the strong, local tidal forcing. The Korea-East 2 eddy/shelf parameter also stands out from the others. Regarding upwelling, generally all sites indicate weak and variable up/downwelling, with exceptions of the strong upwelling in winter in the Yellow Sea and strong downwelling in winter at Korea-East 1.

An extensive error analysis was performed using the Alaska coastal data, because it is the most complete and thus provides the most accurate measure of the actual errors that can be expected at each of the sites. Errors in each of the four classification parameters were computed using values of the standard error of the monthly means of each of the database derived quantities and therefore represent the accuracies to which the parameters are representative of the monthly average conditions. These values are shown in Figure 5, as error bars, and can be seen to be sufficient to allow site comparisons and to distinguish seasonal variations when they are significant. Error estimates based on the Alaska data have also been computed for the derived parameters in the application of the littoral classification discussed in the following section.

In sum, the classification parameter space provides an indication of how these sites would respond to the physical forcing mechanisms and how they compare with each other. Site comparisons for a

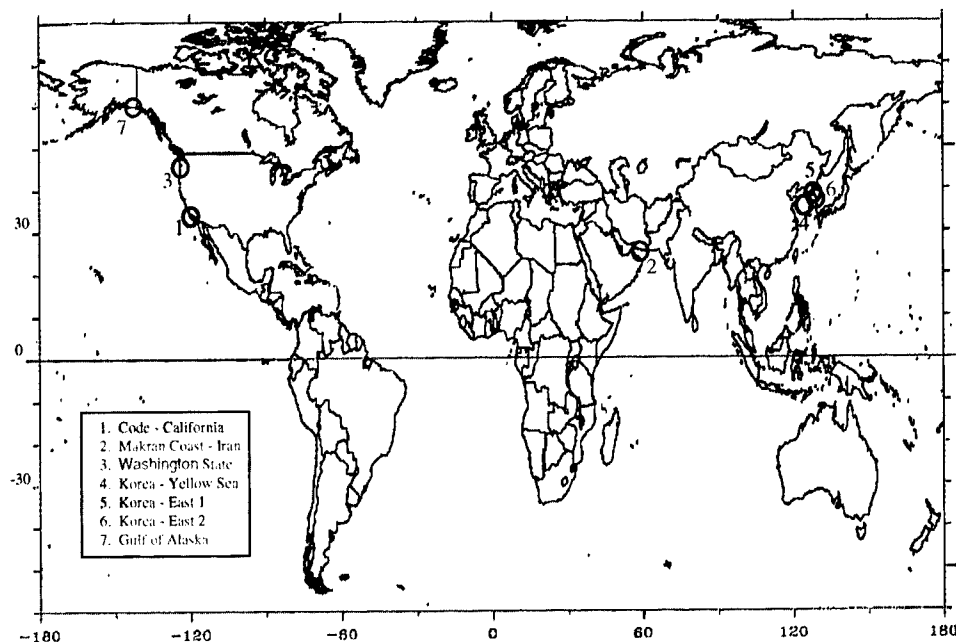


Fig. 4: Littoral sites investigated.

specific application, illustrated in the following section, will use these classification parameters. Additional details of the derivations, especially for the following applications, are given in Brandt *et al.* (1997).

Application of the Littoral Classification System

To illustrate the utility of the littoral classification system, a specific coastal issue has been investigated: the dispersion of a point discharge in coastal waters.

Consider a relatively simple analysis of the dispersion of a point discharge (such as a toxic waste) in the surface layer off the coast. The concentration of discharged material at a specified time, $C(\Delta t)$, is directly related to the volume over which the material has spread during the time interval, Δt , since the initial release. In terms of the average along-shore and cross-shore coastal currents, U and V , respectively, and the vertical depth of mixing, d

$$C(\Delta t) \propto U \Delta t \cdot V \Delta t \cdot d \tag{9}$$

In coastal waters the upper layer will generally be well mixed over short time periods (due primarily to wind-induced mixing) so that it is reasonable to assume that the discharged material will quickly fill the upper mixed layer, h , and that further vertical mixing will result from turbulent entrainment (cf., Csanady, 1990). Extensive studies of turbulent entrainment in stratified fluids, in the laboratory and the ocean (Fernando, 1991), indicate that the entrainment coefficient, defined as the vertical velocity of the interface between the mixed layer and the stratified layer, u_e , scales inversely with the bulk Richardson number, which is directly related to the Froude number (Eq. 7), as $u_e = 0.002(h_i/h)F^2\Delta U$. Expressing the depth of mixing as the sum of the mixed layer depth and the depth of entrainment, $d = h + u_e\Delta t$, and noting that the cross-shore velocity is generally highly variable and significantly less than the along-shore component (e.g., Kosro, 1987), we can approximate $V \cong 0.1 U$, so that

$$C(\Delta t) \propto 0.1 U^2 \Delta t^2 \cdot [h + 0.002 (h_i/h) F^2 \Delta U \Delta t] \tag{10}$$

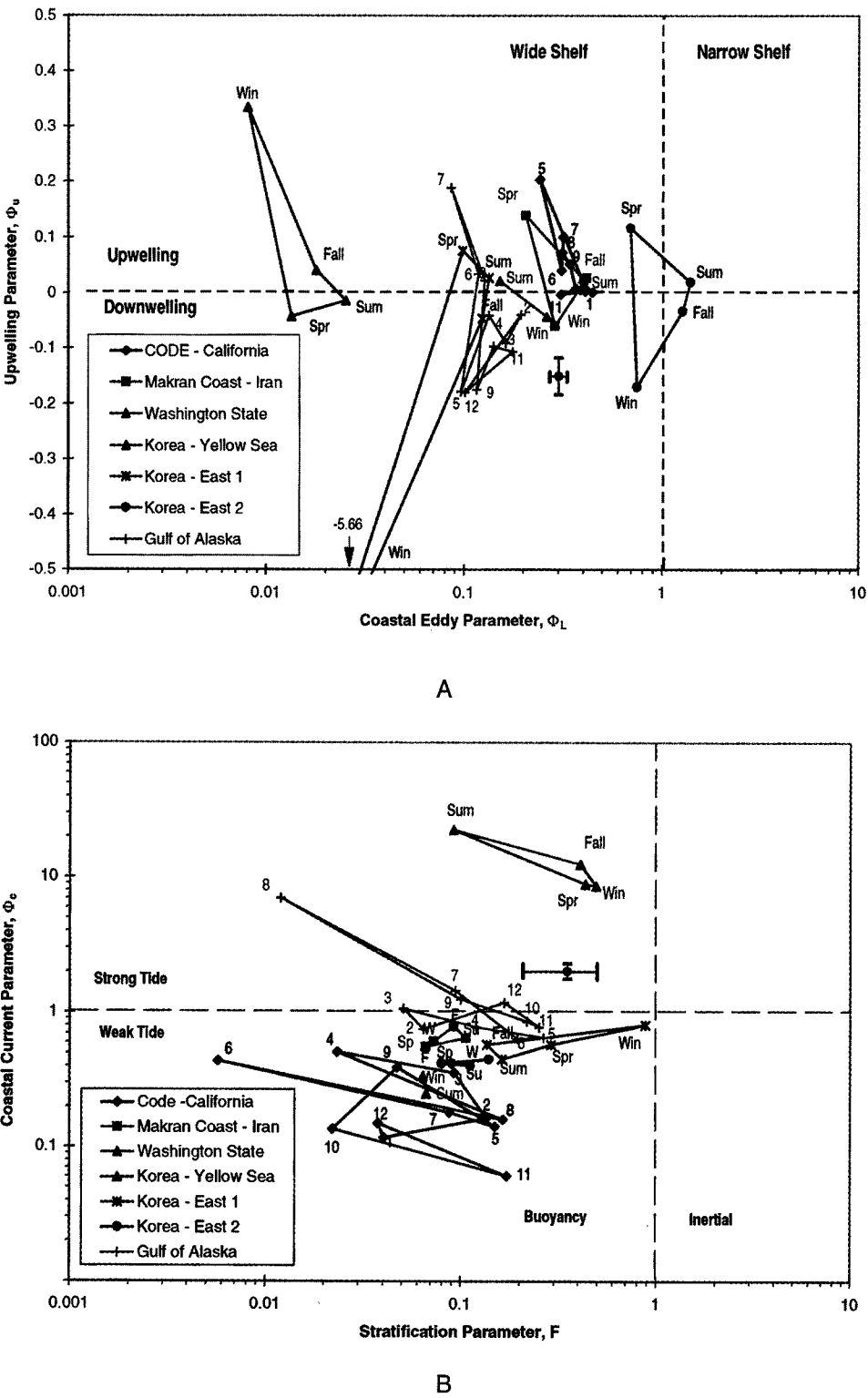


Fig. 5: Coastal shelf site comparison: (a) coastal upwelling and eddy parameters, (b) coastal current and stratification parameters.

To compare the dispersion at various coastal sites, it should be noted that all the quantities required for evaluation of equation (10) are already contained in the classification parameters, Figure 5, or in the data used to derive them. To compare sites it is instructive to separate the hori-

zontal and vertical components of dispersion in equation (10), as

$$C_1 = 0.1 U^2 \Delta t^2$$

$$C_2 = h + 0.002 (h_i/h) F^2 \Delta U \Delta t \tag{11}$$

The values of these two parameters, for each of the seven sites, are shown in Figure 6 (contours of constant volume are indicated by the dotted lines).

The dispersion at some sites does not vary appreciably over the year, as for example, at the CODE and Korea-East 2 sites (Fig. 6). The Washington State, Makran Coast, and Korea-East 1 sites appear to have similar dispersion properties. This would allow for a reasonable extrapolation of observations at the Washington State site to the less accessible Makran Coast and Korea-East 1 locations. Dispersion in the shallow Yellow Sea varies widely with season and, as expected, is dominated by horizontal spreading. The high seasonal variations in the dispersion at the Gulf of Alaska coastal site results from the considerable variation in the winds. With observations such as these it would be possible, for example, to estimate the spread of toxic chemical or biological agents at sites of strategic interest based on measurements in more readily accessible areas.

Summary

A technique for quantitative classification of littoral sites has been developed based on the dimensionless parameters derived from the governing equations for specific physical processes and coastal geographical configurations. The scheme has been used to describe the physical

oceanographic processes on coastal continental shelves resulting in the definition of four dimensionless parameters to represent the large-scale features of coastal regions: eddies, upwelling, currents, and stratification. The processes at seven diverse, worldwide sites have been compared using these parameters. To illustrate the use of the littoral classification system, the coastal shelf classification parameters were used to investigate the dispersion of a point discharge in the surface layer. It was seen that some sites do in fact have similar characteristics, thus allowing extrapolation of information from studied, accessible sites to others of strategic or environmental interest that may not be readily accessible.

The general littoral classification approach could be applied to other areas of interest, such as meteorological and acoustic processes relevant to naval, defense, and civil issues. By identifying analogous sites, data and models could be extrapolated from sites that have been studied to sites that are not generally accessible, providing a basis for assessing, for example, the performance of naval weapon or surveillance systems, coastal radar propagation models, and the environmental impact of accidental or intentional releases.

Current efforts are focused on obtaining data from additional sites for the physical oceanographic-coastal shelf classification, the development of a classification

scheme for near-shore (beach) processes, acoustic propagation in littoral waters, and the use of the general classification framework for additional, practical applications.

Acknowledgements

We thank L.J. Firzzell-Makowski and J.L. Hanson for their careful and constructive review of the manuscript. This effort has been supported by The Office of the Oceanographer of the Navy/Naval Research Laboratory, Tactical Oceanographic Monitoring System Program (K.M. Ferer), Contract SPAWAR N00039-91-C0001; The Office of Naval Research, Tactical Environmental Support Program (E. Hashimoto), Coastal Sciences Program (T.H. Kinder), Contract SPAWAR N00039-95-C0002; and Ocean Executive Agent, Defense Modeling and Simulation Office (D.W. Blake) Contract N0024-98-D-8124.

References

- Brandt, A., J. Calman, and J.R. Rottier, 1997: A Quantitative Littoral Classification System. Johns Hopkins Univ. Applied Physics Lab. Report STD-B-0077, 27 pp.
- Csanady, G.T., 1982: *Circulation in the Coastal Ocean*. Reidel, 279 pp.
- , 1990: Mixing in coastal regions. In: *Ocean Engineering Science, The Sea*, vol. 9A. B. Le Mehaute and D.M. Hanes, eds. Wiley, New York, 593–629.
- Davis, VI, G.W., 1995: Naval oceanography for the future. *Sea Technology*, 36, 13–21.
- Fernando, H.J.S., 1991: Turbulent mixing in stratified fluids. *Annu. Rev. Fluid Mech.*, 23, 455–493.
- Gill, A.E., 1982: *Atmosphere-Ocean Dynamics*. Academic Press, New York, 662 pp.
- Geernaert, G.L., 1990: Bulk parametrization for the wind stress and heat fluxes. In: *Surface Waves and Fluxes, vol. 1. Current Theory*. G.L. Geernaert and W.J. Plant, eds. Kluwer Academic Press, 91–172.
- Hansen, D.V. and M. Rattray, Jr., 1965: Gravitational circulation in straits and estuaries. *J. Mar. Res.*, 23, 104–122.
- Hsu, S.A., 1988: *Coastal Meteorology*. Academic Press, New York, 260 pp.
- Huyer, A., 1990: Shelf circulation. In: *Ocean Engineering Science, The Sea*, vol. 9A. B. Le Mehaute and D.M. Hanes, eds. Wiley, New York, 423–466.
- Jay, D.A. and J.D. Smith, 1988: Residual circulation in and classification of shallow, stratified estuaries. In: *Physical Processes in Estuaries*. J. Dronkers and W. van Leussen, eds. Springer-Verlag, New York, 21–41.
- Kosro, P.M., 1987: Structure of the coastal current field off northern California during the coastal ocean dynamics experiment. *J. Geophys. Res.*, 92, 1637–1654.
- Landry, M.R. and B.M. Hickey, 1989: *Coastal Oceanography of Washington and Oregon*. Elsevier Oceanography Series, vol. 47.
- Lenz, S.J., 1995: Personal communication of CODE data.

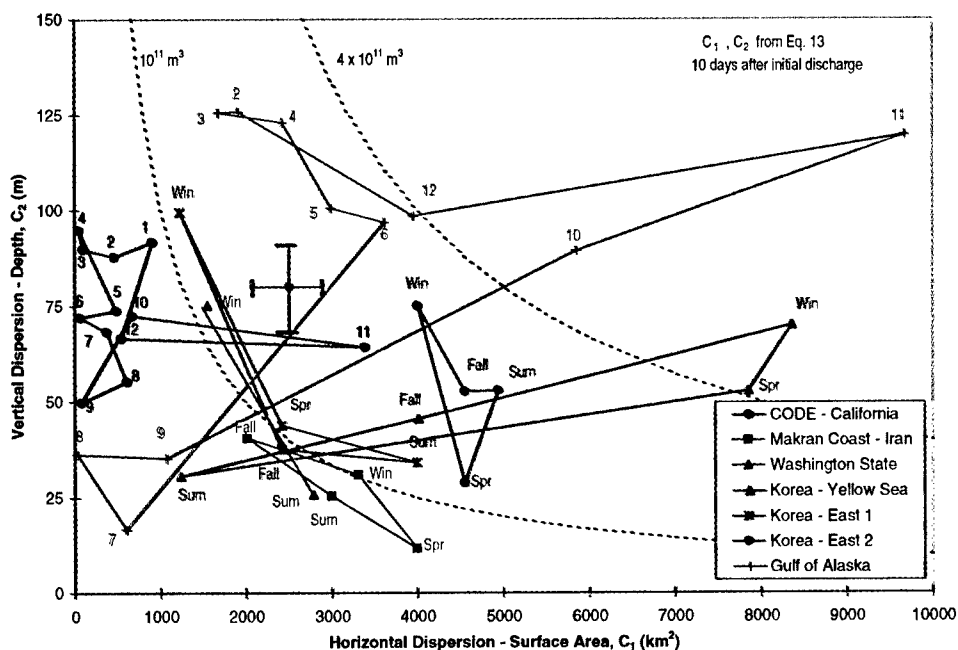
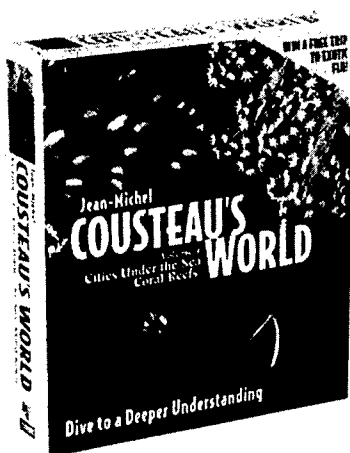


Fig. 6: Dispersion of a point discharge in the coastal ocean.

- _____ and D.C. Chapman, 1989: Seasonal differences in the current and temperature variability over the northern California shelf during the coastal ocean dynamics experiment. *J. Geophys. Res.*, 94, 12571-12592.
- Master Oceanography Observations Data Set*, 1994: US Naval Oceanographic Office.
- Oceanographic Atlas of Korean Waters*, 1987: vol. 1, Yellow Sea, Korea Ocean Research and Development Institute.
- Pedlosky, J., 1987: *Geophysical Fluid Dynamics*, 2nd edition. Springer-Verlag, New York, 710 pp.
- Phillips, O.M., 1977: *The Dynamics of the Upper Ocean*, 2nd edition, Cambridge Univ. Press, 336 pp.
- Pritchard, D.W., 1955: Estuarine circulation patterns. *Proc. Amer. Soc. Civil Eng.*, 81, (717), 1-11.
- _____, 1989: Estuarine classification—a help or a hindrance. In: *Estuarine Circulation*. B.J. Neilson, A. Kuo, and J. Brubaker, eds. Humana Press, Clifton, NJ, 1-38.
- Tarbell, S. 1995: Personal Communication, coastal current meter data.
- Thomson, R.E., 1981: *Oceanography of the British Columbia Coast*. Canadian Special Publication of fisheries and Aquatic Sciences, vol. 56.
- Tide Tables 1994, Central and Western Pacific Ocean and Indian Ocean*, 1993: NOAA.
- U.S. Navy Marine Climatic Atlas of the World*, 1977: vol. 2, North Pacific Ocean, NAVAIR 50-1c-529.
- Warrick, R.A., C. Le Provost, M.F. Meier, J. Oerlemans and P.L. Woodworth, 1996: Changes in sea level. In: *Climate Change 1995, The Science of Climate Change*. J.T. Houghton, L. G. Meira Filho, B.A. Callander, N. Harris, A. Kattenberg and K. Maskell eds., Intergovernment Panel on Climate Change, Cambridge Univ. Press, 359-455. □

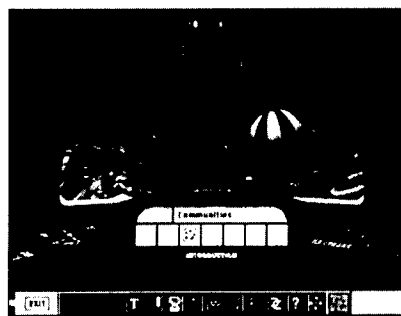
EXPLORE JEAN-MICHEL COUSTEAU'S WORLD!

CITIES UNDER THE SEA: Coral Reefs is a spectacular exploration of undersea "cities" of coral reefs with the world renowned undersea explorer Jean-Michel Cousteau as your host. In this CD-ROM you will travel via the 3-D animated submarine to seven undersea laboratories, each focusing on a different ecological theme to demonstrate how this perfectly balanced ecosystem works. This is a perfect CD-ROM for anyone in the family from ages 10 to adult who is fascinated with coral reefs.



Features:

- All-original full-color photographs, videos, graphics, sound and text created expressly by Jean-Michel Cousteau and his team for CITIES UNDER THE SEA
- Over 700 breathtaking images
- 35 minutes of fascinating, narrated video
- More than 50 minutes of colorful slide shows
- Over 70,000 words of text
- 3-D submarine rides through a virtual reef
- A full course in coral reef ecology
- Two lively "Hot Topic" critical thinking games on ecological/social issues involving coral reefs



visit the web site: <http://www.enteractive.com/jmcousteau>

In-Ovation Award Winner

One of the Top Ten Educational Software Products of 1998
—Edusource.com

"...uncommonly imaginative CD-ROM...enlightening educational material...will yield many hours of enlightening entertainment." — *CD-ROM Today*

"...dazzling CD-ROM...Narrated video and stunning photos provide unforgettable pictures..." — *Home PC*

"...outstanding graphics and 3-D animation."
— *Natural History Magazine*

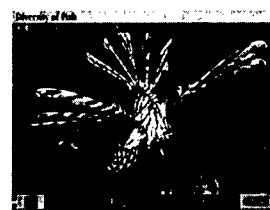
"The photographs of fish and plant life that make up the reef are surprisingly vivid..." — *People Magazine*

"The pick of the lot is *Cities Under the Sea: Coral Reefs*."
— *Publishers Weekly*

(Complete reviews available upon request.)

System Requirements:

- IBM® PC or compatible
- 486SX-33MHz processor or better
- 8 MB RAM
- 5.4 MB hard disc space available
- 640x480 display with 265 colors
- Double speed CD-ROM drive (300KB/sec transfer rate)
- Microsoft® Windows® 3.1 or later or Windows 95®
- Sound card supported by Microsoft Windows
- Mouse



(Macintosh Version Available Summer 1998)

To Order send \$29.95 (check or credit card) to: The Oceanography Society

Quant.	Item	Price	Total
<input type="text"/>	Jean Michel Cousteau Coral Reef PC CD ROM	\$29.95	<input type="text"/>
California residents add 8.25% sales tax (\$2.47 per disc)			

Free shipping via US Priority Mail!

(Make checks drawn on US funds payable to Waveforms) Total

Name: _____
Shipping Address: _____

Phone: (____) _____ Email: _____

Card #: _____ Exp. Date: _____

Signature: _____ Visa M/C

4052 Timber Ridge Dr.
Virginia Beach, VA 23455
(757) 464-0131



The Oceanography Society
will receive a donation of \$5 per disc!

In addition, 10% of the profits from
the sales of the disc will be donated to
coral reef education programs.

International orders shipped duty collect.



NATIONAL SCIENCE FOUNDATION

Fifty Years of Ocean Discovery

This three-day symposium and celebration will gather together many of the leading individuals who have contributed to the past fifty years of ocean discovery, including scientists, engineers, administrators, policymakers, and interested observers. Over the past five decades, NSF has sponsored much of the groundbreaking research that has helped us better understand the ocean and appreciate its importance to the nation and the world.

The symposium will be chaired by **Dr. John Steele** of the Woods Hole Oceanographic Institution and will feature presentations on landmark discoveries in ocean sciences, the institutions that have made these achievements possible, and a glimpse into the future of the field. Former NSF personnel and individuals connected with oceanographic research nationwide will share their experiences and present their views about NSF's ocean history and the future of ocean sciences. Featured speakers will include **Dr. Robert Ballard**, **Dr. Richard Barber**, **Dr. John Farrington**, **Dr. John Knauss**, **Dr. Marcia McNutt**, and **Dr. Walter Munk**.

All interested individuals are encouraged to participate in this event.

WHEN

October 28-30, 1998

WHERE

The historic National Academy of Sciences Building on the Mall in Washington, DC.

REGISTRATION

See registration form on the symposium Website or contact the individuals listed below for more information. The registration fee (\$75 in advance, \$25 for students) includes a copy of a book to be based on the symposium, continental breakfasts and lunches, and evening receptions at the National Academy of Sciences and the National Science Foundation.

For more information, contact

Ann Carlisle or **Ed Urban** at the Ocean Studies Board (202-334-2714, acarlis1@nas.edu) or check the Website at <http://www2.nas.edu/osb/2326.html>.



DIALOG III

Dissertations Initiative for the Advancement of Limnology and Oceanography

Program for Recent Ph.D. Recipients in Limnology, Oceanography and Related Disciplines

PURPOSE

The DIALOG (Dissertations Initiative for the Advancement of Limnology and Oceanography) program seeks to reduce the historical, institutional and philosophical barriers that limit the exchange of information among aquatic scientists, and to expedite the transition from Ph.D. student to independent researcher. Through this program, the dissertation abstracts of program participants are collected and made available, and a symposium is held to foster inter-disciplinary thinking and collaborations. In addition, information on recent Ph.D. recipients is collected for human-resource purposes.

DATA BASE

Information submitted by applicants is used to characterize this most recent group of Ph.D. recipients, and later, as the data base expands, will be used to assess trends. Follow-up studies will be conducted to assess professional progress of participants and long-term outcomes of the program.

Ph.D. ABSTRACTS

Dissertation abstracts are compiled and made available through the ASLO web page (www.aslo.org/dialog.html) to provide a concise introduction to the work of this most recent generation of aquatic science researchers. Abstracts

from dissertations completed after April 1, 1997 are eligible for inclusion. Application for the DIALOG III symposium is not necessary.

SYMPOSIUM

A symposium for up to 40 recent Ph.D. recipients will be held in October, 1999 to foster cross-disciplinary and international understanding and collaborations. Each participant will present a poster and a 10-minute overview of his or her Ph.D. dissertation research, with an additional 5 minutes for questions/discussion. Participants will also form working groups to discuss emerging aquatic science research, education, and policy issues. Funding-agency representatives will present perspectives on interdisciplinary and international aquatic science research programs and building a successful career. Symposium travel subsidies are possible through funding from the agencies listed below. Support from the European Commission is pending.

Symposium Eligibility

The symposium is open to individuals who complete their Ph.D. requirements between April 1, 1997 and March 31, 1999, and whose work in atmospheric, biological, chemical, geological, physical, or terrestrial science is relevant to biologically oriented limnology or oceanography. Individuals from all

nations are eligible for consideration. A committee will select participants based on the application materials submitted. As symposium space is expected to be limited, selection will favor those who wish to pursue interdisciplinary aquatic science research.

Symposium

Dates and Location

October 18 - 24, 1999

Bermuda Biological Station
for Research

Symposium

Application Deadline

May 1, 1999

APPLICATIONS

Dissertation abstract-submission and symposium-application forms are available at:

www.aslo.org/dialog.html



DIALOG is co-sponsored by the American Society of Limnology and Oceanography and Whitman College, and is funded by the U.S. National Science Foundation, National Aeronautics and Space Administration, National Oceanic and Atmospheric Administration, and Office of Naval Research.

Nominations for the Walter Munk Award

In February 1994, the Walter Munk Award Selection Committee, made up of representatives designated by The Oceanography Society, the Chief of Naval Research, and the Oceanographer of the Navy, will begin reviewing nominations. If a worthy candidate is identified, the fifth Walter Munk Award for Distinguished Research in Oceanography Related to Sound and the Sea will be presented at the TOS 1999 scientific meeting in Reno, Nevada, April 27–30.

In keeping with Dr. Munk's contributions to ocean science, nominations for the award will be based upon:

- a. Significant original contributions to the understanding of physical ocean processes related to sound in the sea;
- b. Significant original contributions to the application of acoustic methods to that understanding; and/or
- c. Outstanding service that fosters research in ocean science and instrumentation contributing to the above.

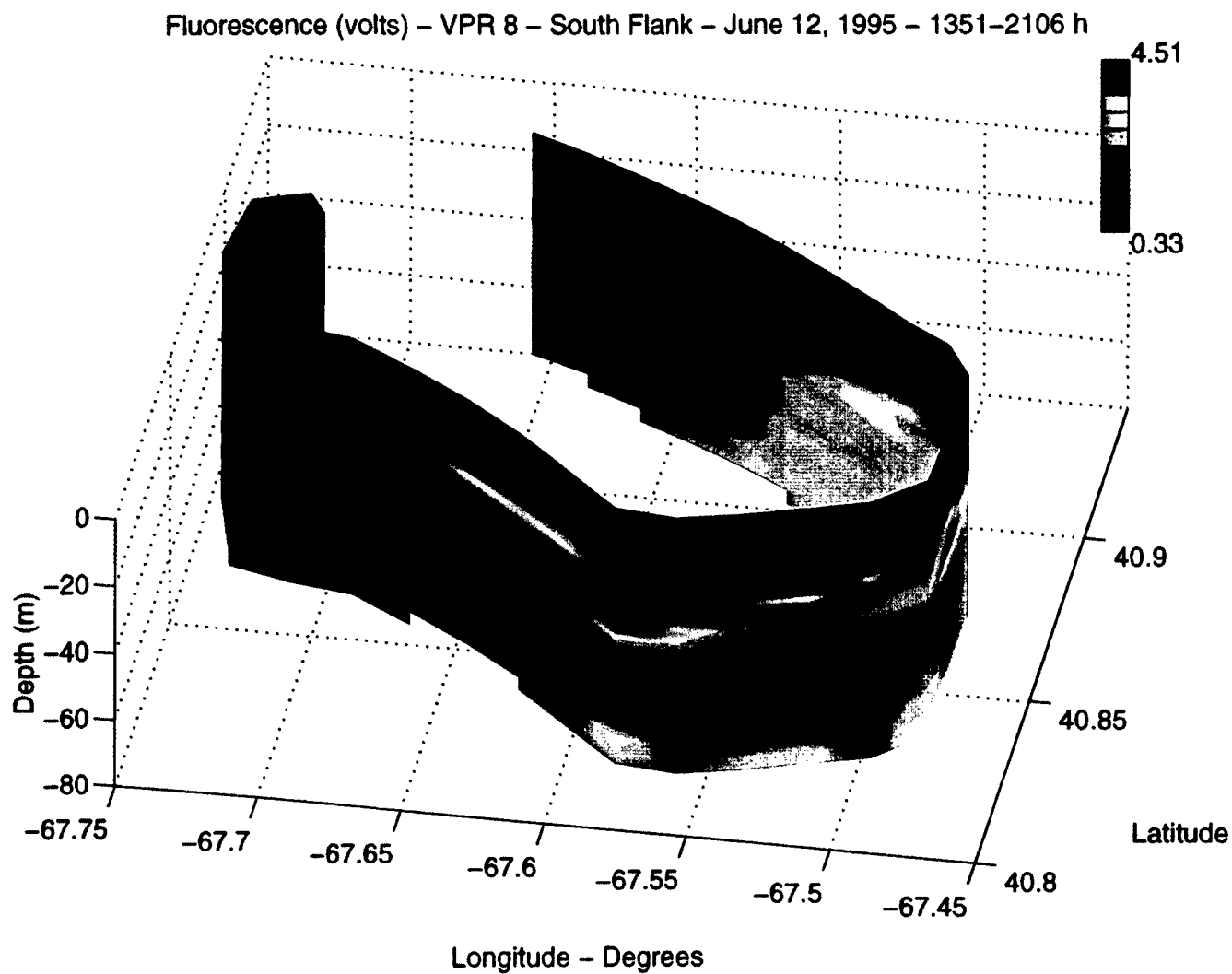
Previous award winners are

- 1993 Walter Munk, Scripps Institution of Oceanography, USA
- 1994 David M. Farmer, Institute of Ocean Sciences, Canada
- 1996 Leonid M. Brekhovskikh, Moscow Institute of Physics and Technology, Russia
- 1997 Stephen A. Thorpe, Southampton Oceanography Centre, UK

Written nominations for the 1999 award should be sent to The Oceanography Society, 1755 Massachusetts Avenue, NW, Suite 800, Washington, DC 20036, USA.



THE OCEANOGRAPHY SOCIETY
4052 Timber Ridge Drive
Virginia Beach, VA 23455 USA
Phone: (757) 464-0131



Units: The International System (SI) should be used throughout. Symbols for a unit of measurement should be used only when preceded by a number (e.g. "10 m" but "several meters"). Unit symbols are not to be punctuated (i.e., they are not treated as abbreviations); the same symbol is used for both singular and plural.

Abbreviations: Abbreviations and acronyms must be identified with their first use. The solitary use of acronyms is unnecessary and discouraged. The abbreviation "U.S." is appropriate when it modifies another word (e.g. U.S. Department of Commerce). Names of states and months should be spelled out except in Table and Reference sections.

Mathematical Formulas: The use of mathematical symbols and formulas should be held to the absolute minimum necessary, and in those cases all symbols must be clearly defined in the text. For detailed guidelines, see the Author's Guide of the American Meteorological Society.

Color Photography/Print Material: The use of color photos or art work is encouraged, if its use enhances the readability, utility, or artistic merit of the article. At present, there are no page charges for publication, but costs for color processing will be charged to the author.

Covers: Any author may submit color material to be considered for use on the front or back covers. Cover material must be pertinent and complementary to the author's published article. In some relevant

cases, cover figures with extended captions will be considered for publication without an accompanying article. Cover figures must be oriented vertically.

Book/Video Reviews: Reviews are solicited for scientific books and videos, and also for published material with a potentially wider appeal (e.g., novels, biographies, historical anecdotes, etc.). Reviewed material must have relevance to the oceans. Reviewers should keep in mind that a well-written review helps readers decide whether or not it is worth their time to read the book in its entirety. The reader of a review expects basic information about the content and organization of the book, as well as a subjective opinion about the quality, style and relevance of the material.

Reviews should include: complete title of book/video, author or editor, year of publication, number of pages, price, format (hardbound, soft-cover, paperback, etc.), name of publisher, city of publication and the reviewer's name, title and affiliation.

Reprints: Offprints of published articles are offered at the time of acceptance and are printed concurrently with the magazine. Contact the editorial office for current estimates of reprint costs.

"Galley" proofs: These will be distributed as soon as they are ready, and the author will have one-day turn around time to return them to the editorial office.

SIGN ME ON!

Please accept my application for membership in The Oceanography Society. My annual membership dues will support the work of the Society and will entitle me to receive *Oceanography*, to register at discounted rates for meetings sponsored and/or co-sponsored by the Society, to vote in Society elections, and to express my opinion on all matters of interest to the Society. I would like to join in the following category (choose one):

- ☐ Regular Member (\$50)
- ☐ Student Member (\$25)*
- ☐ Corporate/Institutional Member (\$500)
- ☐ Library (\$125)
- ☐ Sponsoring Member (\$100)
(\$50 is tax deductible)

* Students must provide the following information to certify student status:

Enrolled at _____ Major Subject _____ Date _____
Certified by _____ Certifier's signature & title _____

Name _____
Affiliation _____
Address _____

Phone _____ ☐ Home ☐ Work
E-Mail _____
Discipline(s): ☐ Biology ☐ Chemistry ☐ Physics
☐ Geology/Geophysics ☐ Applied Technology

- Enclosed is my check for \$ _____
in U.S. funds payable on a U.S. bank.
 - Please charge my credit card: ☐ Mastercard ☐ Visa
- Card # _____
Expiration Date _____
Signature _____



THE OCEANOGRAPHY SOCIETY
4052 Timber Ridge Drive
Virginia Beach, VA 23455 USA
Phone: (757) 464-0131

Non-Profit Org.
U.S. Postage
PAID
Lancaster
PA 17603
Permit 161

THE OCEANOGRAPHY SOCIETY

The Oceanography Society was founded in 1988 to disseminate knowledge of oceanography and its application through research and education, to promote communication among oceanographers, and to provide a constituency for consensus-building across all the disciplines of the field. The Oceanography Society is a non-profit, tax-exempt organization incorporated in the District of Columbia.

MEMBERSHIP

Regular membership is available to oceanographers, scientists or engineers active in ocean-related fields, or to persons who have advanced oceanography by management or other public service. With proper certification, **Student** membership is available for students enrolled at least half-time in an oceanography or ocean-related program at the baccalaureate or higher level. **Life** members pay a one-time fee for lifelong privileges of membership. **Sponsoring** membership is available to individuals who wish to provide enhanced support annually. In the U.S., \$60 of the annual dues in this category is tax-deductible as a charitable contribution, as are any additional contributions, over and above the annual Regular Member dues. *Note:* no portion of Life Member dues qualifies as a charitable contribution. Organizations and companies may subscribe annually as **Corporate/Institutional** members. Annual **Library** subscriptions are also available. All members are entitled to exercise the rights and responsibilities of active participation in the Society, including the vote. All members receive *Oceanography*. All applications for membership are subject to approval by the Membership Committee of the Society. To join, mail the application with completed information and appropriate payment.